Aus dem Charité Comprehensive Cancer Center
der Medizinischen Fakultät Charité – Universitätsmedizin Berlin

DISSERTATION

Bewertung der Kombinationsbehandlung Docetaxel und JQ1 in präklinischen 2D- und 3D-Modellen von Prostatakrebs
Evaluation of the combination treatment docetaxel and JQ1 in 2D and 3D preclinical models of prostate cancer

zur Erlangung des akademischen Grades
Doctor medicinae (Dr. med.)

vorgelegt der Medizinischen Fakultät
Charité – Universitätsmedizin Berlin

Von
Yipeng Xu

aus Linyi, Shandong, China

Datum der Promotion: 30.11.2023.....

Table of Contents

List of Tables

List of Figures

List of Abbreviations

Abbreviations	Full name
ADT	Androgen deprivation therapy
AR	Androgen receptor
AS	Active surveillance
BET	Bromodomain and extra terminal domain
CRPC	Castration-resistant prostate cancer
d_{max}	Major diameter
d_{min}	Minor diameter
mCRPC	Metastatic castration-resistant prostate cancer
mHSPC	Metastatic hormone-sensitive prostate cancer
mPCa	Metastatic Prostate Cancer
nmCRPC	Nonmetastatic castration-resistant prostate cancer
OS	Overall survival
PCa	Prostate cancer
PDXs	Patient-derived xenografts
PFS	Progression-free survival
PSA	Prostate specific antigen
PSA-P	PSA progression
RP	Radical prostatectomy
RT	Radiation therapy
SD	Standard deviation

Title: Evaluation of the combination treatment docetaxel and JQ1 in 2D and 3D preclinical models of prostate cancer

Abstract

Prostate cancer (PCa) remains the most prevalent cancer in men globally, with an increasing burden worldwide. PCa is unique in its dependence on androgen-androgen receptor (AR) signaling for growth and progression, and hormonal therapies have greatly improved the survival of patients with metastatic prostate cancer (mPCa). However, almost all patients with mPCa are resistant to hormonal treatments and ultimately succumb to metastatic castration-resistant prostate cancer (mCRPC), even when new hormonal agents deplete serum androgen levels. Therefore, novel non-AR dependent therapeutic strategies should be explored. JQ1, a potent and selective Bromodomain and extra terminal domain (BET) inhibitor, is a potentially potent therapy for patients with mCRPC. Compared to new hormonal agents, JQ1 more potently abrogates BRD4 localization to the AR target loci and AR-mediated gene transcription. However, a recent study showed that JQ1 promotes PCa invasion and metastasis in a BET protein-independent manner when PCa cell growth is inhibited. Therefore, combination strategies with JQ1 might be more promising than JQ1 alone. This study shows that JQ1 and docetaxel might serve as an effective combination therapy for patients with mPCa. We assessed the combination therapy in 2D and 3D preclinical models, and we also evaluated the susceptibility of 2D-cultured LNCaP cells and 3D-cultured LNCaP cells/spheroids exposed to the same anti-cancer drug. In contrast to 2D LNCaP cells, the evaluation of LNCaP spheroids' susceptibility was more complicated. The IC50 curves were not suitable for evaluating the susceptibility to drugs. Specifically for big-sized LNCaP spheroids, a low maximum inhibition and a low R-squared value were observed. Our results identified the different fitness of IC50 curves for 2D and 3D preclinical models and supported a potential combination treatment (docetaxel and JQ1) for PCa patients.

Titel: Bewertung der Kombinationsbehandlung Docetaxel und JQ1 in präklinischen 2D- und 3D-Modellen von Prostatakrebs

Zusammenfassung

Prostatakrebs (PCa) ist nach wie vor die häufigste Krebserkrankung bei Männern weltweit und nimmt weltweit zunehmend zu. PCa ist einzigartig in seiner Abhängigkeit vom Androgen-Androgen-Rezeptor (AR) -Signal für Wachstum und Progression, und Hormontherapien haben das Überleben von Patienten mit metastasiertem Prostatakrebs (mPCa) erheblich verbessert. Fast alle Patienten mit mPCa sind jedoch gegen hormonelle Behandlungen resistent und erliegen letztendlich metastasiertem kastrationsresistentem Prostatakrebs (mCRPC), selbst wenn neue hormonelle Wirkstoffe den Androgenspiegel im Serum senken. Daher sollten neuartige nicht AR-abhängige Therapiestrategien untersucht werden. JQ1, ein wirksamer und selektiver Bromodomänen- und extra terminaler (BET) Bromodomänenhemmer, ist eine potenziell wirksame Therapie für Patienten mit mCRPC. Im Vergleich zu neuen hormonellen Wirkstoffen hebt JQ1 die BRD4-Lokalisierung an den AR-Zielorten und die AR-vermittelte Gentranskription stärker auf. Eine kürzlich durchgeführte Studie zeigte jedoch, dass JQ1 die PCa-Invasion und -Metastasierung auf BET-Protein-unabhängige Weise fördert, wenn das PCa-Zellwachstum gehemmt wird. Daher sind Kombinationsstrategien mit JQ1 möglicherweise vielversprechender als JQ1 allein. Diese Studie zeigt, dass JQ1 und Docetaxel als wirksame Kombinationstherapie für Patienten mit mPCa dienen können. Wir bewerteten die Kombinationstherapie in präklinischen 2D- und 3D-Modellen und bewerteten auch die Empfindlichkeit von 2D-kultivierten LNCaP-Zellen und 3D-kultivierten LNCaP-Zellen / Sphäroiden, die demselben Krebsmedikament ausgesetzt waren. Im Gegensatz zu 2D-LNCaP-Zellen war die Bewertung der Empfindlichkeit von LNCaP-Sphäroiden komplizierter. Die IC50-Kurven waren zum Teil nicht geeignet, um die Wirksamkeit von Substanzen zu bewerten. Insbesondere bei großen LNCaP-Sphäroiden beobachteten wir eine niedrige maximale Hemmung und niedrige R-Quadrat-Werte. Unsere Ergebnisse identifizierten die unterschiedliche Eignung von IC50-Kurven für präklinische 2D- und 3D-Modelle und unterstützten auch eine mögliche Kombinationsbehandlung (Docetaxel und JQ1) für PCa-Patienten.

1 Introduction

1.1 Prostate cancer

Prostate cancer (PCa) is defined as malignant neoplasm originating from the prostate epithelium, of which prostate adenocarcinoma accounts for more than 95%. PCa remains the most prevalent cancer type in men globally, with approximately 1.6 million newly diagnosed cases and 366,000 deaths each year(Claire H. Pernar, 2018). PCa was once considered a common malignancy in elderly males, while recent studies show that the incidence of PCa in young males is increasing significantly(Archie Bleyer, 2020). This indicates that the global burden of prostate cancer will become more substantial in the future.

1.1.1 The epidemiology of PCa

PCa is a significant public health problem worldwide, particularly in developed countries(Claire H. Pernar, 2018). It is estimated that one in seven men in the USA will be diagnosed with PCa in their lifetime(Barsouk *et al.*, 2020). In the USA and Europe, a large peak in PCa incidence was observed in the early 1990s, when PSA screening was initially introduced at the population level(Rebecca L. Siegel, 2020; Barsouk et al., 2020). As one of the four leading cancers, the incidence of PCa started to increase in 2014 again(Rebecca L. Siegel, 2020). The reduction of PCa mortality was halted during the last decade (2008-2017), while the mortality from the other three most common types of cancer (lung, colorectal, and breast cancer) decreased(Rebecca L Siegel, 2020). Even in Asian countries, where the incidence had previously been low, PCa incidence has increased significantly in recent years(Kimura and Egawa, 2018). The economic burden associated with treatments and prostate cancer monitoring is substantial and growing over time(Smith-Palmer *et al.*, 2019).

1.1.2 Management of PCa

PCa is a heterogeneous disease with a long natural history. Men diagnosed with PCa today have a wide variety of treatment options, such as active surveillance (AS), hormonal therapy, radical prostatectomy (RP), radiation therapy (RT), and chemotherapy. For most patients with low-risk/localized PCa and some selected patients with intermediate-risk disease, AS is the most frequent therapy choice(Chen *et al.*, 2016). Patients in the low-intermediate-risk category can choose for RP or RT with curative intent(Mottet *et al.*, 2017). Patients with PCa with localized or metastatic high-risk disease are typically treated with RT with/without hormonal therapy, while patients with recurrent or metastatic, hormone-sensitive, or castrate-resistant disease are

treated with chemotherapy or next-generation hormonal treatment(Cornford *et al.*, 2017; Min Yuen Teo, 2019).

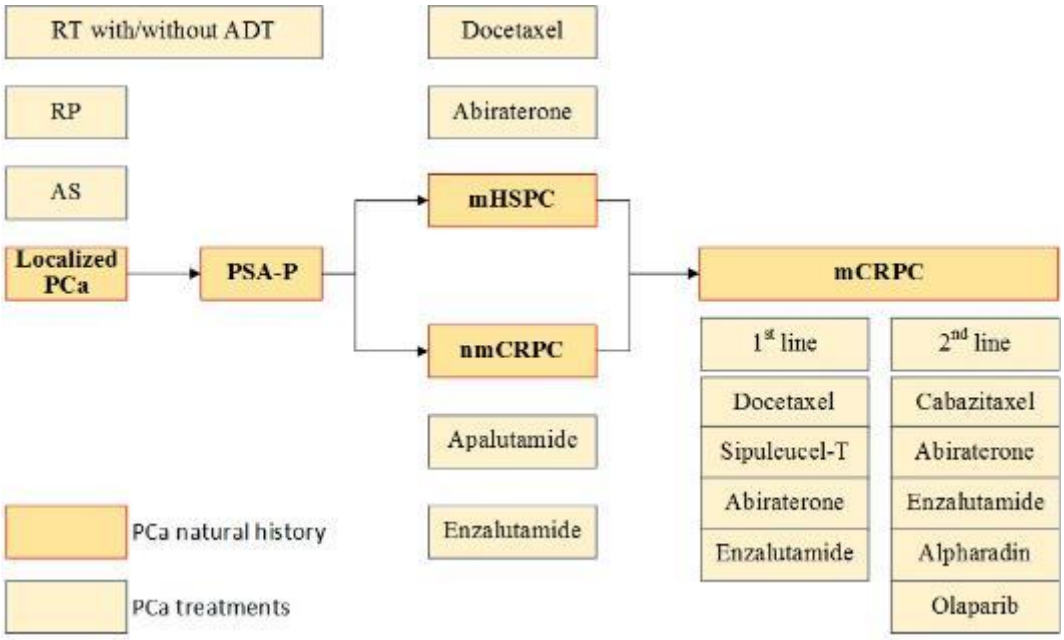

Figure 1. The natural history of PCa and the management options in different clinical states.
Abbreviations: RT (radiation therapy); ADT (androgen deprivation therapy); RP (radical prostatectomy); AS (active surveillance); PSA (prostate-specific antigen); PSA-P (PSA progression); mHSPC (metastatic hormone-sensitive prostate cancer); nmCRPC (nonmetastatic castration-resistant prostate cancer); mCRPC (metastatic castration-resistant prostate cancer).

1.1.3 Drug therapy for PCa

In the 1940s, bilateral orchiectomy and estrogen therapy were first demonstrated as effective therapies for patients with PCa(Huggins and Hodges, 1941). Since then, the androgen receptor (AR) signaling pathway has been identified as a clear target for therapy, and several hormonal therapeutics have been used to treat PCa. PCa was once widely considered as a chemotherapy non-responsive disease until docetaxel was demonstrated to be effective for mCRPC in 2004(Petrylak *et al.*, 2004; Tannock *et al.*, 2004). Several next-generation hormonal treatments have recently improved the overall survival (OS) of patients with metastatic prostate cancer (mPCa) and are used in clinical practice. Even though patients with PCa have a wide variety of therapy options now, hormonal therapy and chemotherapy remain the most important therapies.

1.1.3.1 Hormonal therapy for PCa

PCa is unique in its dependence on the AR signaling pathway for growth and progression, and androgen deprivation therapy (ADT) has been considered the backbone of treatment for

advanced and metastatic PCa(Nader *et al.*, 2018). The original form of ADT was bilateral orchiectomy, which has been replaced by ADT drugs. The validity of ADT has been further demonstrated by the confirmation of the importance of suppressing testosterone activity in the management of mPCa(Crawford *et al.*, 2019). In the initial treatment course, most patients with PCa respond well to medical castration. However, almost all patients become castration-resistant over time and develop castration-resistant prostate cancer (CRPC), wherein prostate cancer cells develop mechanisms to proliferate despite castrate levels of testosterone. Abiraterone(Stein *et al.*, 2012) and enzalutamide(Scher *et al.*, 2012), two next-generation hormonal drugs, resulted in significant improvements in OS and progression-free survival (PFS) for CRPC, but durable responses were also limited. Medical castration involves drugs blocking the AR and drugs blocking the synthesis of testosterone(Evans, 2018). Unfortunately, responses to those treatments are transient, which means that almost all patients with mPCa will become resistant to hormonal therapy. Recently, a new treatment strategy, functioning downstream of the AR, provided an entirely novel approach for the treatment of CRPC. JQ1 is thought to be a potential new therapeutic strategy for patients with mCRPC(Asangani *et al.*, 2014). More of these types of drugs or combination therapies could play an essential role in treating prostate cancer in the future.

1.1.3.2 Chemotherapy for PCa

The role of chemotherapy in PCa has undergone a dramatic and historic landscape change. For decades, chemotherapy was believed ineffective in PCa until 2004, when the results of TAX 327, a randomized nonblinded Phase III trial, were published in the New England Journal of Medicine. This study showed that docetaxel treatment every three weeks leads to superior survival and improves response rates compared to mitoxantrone(Tannock et al., 2004). This study also provided evidence that cytotoxic chemotherapy, such as docetaxel, could significantly prolong survival among patients with hormone-refractory prostate cancer (now named CRPC). Another Phase III trial(Petrylak et al., 2004) was published in the same year and showed that docetaxel treatment combined with estramustine also increased survival, but at the cost of an increased rate of adverse events. Therefore, the combination of docetaxel and estramustine is rarely used. After those initial studies, numerous combination trials were performed to improve the efficacy of docetaxel in patients with CRPC, most of which showed negative results. For patients with mHSPC, three famous clinical trials have been published. The first study (GETUG-AFU(Gravis *et al.*, 2013)) showed that the OS of patients treated with docetaxel combined with ADT was not statistically significantly different from those treated

with ADT alone. In contrast, two other clinical trials (CHAARTED(Sweeney *et al.*, 2015) and STAMPEDE(James *et al.*, 2016)) show significant improvements in OS. Patients who received docetaxel treatment combined with standard therapy had an improved OS, with a 16.6- and 10-month difference. A subsequent meta-analysis reviewed all relevant trials assessing docetaxel combined with standard therapies in patients with mHSPC and showed that docetaxel improves survival in patients with mPCa(Vale *et al.*, 2016).

Cabazitaxel is the second-line chemotherapy drug for patients with mCRPC. A randomized Phase III clinical trial (TROPIC(de Bono *et al.*, 2010)) was first reported on in 2010, in which the median OS of the patient group treated with cabazitaxel was 5.1 months longer than those treated with mitoxantrone. However, cabazitaxel also showed higher adverse events. Another Phase III clinical trial (FIRSTANA(Oudard *et al.*, 2017)) compared cabazitaxel to docetaxel in chemotherapy-naïve mCRPC. There was no superiority in OS for this combination strategy, confirming that docetaxel remains the most appropriate first-line chemotherapy regimen for patients with mCRPC.

1.1.4 Docetaxel treatments for PCa

Docetaxel is a semi-synthetic taxane analog derived from the European yew. The chemical formula of docetaxel is $C_{43}H_{53}NO_{14}$, and its molecular weight is 807.88. Docetaxel has a two-fold mechanism of anti-cancer activity. Docetaxel disrupts the normal physiological functions of microtubules during mitosis, and thus results in cell cycle arrest. On the other hand, docetaxel promotes Bcl-2 phosphorylation, enabling the activation of the Bcl-2 protein, which ultimately results in cell apoptosis(Pienta, 2001). The three-week regimen of docetaxel combined with prednisone is widely used as the first-line chemotherapy regimen for the treatment of CRPC. There are only a few effective treatment options for patients with tumors resistant to docetaxel since cross-resistance between docetaxel and new hormonal agents (e.g., abiraterone, enzalutamide) has been observed in many studies(Mezynski *et al.*, 2012; Nadal *et al.*, 2014; van Soest *et al.*, 2013; Cheng *et al.*, 2015; Schweizer *et al.*, 2014). To date, docetaxel's status as a first-line anti-cancer drug in PCa has not been challenged. Therefore, a combination treatment, which could reduce the dosage of docetaxel and the drug toxicity or delay resistance to docetaxel, might be a solution for patients with mPCa.

1.1.5 JQ1: a novel potential therapeutic for PCa

Bromodomain and extra terminal domain (BET) proteins belong to a family of epigenetic regulators, including three ubiquitously expressed bromodomain-containing proteins (BRD2,

BRD3, and BRD4) and the testis-specific BRDT(Leiming Wang, 2020). In recent years, functional inhibition of BET proteins has been highlighted as an important therapeutic target for cancers(Alghamdi *et al.*, 2016). Several small molecules have been developed to inhibit the function of BET proteins, of which JQ1 was demonstrated to be a potent and selective BRD 4 inhibitor(Alghamdi et al., 2016). BRD4 is a transcription regulator recruiting transcriptional regulatory complex to acetylated chromatin and subsequently regulating the expression of a series of proteins, such as c-Myc. By interfering with the function of BRD4, JQ1 promotes apoptosis and results in cell cycle arrest in the G1 phase(Shi *et al.*, 2018). JQ1 is a new treatment strategy for PCa patients since JQ1 functions downstream of the AR. In contrast to new hormonal agents, JQ1 more potently abrogates BRD4 localization to AR target loci and inhibits AR-mediated gene transcription. The BET bromodomain inhibition was shown to be more efficacious than direct AR antagonism in CRPC xenograft models(Asangani et al., 2014). However, one recently published study showed that JQ1 promoted PCa invasion and metastasis in a BET protein-independent manner when the PCa cell growth was inhibited(Leiming Wang, 2020). This indicates that a combination treatment strategy might be more promising than JQ1 alone. The combined effects of BRD4-targeting therapy and docetaxel were explored in two types of solid tumors, with opposite results. In esophageal adenocarcinoma, the effects of JQ1 are synergistically amplified by docetaxel addition both *in vitro* and *in vivo*(Song *et al.*, 2020). No synergistic activity was observed when docetaxel was combined with BRD4-proteolysis targeting chimeric breast cancer cells(Noblejas-López *et al.*, 2019). In this study, we explored the combined effects of JQ1 and docetaxel in PCa. Our findings in 2D and 3D preclinical models indicate that JQ1 can promote the cell viability inhibition of docetaxel.

1.2 Preclinical models in anti-cancer drug screening

For decades, tremendous progress has been made in commercial drug research and development, but the discovery of novel effective drugs has decreased(Scannell *et al.*, 2012). It has been reported that novel oncology drugs have lower success rates during late clinical development stages than drugs for other diseases(Takebe *et al.*, 2018). A lack of efficacy was suggested as the main reason for this low success rate(Arrowsmith, 2011). Clinical trials are based on evidence of effectiveness in preclinical models; therefore, a preclinical model that mimics human tumors more accurately would be a useful tool for translational research of anti-cancer drugs.

1.2.1 Preclinical models of PCa

Today, most preclinical PCa research is still undertaken in 2D-cultured PCa cell lines, among which, PC3, DU145, and LNCaP are the most widely used (Elbadawy *et al.*, 2020). The advantages of 2D-cultured PCa cell lines are their ease of use, high reproducibility, and cost-effectiveness(Hepburn *et al.*, 2020). However, the cell lines may accumulate multiple additional mutations due to long-term culture. Meanwhile, a lack of essential characteristics can make it challenging to generalize data for clinical practice. For example, DU145 and PC3 cells do not express AR and PSA(Elbadawy et al., 2020; Hepburn et al., 2020).

Compared to cell lines, patient-derived xenografts (PDXs) more appropriately reflect cellular heterogeneity and molecular divergence(Shen and Abate-Shen, 2010; Kopetz *et al.*, 2012). PDXs of PCa were shown to be beneficial in drug screenings for efficacy and toxicity(Nguyen *et al.*, 2017). However, the use of PDXs of PCa is challenging given the low engraftment rate (15-20%), high costs, and long experimental periods (usually several months)(Lin *et al.*, 2014). The murine tumor microenvironment only partially reflects the human tumor microenvironment. The primary sources of PDXs are original tumors obtained by surgical resections, which cannot be obtained repeatedly. As the passages of the PDX model progress, the tumor microenvironment is gradually replaced by a mouse-derived matrix, reducing the PDX passage numbers during application(Cho, 2020).

Given the limitations of 2D-cultured cell lines and PDX models, 3D cell culture systems (organoids, spheroids) are getting increasing attention in PCa research. Organoids and spheroids are both regarded as the intermediate models between *in vitro* 2D-cultured cell lines and PDXs. Spheroids are often formed from cancer cell lines or tumor biopsies, whereas organoids are derived from primary tumor tissues(Colella *et al.*, 2018). Organoids offer a higher complexity and are more *in vivo*-like than spheroids, while unfortunately, the efficiency for PCa organoid establishment is only 15-20%(Gao *et al.*, 2014). Compared with PCa organoids, the efficiency of establishing PCa spheroids based on PCa cell lines is much higher, allowing them to be widely used in novel anti-cancer drug therapies(Thakuri *et al.*, 2019), treatment-induced drug resistance(Shahi Thakuri *et al.*, 2019), and drug screening(Mulholland *et al.*, 2018).

1.2.2 Challenges for spheroids in drug screening

Despite the advantages of spheroids over 2D-cultured cells and animal models, their employment in drug screening as preclinical models is still limited. There are multiple challenges to be addressed for spheroid experimental protocols to be widely adopted and used in fundamental research and drug screening(Ham *et al.*, 2016).

1.2.2.1 The most desired application of spheroids is drug testing and screening. However, compared to 2D-cultured cells, the routine use of spheroids is more complex and expensive. The design of new platforms or protocols is prompted, which could simplify the spheroids' culture and maintenance, and could improve their availability for drug testing work.

1.2.2.2 The analyses of drug testing experiments based on spheroids also rely on colorimetric, luminescence or fluorescence assays, originally developed for 2D-monolayer cultured cells. The evaluation indexes of drug effectiveness for spheroids are based on the IC50 values generated from 2D monolayer cultured cells. Many studies showed that spheroids are much more drug-resistant than 2D cultured cells(Shahi Thakuri *et al.*, 2016). A new evaluation system or combined evaluation indexes should be explored for spheroid drug testing experiments.

1.2.2.3 Cancer organoids based on primary cancer tissues are composed of cancer cells and mesenchymal cells. The mesenchymal cells stimulate the growth of cancer cells and provide treatment protection from anti-cancer drugs(Stock *et al.*, 2016). The proportion of cancer and stromal cells could also be variable in different tumor models. Fortunately, one study revealed that Matrigel, containing growth factors, could partially replace the effect of the stromal cells(Stock et al., 2016).

Even though there are limitations in all models, we sought to mimic cancer *in vivo* as much as possible. Our study's experiments were based on cells/spheroids obtained from the prostate cancer LNCaP cell line, which express AR and PSA. We used Matrigel to replace the effect of stromal cells. The CellTiter Glo is the standard assay in spheroid drug testing experiments, and we used multi-parameters to analyze the drug effectiveness.

1.3 Aims of the research

Based on previous evidence for the role of JQ1 as a potential anti-cancer drug in PCa and the possible synergistic activity with docetaxel, we aimed to answer the following research questions:

1. Can we harvest spheroids from the LNCaP cell line?
2. What are the differences between 2D and 3D drug testing experiments?
3. Is IC50 a suitable tool for 3D drug sensitivity evaluation?
4. How can drug effectiveness be assessed in spheroid drug testing experiments?
5. Can JQ1 promote drug sensitivity to docetaxel, as assessed in PCa cells/spheroids?

2 Methodology

2.1 Lists

2.1.1 List of commercial reagents

Reagent	Company	Catalogue Number
Albumin bovine (BSA)	Serva	11926.03
Docetaxel, Cytotoxic agent	Abcam	ab141248
Dulbecco's phosphate buffered saline (DPBS)	Life Technologies	14190169
Ethanol (≥70%)	Roth	T913.3
Ethanol (≥99.8%)	Roth	K928.4
Fetal Bovine Serum (FBS), qualified, heat inactivated	Gibco	10500064
HISTOGEL	Thermo Scientific	R904012
JQ1	BPS	27402
Matrigel® Growth Factor Reduced (GFR) Basement Membrane Matrix, Phenol Red-free	Corning	356231
Penicillin-Streptomycin	Gibco	15140-148
Recover cell culture freezing medium	Gibco	12648-010
TrypLE Express	Gibco	12604-013

2.1.2 List of kits

Name	Components
CellTiter-Glo® Luminescent Cell Viability Assay kit (Catalog No. G755A)	10×10ml CellTiter-Glo® Substrate Lyophilized 10×10ml CellTiter-Glo® Buffer

2.1.3 List of consumables

Name	Company	Catalogue Number
1.5 ml MicroTubes	SARSTEDT	72.706.400
1000 µl Pipette tips	SARSTEDT	70.760.002
20 µl Pipette tips	SARSTEDT	70.116
200 µl Pipette tips	SARSTEDT	70.762.411

Corning® 96-well Black/Clear Round Bottom Ultra-Low Attachment Spheroid Microplate, with Lid, Sterile	Corning	4515
Corning® 96-well Flat Clear Bottom Black Polystyrene TC-treated Microplates, Individually Wrapped, with Lid, Sterile	Corning	3603
Falcon® 10 mL Serological Pipet, Polystyrene, 0.1 Increments, Individually Packed, Sterile	Corning	357551
Falcon® 100 mm TC-treated Cell Culture Dish	Corning	353003
Falcon® 15 mL High Clarity PP Centrifuge Tube, Conical Bottom, with Dome Seal Screw Cap, Sterile	Corning	352097
Falcon® 24-well Clear Flat Bottom plates	Corning	353047
Falcon® 25 mL Serological Pipet, Polystyrene, Space Saver, 0.25 Increments, Sterile	Corning	357525
Falcon® 25cm² Rectangular Canted Neck Cell Culture Flask with Vented Cap	Corning	353108
Falcon® 5 mL Serological Pipet, Polystyrene, 0.1 Increments, Individually Packed, Sterile	Corning	357543
Falcon® 50 mL High Clarity PP Centrifuge Tube, Conical Bottom, Sterile	Corning	352098
Falcon® 75cm² Rectangular Canted Neck Cell Culture Flask with Vented Cap	Corning	353136
Falcon® 96-well Clear Flat Bottom TC-treated Culture Microplate, with Lid, Individually Wrapped, Sterile	Corning	353072
MACS® SmartStrainers 100 µm	Miltenyi Biotec	130-098-463
MACS® SmartStrainers 30 µm	Miltenyi Biotec	130-098-458
MACS® SmartStrainers 70 µm	Miltenyi Biotec	130-098-462
Pipetus® Junior Pipettencontroller	Hirschmann	HI9907200

2.1.4 List of devices

Product	**Manufacturer**
ASPIRE Laboratory Aspirator	Accuris

Centrifuge 320R	Hettich® Universal
Centrifuge 5810	Eppendorf
Centrifuge 5810	Eppendorf
Centrifuge 5810R	Eppendorf
Centrifuge 8510R	Eppendorf
Incubator B6120 microbiological	Heraeus
Incubator(CO_2) 240i	Hettich
Incubator(CO_2) CB160	Binder
Incubator(CO_2) Midi 40	Thermo Scientific™
Laboratory shaker 34524-200	CENCO
Microscope TCS SPE confocal system	Leica
Microwave M1913	Samsung
Research pipette 0.1-0.25 µl	Eppendorf
Research pipette 0.5-10 µl	Eppendorf
Research pipette 100-1000 µl	Eppendorf
Research pipette 10-100 µl	Eppendorf
Research pipette 2-20 µl	Eppendorf
Research pipette(12-channel) 30-300 µl	Eppendorf
Research pipette(8-channel) 30-300 µl	Eppendorf
Safety workbenches(DIN12950)	Heraeus
Water Bath 1004	GFL

2.2 Cell culture conditions and cell cryopreservation

The LNCaP cell line was a kind gift from the Urology Department of Charité Campus Mitte. All the 2D and 3D cultured cells were cultured in a humidified incubator with 5% CO_2 (carbon dioxide) at 37℃.

2.2.1 Complete growth medium: The 2D cultured LNCaP cells were maintained in RPMI 1640 medium supplemented with 10% FBS (fetal bovine serum) and 1% PS (penicillin /streptomycin antibiotics) according to the complete growth medium described on the ATCC website(https://www.lgcstandards-atcc.org/products/all/CRL-1740.aspx#culturemethod).

However, for the 3D cultured cell/spheroids, we first carried out the experiment based on RPMI + 1% PS supplemented with 2%, 5%, 7.5% and 10% FBS(Subheading 2.4), since different concentrations of FBS were applied according to various pieces of literature (Song *et al.*, 2003;

Ziaee and Chung, 2014; Härmä *et al.*, 2015; Ma *et al.*, 2017; Ballangrud *et al.*, 2001). The results showed that lower FBS concentrations were not suitable for the survival and growth of embedded cultured LNCaP spheroids except 10% FBS(Subheading 3.1), so all the 3D cultured LNCaP cells/spheroids were maintained in RPMI + 10% FBS + 1% PS in the subsequent experiments, irrespective of whether the cells/spheroids were embedded cultured in Matrigel or floating cultured in spheroid microplates.

2.2.2 Cell cryopreservation: Long-term storage of the 2D/3D LNCaP cells was achieved by resuspending the cells in RPMI+50% FBS +10% DMSO without antibiotics and preserving in the liquid nitrogen.

2.3 3D cell/spheroid workflow: The LNCaP cells were set up as 2D or 3D preclinical models in this research. Two kinds of 3D culture protocols were carried out in this research (3D embedded culture and 3D floater culture, Figure 2). The growth of the 3D cultured cells/spheroids was monitored via images of LNCaP cells/spheroids by microscopy, and the susceptibilities of LNCaP cells/spheroids were evaluated by spheroid formation and IC50 curves.

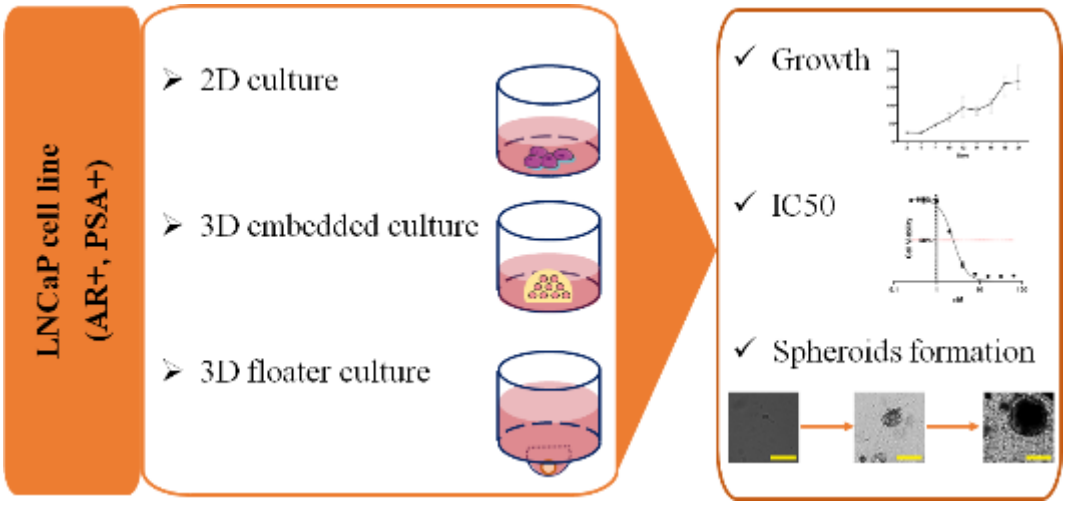

Figure 2. The 2D/3D preclinical models of prostate cancer workflow.

2.3.1 3D embedded cell/spheroid culture: The 3D cultured LNCaP cells/spheroids were initiated from 2D cultured LNCaP cells. The cryotubes of the 2D cultured LNCaP cells were removed from liquid nitrogen storage and quickly thawed into a 37℃ water bath to be melted. The cell precipitation was resuspended in complete growth medium (RPMI + 10% FBS + 1% PS), then removed into the cell flasks after centrifugation (1,000rpm×3min) and supernatant removal. From the 3rd passages after cell thawing, a certain number of 2D cultured LNCaP

cells were resuspended in the Matrigel and plated into the center of each well (TC-treated 96-well microplates, 24-well plates) according to the protocols below.

2.3.1.1 3D embedded cell culture protocols: The Matrigel was divided into separate 1.5ml sterile EP tubes and preserved at -20℃. Matrigel split tubes were thawed on ice overnight before subsequent experiments, while the plates were maintained in the incubator at 37℃ overnight. The cool PBS was divided into 50ml tubes and kept on ice overnight, while the PBS at room temperature was kept at room temperature for at least 2 hours before the following experiments. The complete growth medium was divided into 50ml centrifuge tubes and preserved at 4℃. The complete growth medium's separated tubes should be prewarmed at 37℃ for at least 2 hours before the subsequent experiments.

2.3.1.1.1 Establishing and culturing LNCaP cells/spheroids

2.3.1.1.1.1 Take one flask(75cm^2) of LNCaP cells (80-90% proportion) from the incubator and exchange the complete growth medium 24 hours before the experiments.

2.3.1.1.1.2 Culture the cells overnight in the incubator.

2.3.1.1.1.3 Wash the LNCaP cells in the cell flask with 10ml PBS (room temperature) twice.

2.3.1.1.1.4 Pipet 2ml Accutase Cell Dissociation Reagent into the cell flask, and maintain the flask at 37℃ for 5 min.

2.3.1.1.1.5 Pipet the cell suspension into a 15ml centrifuge tube and wash the flask with 5ml PBS twice, which is also pipetted into the 15ml centrifuge tube.

2.3.1.1.1.6 Centrifuge: 1000rpm×3min.

2.3.1.1.1.7 Resuspend the cell pellet with 2ml cool PBS after supernatant removal.

2.3.1.1.1.8 Filter the cell suspension with a 30 μm cell strainer and count the cells using a hemocytometer.

2.3.1.1.1.9 Resuspend the cells (500 cells per well) in Matrigel and plate the cell-Matrigel (6 μl/well for 96-well TC-treated microplates, and 15 μl/well for 24-well plates) into the center of each well of a preheated plate (Figure 3).

2.3.1.1.1.10 Place the plate upside down in the CO_2 incubator (Figure 3) while the Matrigel containing the cells solidifies for 15 min at 37℃.

2.3.1.1.1.11 Gently add the prewarmed complete growth medium into each well (1 ml/well for 24-well plates and 200 μl/well for 96-well plates), then place the plates into the incubator.

2.3.1.1.1.12 Refresh the complete growth medium every three days in the 24-well plates, while half exchanging the complete growth medium every other day in the 96-well plates.

2.3.1.1.1.13 Check the cells/spheroids with a microscope daily and record the spheroids' growth three times per week.

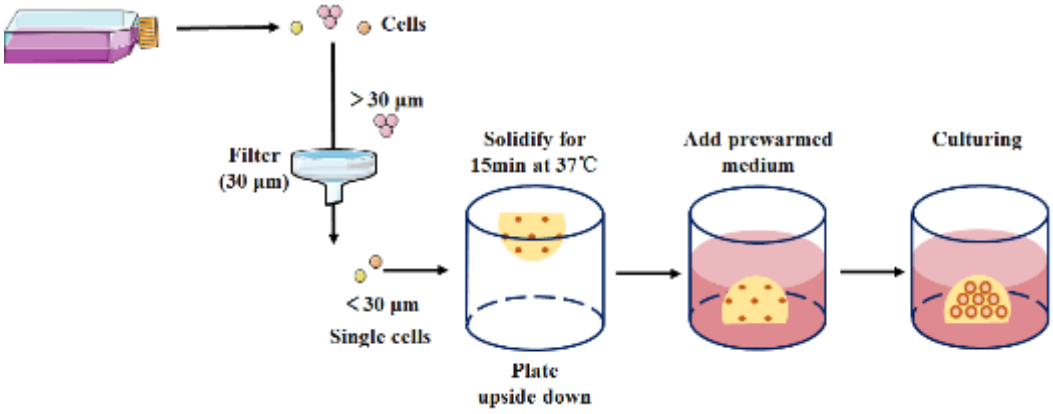

Figure 3. Protocol for establishing 3D embedded LNCaP cells/spheroids.

2.3.1.1.2 Passaging LNCaP spheroids in the 24-well plates

2.3.1.1.2.1 Pipet out the complete growth medium with 1 ml pipette tips, and add 1 ml cool PBS into each well.

2.3.1.1.2.2 Release the spheroid-Matrigel lenses from each well with 1 ml pipette tips and transfer them into a 15 ml centrifuge tube which has been coated with 1% BSA in PBS.

2.3.1.1.2.3 Wash each well with cool PBS to obtain all the spheroids and add them into the centrifuge tube described above.

2.3.1.1.2.4 Pipet thoroughly using a 100 μl tip (without filter) on a 1ml pipette tip to release the spheroids from the Matrigel.

2.3.1.1.2.5 Filter the cell suspension through a 70 μm cell strainer to eliminate the dead cells and the cells not within the growing spheroids.

2.3.1.1.2.6 Wash the strainer with 5 ml cool FBS and invert the cell strainer onto a 10 cm^2 dish.

2.3.1.1.2.7 Wash the retained spheroids from the strainer with 10 ml cool FBS and collect the spheroids into a new 15 ml centrifuge tube.

2.3.1.1.2.8 Centrifuge at 1,000 rpm for 5 min at 4℃, then aspirate the supernatant and Matrigel above the cell pellet.

2.3.1.1.2.9 Resuspend the spheroids in Matrigel and plate 15 μl spheroid-Matrigel drops into the center of the well of a prewarmed 24-well plate. The spheroids are passaged in a 1:2 dilution (Figure 4).

2.3.1.1.2.10 Place the plate upside down in the incubator while the Matrigel containing the spheroids solidifies for 15 min at 37℃.

2.3.1.1.2.11 Gently add 1ml prewarmed complete growth medium into each well and place the plates into the incubator.

2.3.1.1.2.12 Refresh the cell culture fluids every three days.

2.3.1.1.2.13 Check the spheroids with a microscope daily and record the spheroids' growth three times per week.

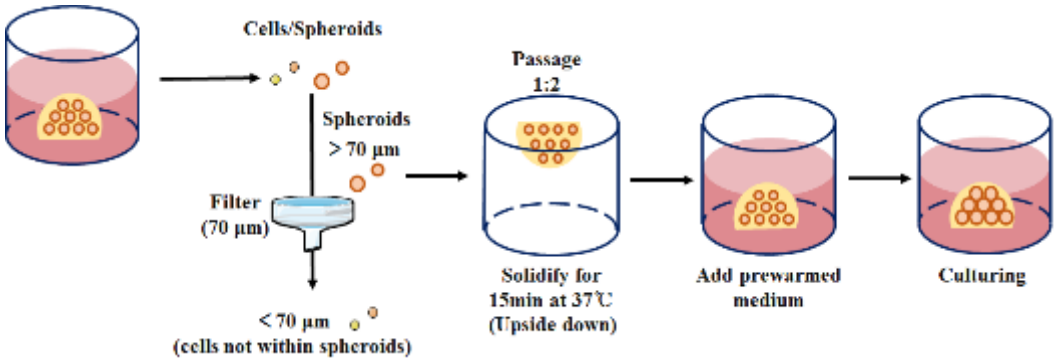

Figure 4. Protocol for passaging 3D embedded LNCaP spheroids.

2.3.2 3D floater culture: Unlike the 3D embedded cell/spheroid culture, the cells/spheroids in this protocol were floaters at the U-bottom of each well instead of embedding in Matrigel. The low attachment U-bottom 96-well spheroid microplates were applied in these cell culture experiments and drug testing work according to the protocol below.

2.3.2.1 The 2D cultured LNCaP cells were collected from the cell flasks (repeat Subheadings 2.3.1.1.1.1 - 2.3.1.1.1.6).

2.3.2.2 Resuspend the cell pellet with 2 ml complete growth medium after the supernatant removal.

2.3.2.3 Count the cells using a hemocytometer.

2.3.2.4 Resuspend the cells with the prewarmed complete growth medium and add the cell suspension (200 μl/well) into the 96-well spheroid microplates.

2.3.2.5 Place the plates in the CO_2 incubator, then half exchange the cell culture fluids every other day.

2.3.2.6 Check the spheroids with a microscope daily and record the spheroids' growth.

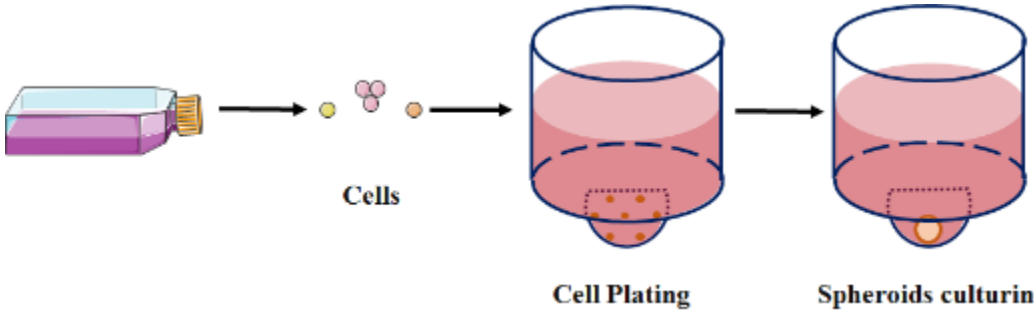

Figure 5. Protocol for establishing 3D floater cultured LNCaP spheroids.

2.4 Exploring for a suitable FBS concentration for LNCaP spheroid culture: Many studies have shown that the LNCaP spheroids can be cultured in RPMI supplemented with PS and FBS, but the FBS concentrations were different across the literature(Song et al., 2003; Ziaee and Chung, 2014; Härmä et al., 2015; Ma et al., 2017; Ballangrud et al., 2001). Therefore, we first carried out a 3D culturing experiment to define a suitable FBS concentration for LNCaP spheroids. The establishment of LNCaP spheroids in 24-well plates was done according to the steps from Subheadings 2.3.1.1.1.1 to 2.3.2.1.10, after which 1ml prewarmed RPMI 1640 medium supplemented with 1% PS and varying FBS concentrations (2%, 5%, 7.5%, and 10%) was gently added into each well. The LNCaP spheroids were checked and recorded with a microscope for 18 days.

2.5 LNCaP spheroid formation and its growth kinetics in Matrigel: The establishment of LNCaP spheroids in TC-treated 96-well microplates was done according to the steps from Subheadings 2.3.1.1.1.1 to 2.3.2.1.10, after which 200μl prewarmed complete growth medium (RPMI + 10% FBS + 1% PS) were gently added into each well. The complete growth medium was half exchanged every other day, and the LNCaP spheroids were checked and recorded with a microscope for three weeks.

2.6 Drug testing experiments: Our drug testing experiments were based on two different drugs (docetaxel and JQ1), the states of matter of which were both powders at the very beginning. We first dissolved them in DMSO into the storage concentrations at 50mM (millimoles) and 10mM, and maintained them at -20℃. The storage concentrations diluted all the drug concentrations described below. We first experimented with detecting the cell viability of 2D cultured LNCaP cells exposed to varying DMSO concentrations to evaluate the effect of DMSO in the final drug concentrations.

2.6.1 2D drug testing experiments exposed to DMSO: The final concentrations of docetaxel in the following drug testing experiments were from 0.25 to 2048 nM, while 8 - 4096nM for JQ1. So the final concentrations of DMSO were from 4.096×10^{-2} % to 5×10^{-7} %. CellTiter Glo assays were performed to analyze the influences of cell viability exposed to varying final DMSO concentrations of 5×10^{-7} %, 5×10^{-6} %, 5×10^{-5} %, 5×10^{-4} %, 5×10^{-3} %, and 5×10^{-2} %.

2.6.1.1 Collect the 2D cultured LNCaP cells from the cell flasks (repeat Subheadings 2.3.1.1.1.1 - 2.3.1.1.1.6).

2.6.1.2 Resuspend the cell pellet with 2 ml complete growth medium after the supernatant removal.

2.6.1.3 Count the cells using a hemocytometer.

2.6.1.4 Resuspend the cells with room temperature complete growth medium and add the cell suspension (100 µl/well, 2000 cells/well) into the 96-well TC-treated microplates.

2.6.1.5 Place the plates in the CO_2 incubator for 48 hours.

2.6.1.6 Add 100 µl cell culture fluids containing 2× DMSO final concentrations (10^{-6}, 10^{-5}, 10^{-4}, 10^{-3}, 10^{-2}, 0.1 %) into each well, while 0 concentration of DMSO serves as negative control.

2.6.1.7 Culture the LNCaP cells for five days.

2.6.1.8 CellTiter Glo assay (2D, Subheading 2.8.1).

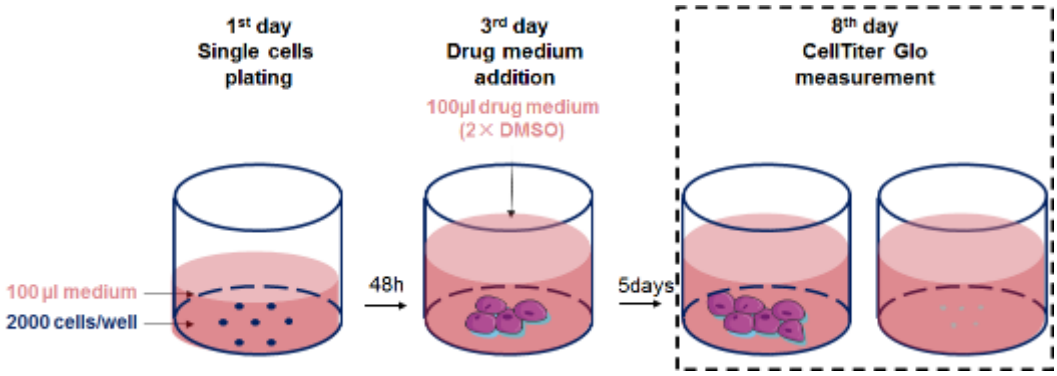

Figure 6. Protocol for 2D drug testing experiment exposed to DMSO.

2.6.2 2D drug testing experiments exposed to docetaxel / JQ1:

2.6.2.1 The 2D cultured LNCaP cells were collected from the cell flasks (repeat Subheadings 2.3.1.1.1.1 - 2.3.1.1.1.6).

2.6.2.2 Resuspend the cell pellet with 2 ml complete growth medium after the supernatant removal.

2.6.2.3 Count the cells using a hemocytometer.

2.6.2.4 Resuspend the cells with the complete growth medium (room temperature), then add the cell suspension (100 µl/well, 2000 cells/well) into the 96-well TC-treated microplates.

2.6.2.5 Place the plates in the CO_2 incubator for 48 hours.

2.6.2.6 Add 100 µl complete growth medium with the 2× docetaxel / JQ1 final concentrations as described below, while the negative control contains no drug at all.

Final drug concentrations in the plates: The 2D cultured LNCaP cells were exposed to a varying final concentration of docetaxel / JQ1 as follows:

	Final docetaxel concentrations
Docetaxel	0, 0.25, 0.5, 1, 2, 4, 8, 16, 32, 64 nM
	0, 0.25, 0.5, 1, 2, 4, 8, 16, 32, 64 nM
	0, 0.125, 0.25, 0.5, 1, 2, 4, 8, 16, 32 nM
JQ1	0, 8, 16, 32, 64, 128, 256, 512, 1024, 2048 nM
	0, 8, 16, 32, 64, 128, 256, 512, 1024, 2048 nM
	0, 16, 32, 64, 128, 256, 512, 1024, 2048, 4096 nM

Table 1. Varying final concentrations of docetaxel/JQ1 for 2D drug testing experiments.

2.6.2.7 Culture the LNCaP cells for five days.

2.6.2.8 CellTiter Glo assay (2D, Subheading 2.8.1).

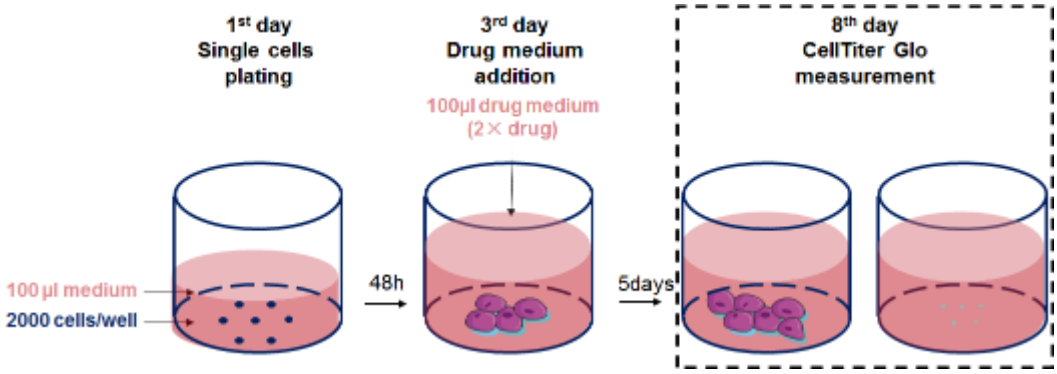

Figure 7. Protocol for 2D drug testing experiments exposed to docetaxel/JQ1.

2.6.3 3D drug testing experiments based on embedded cultured LNCaP cells (2 days):

2.6.3.1 The 2D cultured LNCaP cells were collected from the cell flasks and embedded in Matrigel then plated into the 96-well TC-treated microplates (repeat Subheadings 2.3.2.1.1 - 2.3.2.1.10).

2.6.3.2 Gently add the prewarmed complete growth medium into each well (200 µl/well), and place the plates into the incubator.

2.6.3.3 Place the plates in the CO_2 incubator for 48 hours.

2.6.3.4 Pipet out 100 µl complete growth medium, and then add 100 µl new complete growth medium with the 2× docetaxel / JQ1 final concentrations as described below, while the negative control contains no docetaxel at all.

Final drug concentrations in the plates:

	Final docetaxel concentrations
Docetaxel	0, 0.25, 0.5, 1, 2, 4, 8, 16, 32, 64 nM
	0, 0.25, 0.5, 1, 2, 4, 8, 16, 32, 64 nM

	0, 0.125, 0.25, 0.5, 1, 2, 4, 8, 16, 32 nM
JQ1	0, 8, 16, 32, 64, 128, 256, 512, 1024, 2048 nM
	0, 8, 16, 32, 64, 128, 256, 512, 1024, 2048 nM
	0, 16, 32, 64, 128, 256, 512, 1024, 2048, 4096 nM

Table 2. Varying final concentrations of docetaxel/JQ1 for 3D drug testing experiments based on embedded cultured LNCaP cells (2 days).

2.6.3.5 Culture the LNCaP cells for five days.

2.6.3.6 CellTiter Glo assay (3D, Subheading 2.8.2).

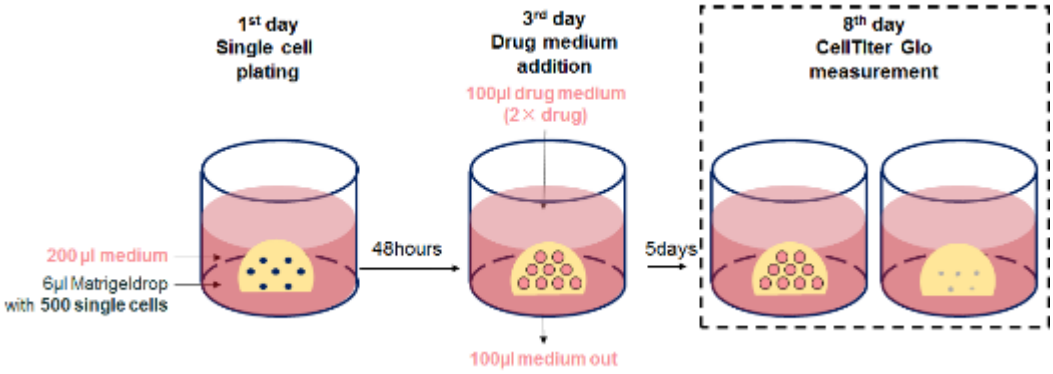

Figure 8. Protocol for 3D drug testing experiments (2 days) exposed to docetaxel / JQ1.

2.6.4 3D drug testing experiments based on embedded cultured cells/spheroids (4-21 days):

2.6.4.1 The 2D cultured LNCaP cells were collected from the cell flasks and embedded in Matrigel then plated into the 96-well TC-treated microplates (repeat Subheadings 2.3.1.1.1.1 - 2.3.1.1.1.10).

2.6.4.2 Gently add the prewarmed complete growth medium into each well (200 µl/well), and place the plates into the incubator.

2.6.4.3 Place the plates in the CO_2 incubator for 4, 7, 14, and 21 days to get different sized spheroids. Half exchange the complete growth medium (100 µl/well) every other day.

2.6.4.4 Pipet out 100 µl complete growth medium, and then add 100 µl new complete growth medium with the 2× docetaxel final concentrations as described below, while the negative control contains no docetaxel at all. All the experiments were repeated three times.

Final docetaxel concentrations in the plates:

	Final docetaxel concentrations
4 days spheroids	0, 0.25, 0.5, 1, 2, 4, 8, 16, 32, 64 nM
	0, 0.25, 0.5, 1, 2, 4, 8, 16, 32, 64 nM
	0, 0.25, 0.5, 1, 2, 4, 8, 16, 32, 64 nM

7 days spheroids	0, 0.5, 1, 2, 4, 8, 16, 32, 64, 128 nM
	0, 1, 2, 4, 8, 16, 32, 64, 128, 256 nM
	0, 2, 4, 8, 16, 32, 64, 128, 256, 512 nM
14 days spheroids	0, 2, 4, 8, 16, 32, 64, 128, 256, 512 nM
	0, 1, 4, 8, 16, 32, 64, 128, 256, 512 nM
	0, 4, 8, 16, 32, 64, 128, 256, 512, 1024 nM
21 days spheroids	0, 1, 2, 4, 8, 16, 32, 64, 128, 256 nM
	0, 4, 8, 16, 32, 64, 128, 256, 512, 1024 nM
	0, 8, 16, 32, 64, 128, 256, 512, 1024, 2048 nM

Table 3. Varying final concentrations of docetaxel/JQ1 for 3D drug testing experiments based on embedded cultured LNCaP cells (4-21 days).

2.6.4.5 Culture the LNCaP cells/spheroids for five days.

2.6.4.6 CellTiter Glo assay (3D, Subheading 2.8.2).

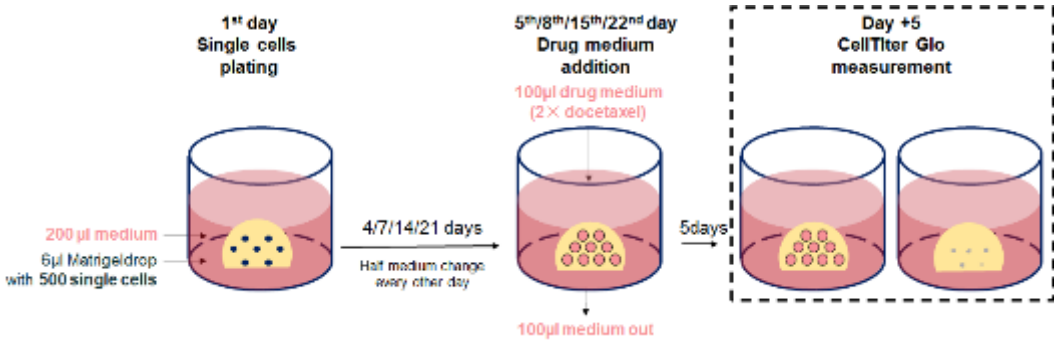

Figure 9. Protocol for 3D drug testing experiments (4-21 days) exposed to docetaxel.

2.6.5 3D drug testing experiments based on embedded cultured spheroid aliquots:

2.6.5.1 The 2D cultured LNCaP cells were collected from the cell flasks and embedded in Matrigel then plated into the 24-well plates (repeat Subheadings 2.3.1.1.1.1 - 2.3.1.1.1.10).

2.6.5.2 Gently add the prewarmed complete growth medium into each well (1 ml/well), and place the plates into the incubator.

2.6.5.3 Place the plates in the CO_2 incubator for 21 days to get different sized spheroids. Refresh the complete growth medium every three days.

2.6.5.4 Collect all the spheroids from the 24-well plates (repeat Subheadings 2.3.1.1.2.1 - 2.3.1.1.2.8).

2.6.5.5 Resuspend the spheroids in Matrigel and plate 6 µl spheroid-Matrigel drops into the center of the well of prewarmed 96-well TC-treated microplates (Figure 9).

2.6.5.6 Place the plate upside down in the incubator while the Matrigel containing the spheroids solidifies for 15 min at 37℃.

2.6.5.7 Gently add 200 µl prewarmed complete growth medium into each well and place the plates into the incubator.

2.6.5.8 Culture the LNCaP spheroids for 48 hours in the incubator.

2.6.5.9 Pipet out 100 µl complete growth medium, and then add 100 µl new complete growth medium with the 2× docetaxel final concentrations as described below, while the negative control contains no docetaxel at all.

Final docetaxel concentrations in the plates: 0.5, 1, 2, 5, 10, 20, 30, 50, 100 nM.

2.6.5.10 Culture the LNCaP spheroids for five days.

2.6.4.6 CellTiter Glo assay (3D, Subheading 2.8.2).

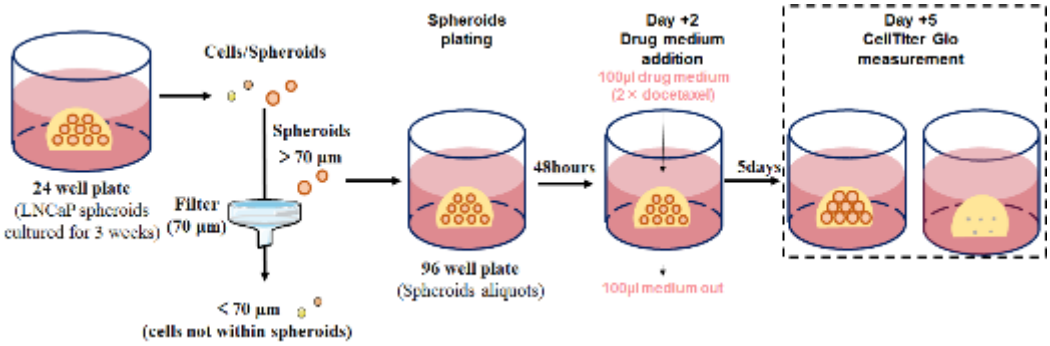

Figure 10. Protocol for 3D drug testing experiments based on embedded cultured spheroid aliquots exposed to docetaxel.

2.6.6 3D drug testing experiments based on floating LNCaP spheroids:

2.6.6.1 Effect of LNCaP cell numbers plated into the spheroid microplates: We first experimented to explore the spheroid formation in spheroid microplates, and the protocol was based on Subheading 2.3.2. Different numbers of LNCaP cells (312 cells/well, 625 cells/well, 1250 cells/well, 2500 cells/well, 5000 cells/well, 10^4 cells/well, 2×10^4 cells/well, 4×10^4 cells/well, 8×10^4 cells/well, and 16×10^4 cells/well) were resuspended and seeded into the spheroid microplates with a volume of 200 µl/well. The spheroids were checked and recorded by a microscope daily for five days.

2.6.6.2 3D drug testing experiments based on different sized floating LNCaP spheroids:

2.6.6.1 Collect the 2D cultured LNCaP cells from the cell flasks and seed them into a spheroid microplate (300/3000 cells per well with 200 µl volume, repeat Subheadings 2.3.2.1 - 2.3.2.4).

2.6.6.2 Culture the LNCaP cells/spheroids for 48 hours.

2.6.6.3 Pipet out 100 µl complete growth medium, and then add 100 µl complete growth medium with the 2× docetaxel final concentrations as described below, while the negative control contains no docetaxel at all.

Final docetaxel concentrations in the plates:

300 cells/well: 0, 0.25, 0.5, 1, 2, 4, 8, 16, 32, 64 nM.

3000 cells/well: 0, 1, 2, 4, 8, 16, 32, 64, 128, 256 nM.

2.6.6.4 Culture the LNCaP cells for five days.

2.6.6.5 CellTiter Glo assay (3D, Subheading 2.8.2).

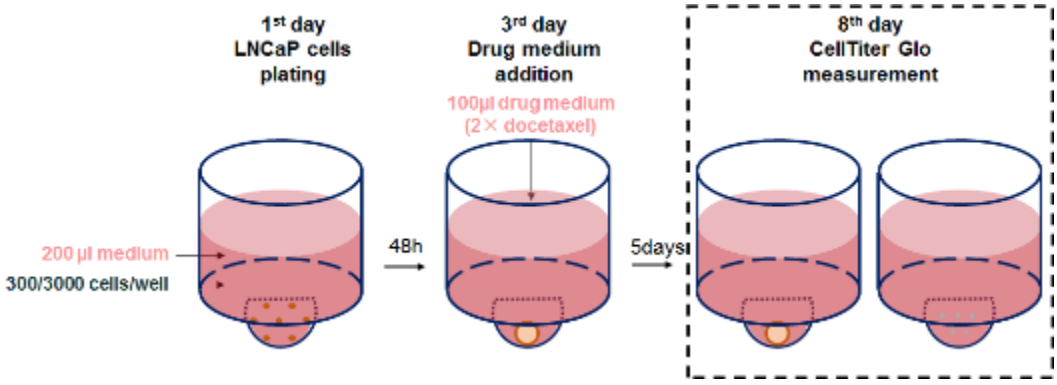

Figure 11. Protocol for 3D drug testing experiments based on different sized floating LNCaP spheroids exposed to docetaxel.

2.7 Drug testing experiments based on the combination treatment of JQ1 and docetaxel:

2.7.1 Diagonal method to evaluate the combinatory drug effects of docetaxel and JQ1 based on 2D LNCaP cells:

2.7.1.1 LNCaP cells were collected and then plated into 96-well TC-treated black microplates (repeat Subheadings 2.6.2.1 - 2.6.2.4).

2.7.1.2 Place the plates in the CO_2 incubator for 48 hours.

2.7.1.3 Prepare a new 96-well clear plate, and prepare the complete growth medium with 4× docetaxel/JQ1 final concentrations as described below (300 µl/well).

	1	2	3	4	5	6	7	8	9	10	11	12
A												
B		NC		JQ1 32 nM	JQ1 32 nM		NC	NC		Docetaxel 16 nM	Docetaxel 16 nM	
C		NC		JQ1 64 nM	JQ1 64 nM		Docetaxel 1 nM	Docetaxel 1 nM		Docetaxel 32 nM	Docetaxel 32 nM	
D		NC		JQ1 128 nM	JQ1 128 nM		Docetaxel 2 nM	Docetaxel 2 nM		Docetaxel 64 nM	Docetaxel 64 nM	
E		NC		JQ1 256 nM	JQ1 256 nM		Docetaxel 4 nM	Docetaxel 4 nM		NC	NC	
F		NC		JQ1 512 nM	JQ1 512 nM		Docetaxel 8 nM	Docetaxel 8 nM		NC	NC	
G		NC		JQ1 1024 nM	JQ1 1024 nM							
H												

Figure 12. Preparation of the complete growth medium with 4× docetaxel/JQ1 final concentrations in 96-well clear plate.

NC: complete growth medium without docetaxel, JQ1, and DMSO.

2.7.1.4 Pipet out 50 µl/well complete growth medium with a 4× varying final concentration of JQ1 from the 96-well clear plate described above (Columns 4/5, Lines B to G) of the clear plate, and then add this into the TC-treated black microplate (Columns 2-9, Lines B to G) with a multichannel pipette (Figure 13, blue wells from A to B).

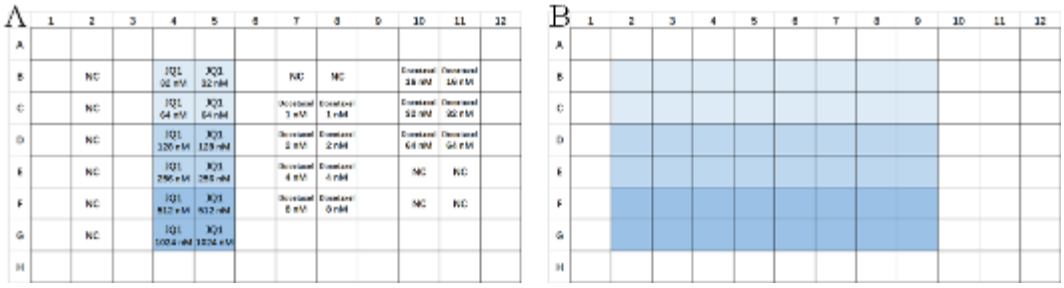

Figure 13. JQ1 medium addition from clear plate to the wells with combination treatment in TC-treated black plate.

A. The complete growth medium with 4× JQ1 final concentrations in the 96-well clear plate (blue wells). **B.** The TC-treated 96-well black plates after JQ1 medium addition (blue wells).

2.7.1.5 Turn the 96-well black plates 90° clockwise. Pipet out 50 µl complete growth medium with NC/4× varying the final concentration of docetaxel/NC from the clear plate (Columns 7/8/10/11, Lines B to F), and then add this into the black plate (Lines B to G, Columns 2-11) with a multichannel pipette(Figure 14, grey and orange wells from A to B).

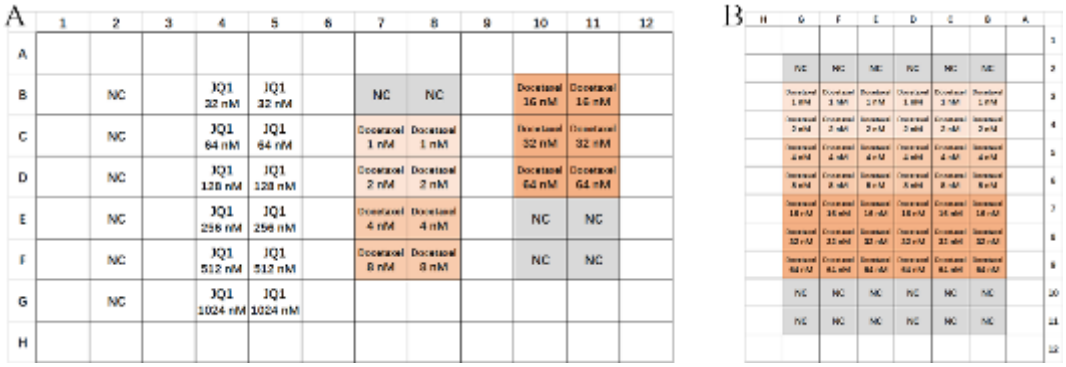

Figure 14. Docetaxel medium addition from the clear plate to the wells with combination treatment/NC in TC-treated black plate.

A. The complete growth medium with NC/4× varying the final concentration of docetaxel/NC in the 96-well clear plate (grey and orange wells). **B.** The TC-treated 96-well black plate after NC/docetaxel medium addition (grey and orange wells).

2.7.1.6 Turn the 96-well black plates 90° counterclockwise. Pipet out 50 µl complete growth medium with 4× varying final concentration of docetaxel from the clear plate (Columns 7/8, Lines C to F and Columns 10/11, Lines B to C), and then add this into the black plate (Columns 11, Lines B to G) with a multichannel pipette (Figure 15, orange wells from A to B).

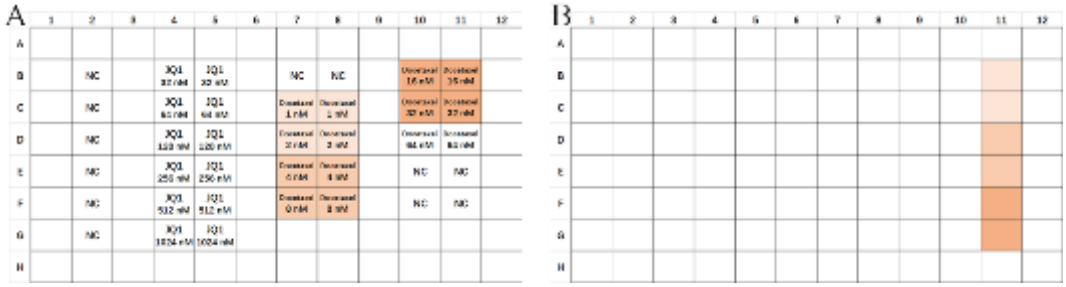

Figure 15. Docetaxel medium addition from clear plate to the wells with docetaxel alone in TC-treated black plate.

A. The complete growth medium with 4× varying final concentration of docetaxel in the 96-well clear plate (orange wells). **B.** The TC-treated 96-well black plates after docetaxel medium addition (orange wells).

2.7.1.7 Pipet out 50 µl complete growth medium without any drugs (NC) from the clear plates (Columns 2, Lines B to G), and then add this into the black plate (Columns 10, Lines B to G) with a multichannel pipette (Figure 16, grey wells from A to B).

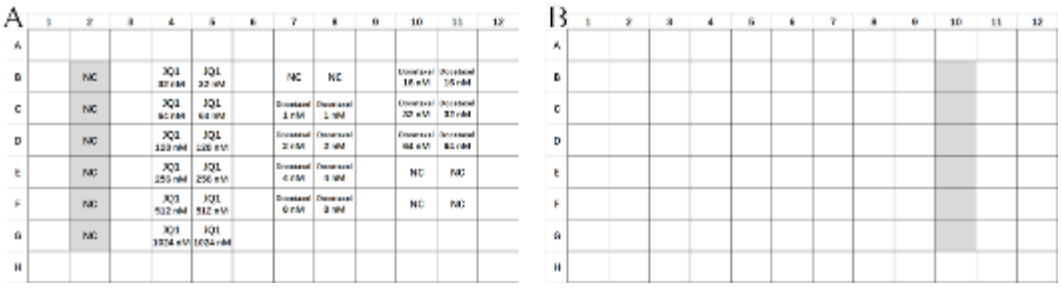

Figure 16. Complete growth medium addition from clear plate to the wells with docetaxel alone in TC-treated black plate.

A. The NC complete growth medium in the 96-well clear plate (grey wells). **B.** The TC-treated 96-well black plates after medium addition (grey wells).

2.7.1.8 Culture the LNCaP cells for 5 days.

2.7.1.9 CellTiter Glo assay (2D, Subheading 2.8.1).

2.7.2 3D LNCaP spheroid formation experiments:

2.7.2.1 The LNCaP spheroid formation when exposed to JQ1/docetaxel alone:

2.7.2.1.1 The 2D cultured LNCaP cells were collected from the cell flasks and embedded in Matrigel then plated into the 24-well plates (repeat Subheadings 2.3.1.1.1.1 - 2.3.1.1.1.10).

2.7.2.1.2 Prepare a varying final concentration of docetaxel (0.25 nM, 0.5 nM, 1 nM, 2 nM, and 4 nM) and JQ1(8 nM, 16 nM, 32 nM, 64 nM, 128 nM, and 256 nM). Then gently add the prewarmed complete growth medium into each well (1ml/well), while the negative control contains no drug at all. Refresh the complete growth medium every three days.

2.7.2.1.3 Culture for 2 weeks. The spheroids were checked with a microscope twice a week and the spheroids' growth were recorded every week.

2.7.2.2 The LNCaP spheroid formation when exposed to JQ1/docetaxel alone or combination:

2.7.2.2.1 The 2D cultured LNCaP cells were collected from the cell flasks and embedded in Matrigel then plated into the 24-well plates (repeat Subheadings 2.3.1.1.1.1 - 2.3.1.1.1.10).

2.7.2.2.2 Prepare 4 kinds of complete growth medium (NC, 0.25 nM docetaxel, 128 nM JQ1, and 0.25 nM docetaxel + 128 nM JQ1). Then gently add the prewarmed complete growth medium into each well (1 ml/well).

2.7.2.2.3 Culture for 2 weeks. The spheroids were checked with a microscope twice a week and the spheroids' growth were recorded every week.

2.7.3 Cell viability detection following JQ1/docetaxel treatment alone or combination treatment

2.7.3.1 2D cell viability detection following JQ1/docetaxel treatment alone or combination treatment:

2.7.3.1.1 The 2D cultured LNCaP cells were collected and seeded into the 96-well TC-treated black microplates (repeat Subheadings 2.6.2.1 - 2.6.2.4).

2.7.3.1.2 Place the plates in the CO_2 incubator for 48 hours.

2.7.3.1.3 Add 100 µl new complete growth medium with 2× docetaxel/JQ1 final concentrations as described below, while the negative control contains no docetaxel at all.

Final docetaxel concentrations in the plates:

Docetaxel treatment: 2 nM.

JQ1 treatment: 128 nM.

Combination treatment: Docetaxel: 2 nM + JQ1: 128 nM.

2.7.3.1.4 Culture the LNCaP cells for 5 days.

2.7.3.1.5 CellTiter Glo assay (2D, Subheading 2.8.1).

2.7.3.2 3D cell viability detection following JQ1/docetaxel treatment alone or combination treatment:

2.7.3.2.1 The 2D LNCaP cells were collected and seeded into the 96-well TC-treated black microplates (repeat Subheadings 2.6.3.1 – 2.6.3.2).

2.7.3.2.2 Place the plates in the CO_2 incubator for 48 hours.

2.7.3.2.3 Pipet out 100 µl complete growth medium, and then add 100 µl new complete growth medium with the 2× docetaxel / JQ1 final concentrations as described below, while the negative control contains no docetaxel at all.

Final docetaxel concentrations in the plates:

Docetaxel treatment: 2 nM.

JQ1 treatment: 128 nM.

Combination treatment: Docetaxel: 2 nM + JQ1: 128 nM.

2.7.3.2.4 Culture the LNCaP cells for 5 days.

2.7.3.2.5 CellTiter Glo assay (3D, Subheading 2.8.2).

2.8 Cell viability detection by CellTiter Glo assay: The cell viability of the treated LNCaP cells/spheroids was measured using CellTiter-Glo® Luminescent Cell Viability Assay.

2.8.1 CellTiter Glo assay for 2D cultured cells and spheroids in spheroid microplates.

2.8.1.1 Having stored the CellTiter Glo reagents at -20℃, thaw and equilibrate the reagents to room temperature.

2.8.1.2 Mix the powder and the solvent and store at 4℃.

2.8.1.3 Equilibrate the CellTiter Glo reagents to room temperature for 2 hours.

2.8.1.4 Remove 100 µl supernatant from each well carefully (100 µl left).

2.8.1.5 Add 100 µl CellTiter Glo reagents and wrap the plate in aluminum foil.

2.8.1.6 Read the plates.

2.8.2 3D embedded cell/spheroid CellTiter Glo assay.

2.8.1.1 Repeat Subheadings 2.8.1.1 - 2.8.1.5.

2.8.1.2 Shake the plates for 1 hour at 300 rpm.

2.8.1.3 Equilibrate plate for 1 hour in the incubator (remove bubbles if necessary with a needle).

2.8.1.4 Read the plates.

2.9 Statistics

2.9.1 The normality tests of LNCaP cell/spheroid size were analyzed with GraphPad Prism 8 software, including frequency distribution and Gaussian distribution (D'Agostino-Pearson omnibus normality test).

2.9.2 The line charts and violin plots of spheroid parameters (d_{max}, spheroid volume, and lg volume) were plotted with GraphPad Prism 8 software.

2.9.3 The IC50 values and R^2 of the drug testing experiments were analyzed with GraphPad Prism 8 software, while the maximum inhibitions were averaged according to the last three cell viabilities at the 2^{nd} plateau phase with Excel 2016.

2.9.4 The unpaired t-tests of the spheroid formation parameters (d_{max}, lg volume) were also analyzed with GraphPad Prism 8 software.

3 Results

3.1 Evaluation of LNCaP cell/spheroid growth in medium with variable FBS concentrations

We first evaluated the LNCaP cell/spheroid growth in different FBS concentrations (2%, 5%, 7.5% and 10%) for 18 days. We found that no living cells/spheroids could be observed after the tenth day (Figure 17. A3), when the LNCaP cells/spheroids were cultured in medium with 2% FBS. However, for the LNCaP cells/spheroids cultured in the medium with 5% or 7.5% FBS, the timepoint for no living cells/spheroids being observed was the fourteenth day (Figure 17. B4/C4). With the LNCaP cells/spheroids cultured in medium with 10% FBS, living cells/spheroids were observed, and the size of the cells/spheroids grew over time (Figure 17. D1-D5). These results show that lower FBS concentrations are not suitable for the embedded cultured LNCaP spheroids' survival and growth. Therefore, all our subsequent experiments based on 3D cultured LNCaP cells/spheroids were maintained in RPMI + 10% FBS + 1% PS.

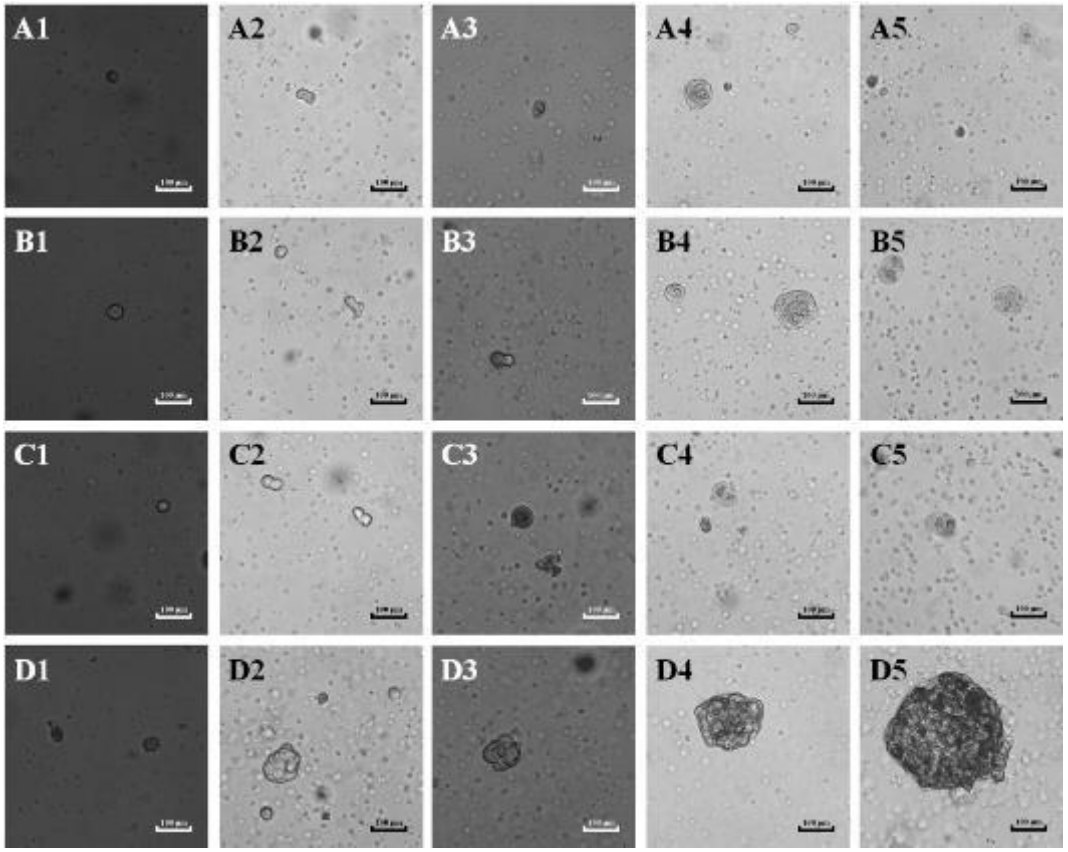

Figure 17. Representative images of LNCaP cells/spheroids cultured in varying FBS concentration.

A1-A5: Images of LNCaP cells/spheroids cultured in 2% FBS on the 3rd, 7th, 10th, 14th, 18th days; **B1-B5:** Images of LNCaP cells/spheroids cultured in 5% FBS on the 3rd, 7th, 10th, 14th, 18th days; **C1-C5:** Images of LNCaP cells/spheroids cultured in 7.5% FBS on the 3rd, 7th, 10th,

14th, 18th days; **D1-D5:** Images of LNCaP cells/spheroids cultured in 10% FBS on the 3rd, 7th, 10th, 14th, 18th days.

3.2 Formation inconsistency of LNCaP spheroids in Matrigel

Single LNCaP cells were plated into the TC-treated 96-well black microplates according to the 3D embedded cell culture protocols (Subheading 2.3.1.1.1), and morphological changes from single cells to spheroids were observed under the microscope over time. To clarify the consistency of LNCaP spheroid sizes, we collected three parameters (long diameter/d_{max}, spheroid volume, and lg volume) at different time points (2, 4, 7, 10, 12, 14, 16, 18, and 21 days). Normality tests were performed to determine if the size of LNCaP spheroids was normally distributed.

3.2.1 Formation inconsistency of LNCaP spheroids based on major diameter (d_{max}): For both LNCaP cells/spheroids, we measured two diameters (d_{max}: major diameter, d_{min}: minor diameter), of which the d_{max} has previously been shown to be a useful parameter to represent the spheroids' size(Shahi Thakuri et al., 2016). We chose to use a histogram (Figure 18) to show the distribution of spheroids d_{max}. Frequency distribution and D'Agostino-Pearson omnibus normality tests were performed in GraphPad Prism 8 to determine whether the d_{max} fitted to a normal distribution. We found that all the d_{max} data at different time points passed the normality test ($P > 0.05$), in which the p-value of the tenth day was 0.0547 (relatively close to 0.05) (Table 4).

Day	2	4	7	10	12	14	16	18	21
D'Agostino-Pearson omnibus (K2)	1.01	1.95	0.8864	5.814	1.059	3.379	2.508	0.5105	1.252
p-value	0.6034	0.3773	0.642	0.0547	0.5888	0.1846	0.2853	0.7747	0.5347
Passed normality test (alpha=0.05)?	Yes	Yes	Yes	Yes	Yes	Yes	Yes	Yes	Yes

Table 4. Results of the normality tests for LNCaP cells/spheroids at different time points (d_{max}).

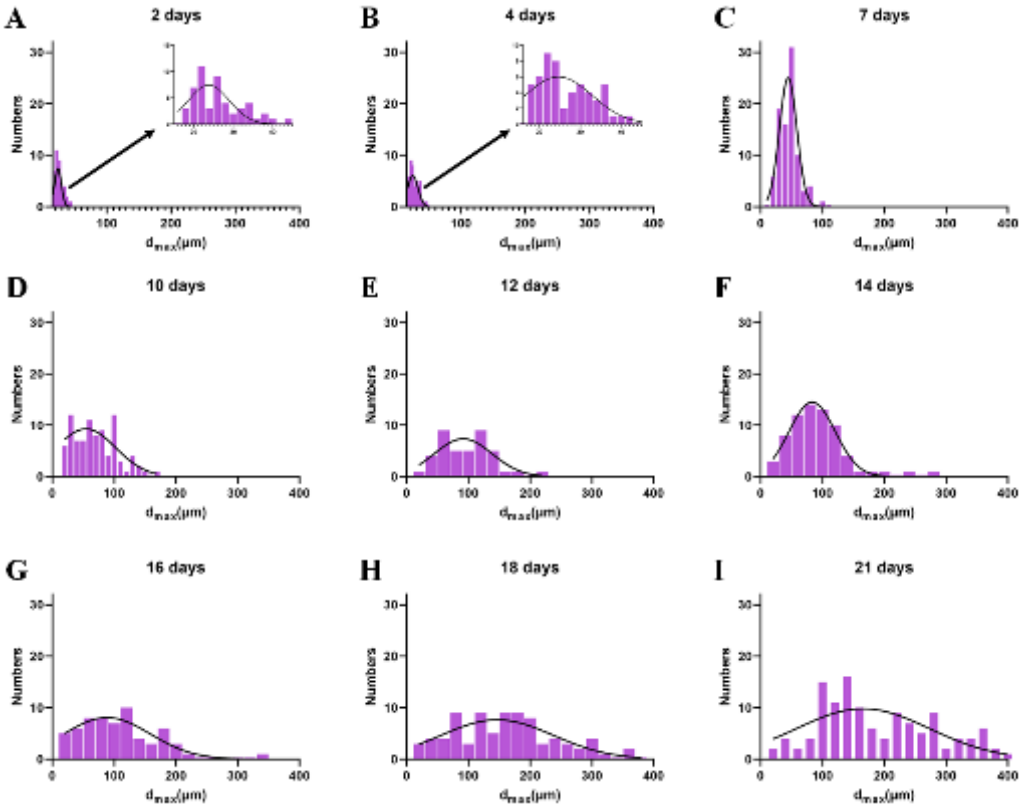

Figure 18. Histogram of d_{max} of LNCaP spheroids from day 2 to day 21.

3.2.2 Formation inconsistency of LNCaP spheroids based on spheroid volume: The volume is another parameter representing the size of LNCaP spheroids. The LNCaP spheroid volume can be calculated as $V = \pi \times d_{max} \times d_{min}^2 / 6$, according to the literature(Ballangrud *et al.*, 1999). We also used the histogram (Figure 19) to show the distribution of spheroid volume. Frequency distribution and D'Agostino-Pearson omnibus normality tests showed that the data at days 10, 16, 18, and 21 did not pass the normality test ($P < 0.05$) (Table 5).

Day	2	4	7	10	12	14	16	18	21
D'Agostino-Pearson omnibus (K2)	0.1069	0.3103	2.676	*	0.7963	5.601	7.453	6.231	*
p-value	0.948	0.8563	0.2624	*	0.6715	0.0608	0.0241	0.0443	*
Passed normality test (alpha=0.05)?	Yes	Yes	Yes	No	Yes	Yes	No	No	No

Table 5. Results of the normality tests for LNCaP cells/spheroids at different time points (volume).

*: Gaussian was interrupted in GraphPad Prism 8, which means the data simply does not fit the model (according to the GraphPad Prism 8 User Guide: https://www.graphpad.com/guides/prism/8/curve-fitting/reg_analysischeck_nonlin_interrupted.htm?q=interrupted).

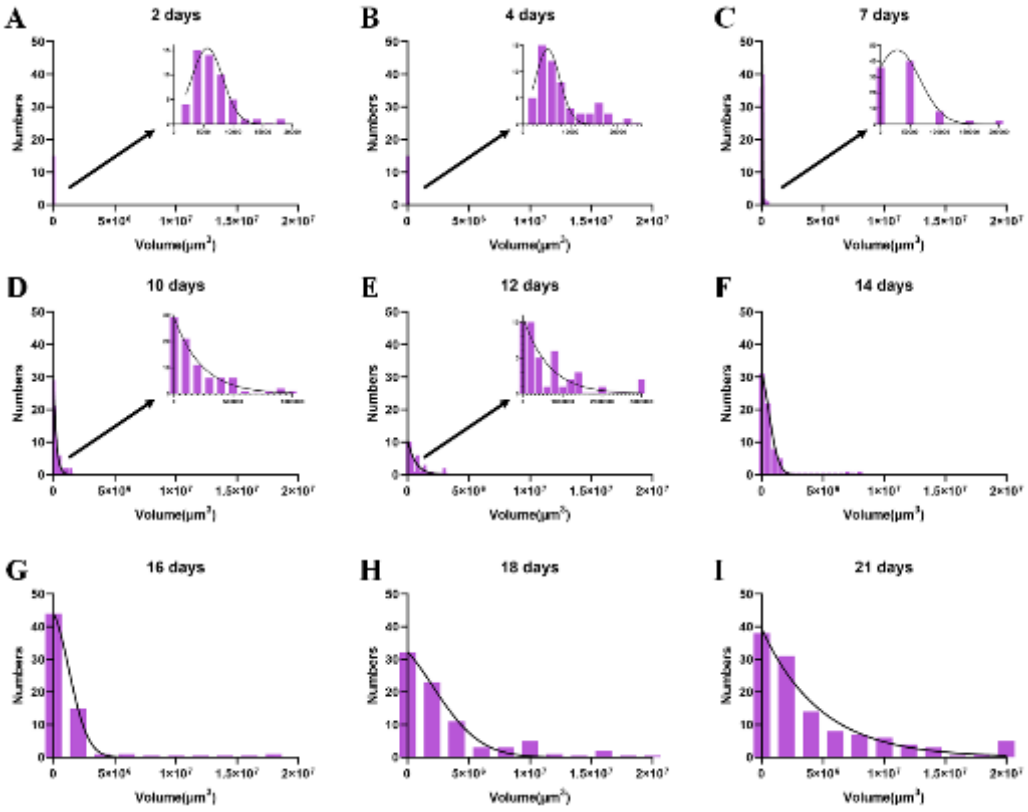

Figure 19. Histogram of the volume of LNCaP spheroids from day 2 to day 21.

3.2.3 Formation inconsistency of LNCaP spheroids based on spheroid lg volume: The results above show that the LNCaP spheroid volumes at some time points did not pass the normality test, in particular when the spheroids were big. One explanation might be the long span of spheroid volume by time. Therefore, we performed frequency distribution and D'Agostino-Pearson omnibus normality tests to evaluate whether the lg volume (log_{10} volume) values fit the normal distribution (Figure 20). Almost all the lg volume of the LNCaP spheroids passed the normality test at different time points, except day 2 and day 18.

Day	**2**	**4**	**7**	**10**	**12**	**14**	**16**	**18**	**21**
D'Agostino-Pearson omnibus (K2)	7.852	3.551	0.8613	0.716	0.4944	2.397	1.387	10.02	0.3856
p-value	0.0197	0.1694	0.6501	0.6991	0.781	0.3017	0.4998	0.0067	0.8246
Passed normality test (alpha=0.05)?	No	Yes	Yes	Yes	Yes	Yes	Yes	No	Yes

Table 6. Results of the normality tests for LNCaP cells/spheroids at different time points (lg volume).

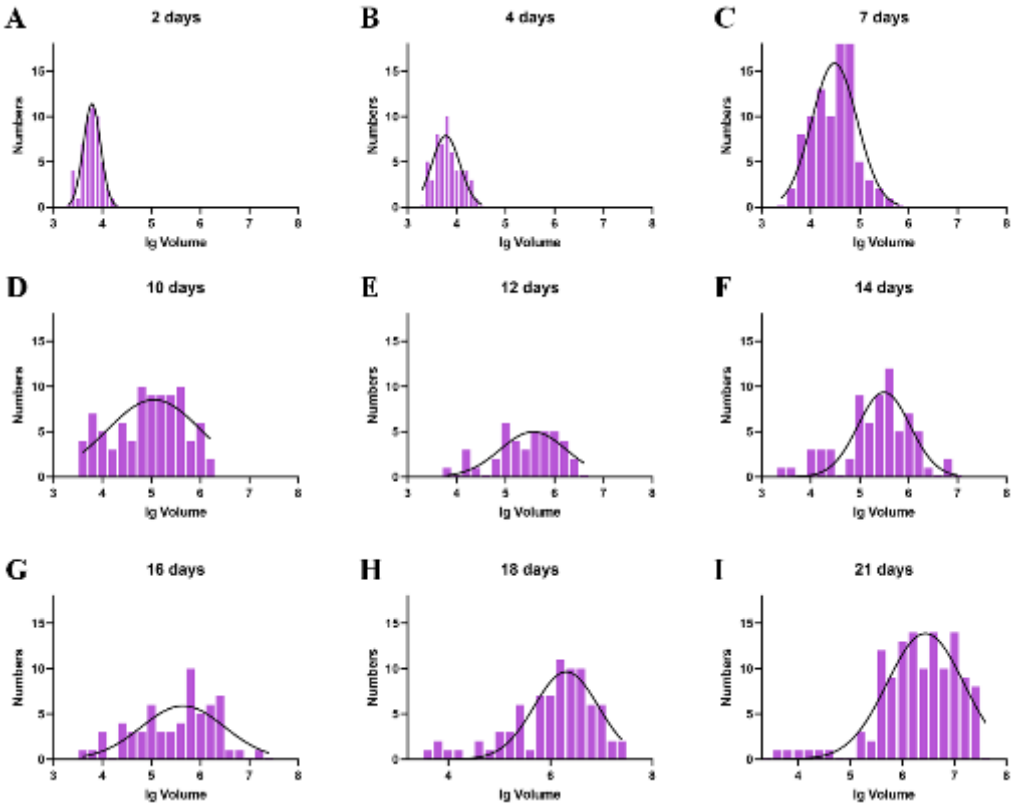

Figure 20. Histogram of lg volume of LNCaP spheroids from day 2 to day 21.

3.2.4 Variations in the size of LNCaP cell/spheroid distribution

According to the results above, we found that the peak of each parameter's distribution moves from the left to the right (small size to large size) over time. Almost all the cells were single initially, and most of them became spheroids at day 21. The difference between the volumes of the biggest and smallest LNCaP spheroids was 7.241 times (2377 vs. 17214 μm^3) on the second day, and 8433 times (3730 vs. 31465801 μm^3) on the twenty-first day. Single LNCaP cells could still be observed on day 21 (Figure 21. D), even though the percentage of single cells was relatively low. For the three parameters we used to describe the spheroid size, the mean value of d_{max} for LNCaP spheroids cultured at day 21 became 6.587 times than that of single LNCaP cells (168.5 vs. 25.58 μm). The difference between the lg volume of spheroids was only 1.681 times (6.360 vs. 3.784). The frequency distributions and D'Agostino-Pearson omnibus normality tests described above showed that mostly d_{max} and lg volume were normally distributed, while 4/9 of the data on the spheroid volume did not pass the normality tests. Based on the above results, we chose each parameter's median to describe the size of the LNCaP cells/spheroids in the following evaluation of LNCaP cell/spheroid growth kinetics.

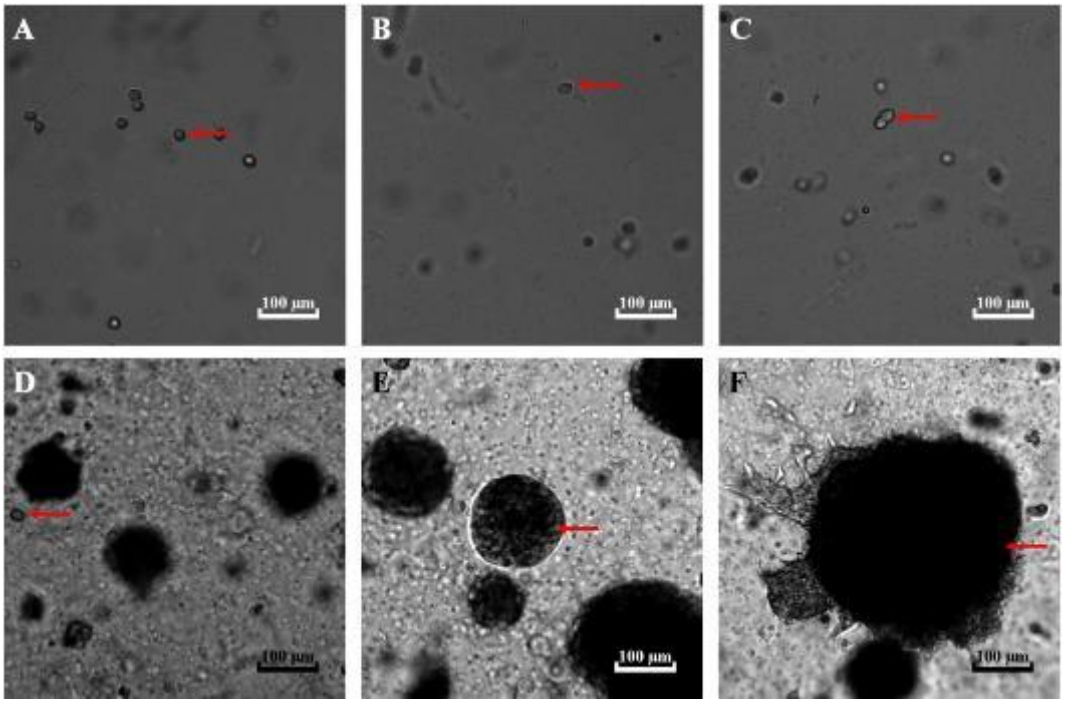

Figure 21. Images of LNCaP cells and spheroids on day 2 and day 21.

A. Image of the smallest LNCaP cell on day 2 (red arrow). **B.** Image of the median LNCaP cell on day 2 (red arrow). **C.** Image of the biggest LNCaP cell on day 2 (red arrow). **D.** Image of the smallest LNCaP cell and spheroid on the day 21 (red arrow, still single cell). **E.** Image of the median LNCaP cell and spheroid on day 21 (red arrow). **F.** Image of the biggest LNCaP cell and spheroid on the day 21 (red arrow).

3.3 Growth kinetics of 3D-embedded LNCaP cells/spheroids

In contrast to the proliferation of 2D cultured cells, the growth of LNCaP cells/spheroids in Matrigel was evaluated as increases in spheroid size. To show the continuous changes of the LNCaP cells/spheroids, we used three parameters (long diameter/d_{max}, spheroid volume, and lg volume) to describe the size of the LNCaP spheroids. The line chart of each parameter was used to show the growth curves, while the violin plots also showed the frequency distribution. Instead of the mean, the median was used to describe the size of the LNCaP spheroids, since not all data were normally distributed.

3.3.1 Growth kinetics of 3D-embedded LNCaP cells/spheroids based on d_{max}: As shown in Figure 22A (the line chart of d_{max}), Figure 22B (the violin plots of d_{max}), and the cell/spheroid images below, the LNCaP spheroids were initiated from single LNCaP cells, and kept single at days 2 and 4. The formation of LNCaP spheroids could be observed from the seventh day. The images represent the median-sized spheroids at various time points.

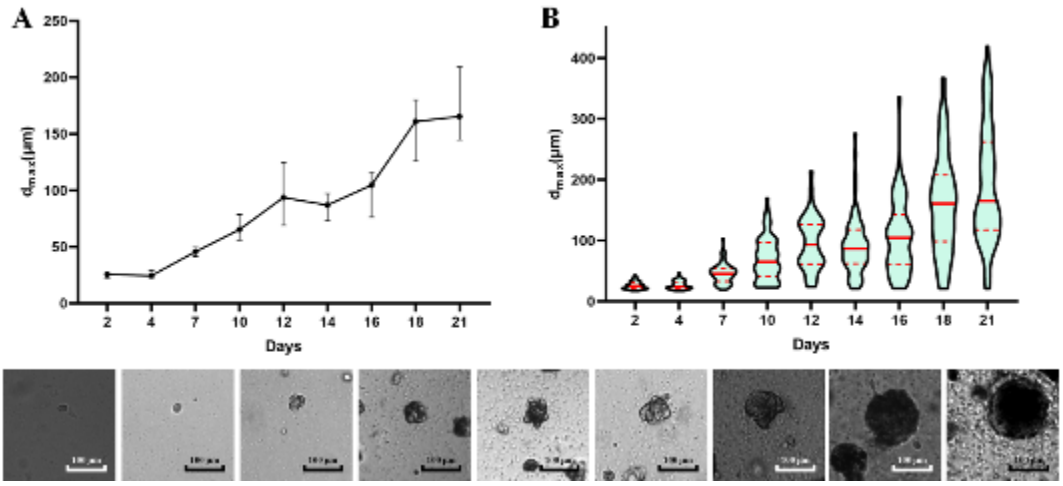

Figure 22. Growth kinetics of 3D embedded LNCaP cells/spheroids (d_{max}).

3.3.2 Growth kinetics of 3D-embedded LNCaP cells/spheroids based on spheroid volume: The trends of LNCaP cell/spheroid volume were similar to the d_{max}. However, the line chart (Figure 23. A) and violin plots (Figure 23. B) could not display the cell/spheroid size initially since the volume span was much greater than the d_{max}, resulting in volumes too close to the X-axis.

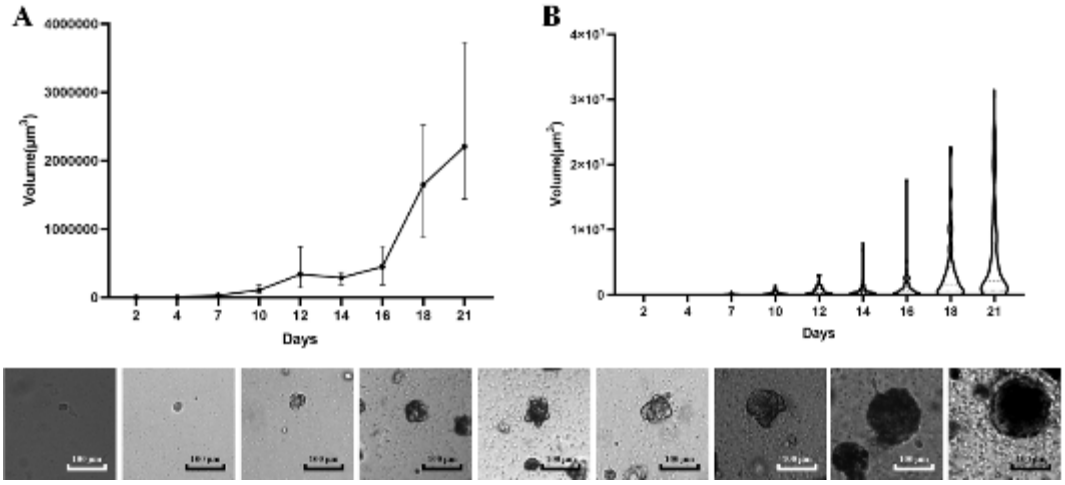

Figure 23. Growth kinetics of 3D embedded LNCaP cells/spheroids (volume).

3.3.3 Growth kinetics of 3D-embedded LNCaP cells/spheroids based on spheroid lg volume: According to the results above, the volume could not display the growth kinetics effectively. Therefore, we next evaluated the lg volume of the LNCaP cells/spheroids to show the growth kinetics. The lg volume seems to be a useful parameter to display the LNCaP cells/spheroids and for the evaluation of growth kinetics (Figure 24).

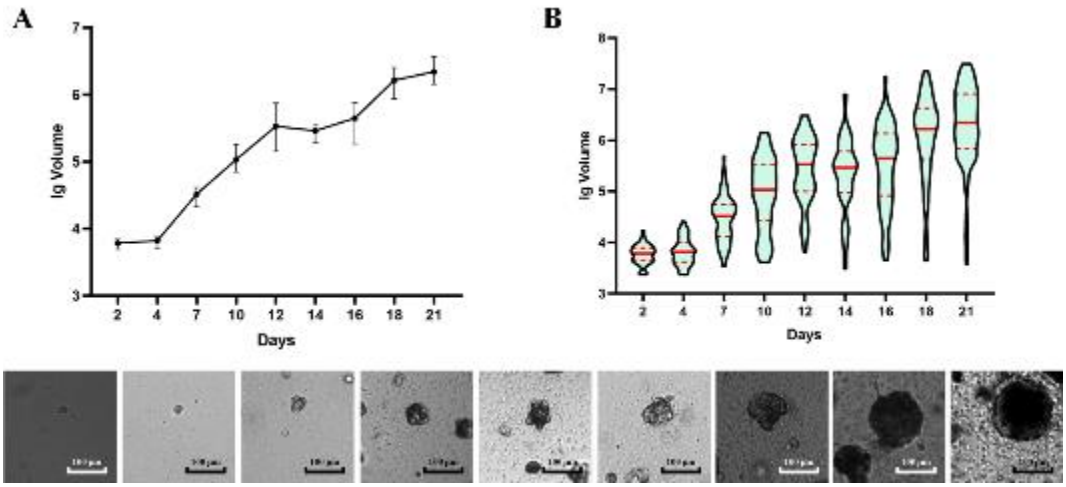

Figure 24. Growth kinetics of 3D embedded LNCaP cells/spheroids (lg volume).

3.4 Evaluation of Matrigel stability according to the images under the microscope

Most of our subsequent 3D drug testing experiments were based on LNCaP spheroids cultured for 2-3 weeks in Matrigel. Before the drug testing experiments, we performed a long term 3D-embedded LNCaP spheroid culture experiment to evaluate the stability of Matrigel in the TC-treated 96-well black microplates. The LNCaP cells/spheroids in Matrigel were checked daily with a microscope, and we found that the Matrigel was not stable after day 21. Some concaves were observed in the Matrigel, where some spheroids were previously localized (Figure 25. C). We also acquired an image that contained the concave and escaped spheroids (Figure 25. D, yellow arrow). The formation of the concaves might result from two factors: ① The Matrigel was not stable enough for a long-term culturing. ② The space for LNCaP spheroids, which accommodated single LNCaP cells when plating, could not effectively accommodate the large-sized spheroids. Therefore, culturing beyond three weeks might not be suitable for LNCaP spheroid experiments.

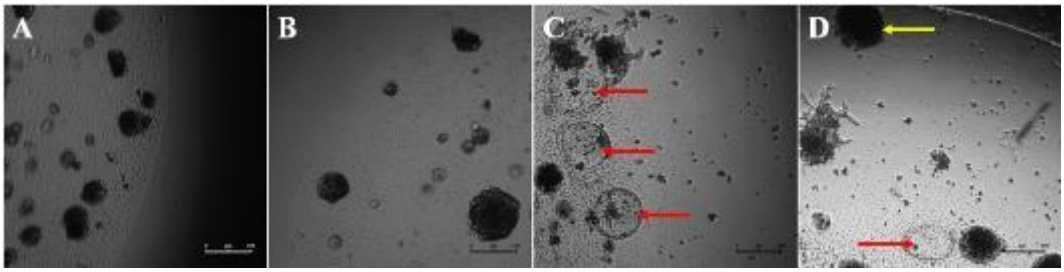

Figure 25. Representative images of Matrigel from 1 week to 3 weeks.

A: Image of Matrigel at 1 week of culture. **B:** Image of Matrigel after 2 weeks of culture. **C:** Image of Matrigel at 3 weeks of culture: some concaves (red arrow) could be observed. **D:** Image of Matrigel at 3 weeks: the concave (red arrow) and the escaped spheroids (yellow arrow) were observed in the same image.

3.5 Susceptibility of LNCaP cells/spheroids exposed to docetaxel / JQ1 treatment

3.5.1 Evaluation of the LNCaP cell viability exposed to DMSO: CellTiter Glo assays were performed to analyze the LNCaP cell viability exposed to different DMSO concentrations, which represented the DMSO concentrations in the subsequent drug testing experiments (Subheading 2.6.1). We found that DMSO did not significantly inhibit the cell viability in concentrations ranging from 5×10^{-7} % to 5×10^{-2} % (Figure 26).

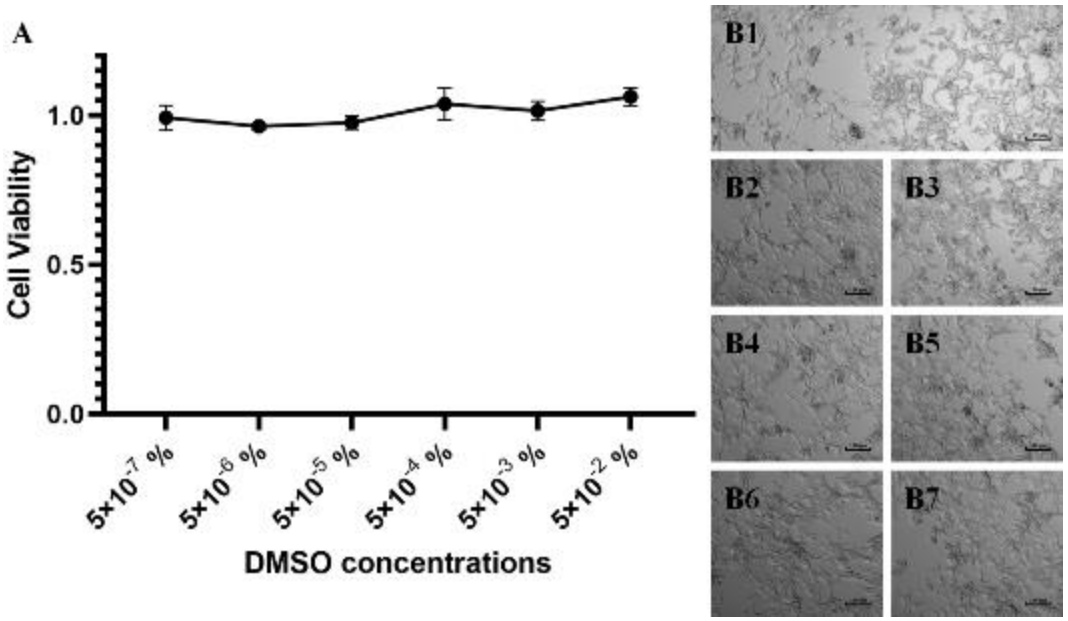

Figure 26. LNCaP cell viability exposed to DMSO.

A. LNCaP cell viability exposed to different DMSO concentrations. **B1-B7.** Images of LNCaP cells exposed to different DMSO concentrations for 5 days: B1: 0 (NC), B2: 5×10^{-7} %, B3: 5×10^{-6} %, B4: 5×10^{-5} %, B5: 5×10^{-4} %, B6: 5×10^{-3} %, and B7: 5×10^{-2} %.

3.5.2 Susceptibility of 2D/3D LNCaP cells exposed to docetaxel / JQ1 treatment

According to our previous results (Subheading 3.3.1), the LNCaP cells were still single in Matrigel when cultured for two days. We first carried out the experiments to compare any significant differences between the drug testing experiments based on 2D-cultured LNCaP cells and 3D-embedded cultured LNCaP cells.

3.5.2.1 Susceptibility of 2D/3D LNCaP cells exposed to docetaxel treatment

The drug testing experiments based on 2D- and 3D-cultured LNCaP cells were performed in the same plates, and all tests were performed in triplicate. The IC50 values and R^2 were analyzed using GraphPad Prism 8 software, and the maximum inhibitions were averaged in Excel 2016 according to the last three cell viabilities at the second plateau phase. All IC50

values of 3D-cultured LNCaP cells were slightly higher than those of corresponding 2D-cultured LNCaP cells (Figure 27. G). The images of the cells showed that the proliferation of 2D-cultured cells was significantly inhibited by docetaxel at high concentrations, while the inhibition of 3D-cultured cells was reflected both in cell numbers and spheroid sizes (Figure 28). There were almost no living 2D-cultured cells after five days of exposure to 32nM docetaxel, while some living 3D-cultured cells could still be observed. In the IC50 curves, the second plateau phase of the 3D-cultured cells was much higher than that of the 2D-cultured cells, and the IC50 curves of the 3D-cultured cells were much flatter than those of the 2D-cultured cells. We additionally analyzed the maximum inhibition (the mean values of the cell inhibitions at the highest three concentrations at the second plateau phase) and R^2 (quantifying the goodness of fit) for each IC50 curve. The maximum inhibition values of the 3D drug testing experiments were lower than corresponding 2D drug testing experiments (Figure 27. H), and the R^2 values of 3D drug testing experiments were also lower (Figure 27. I).

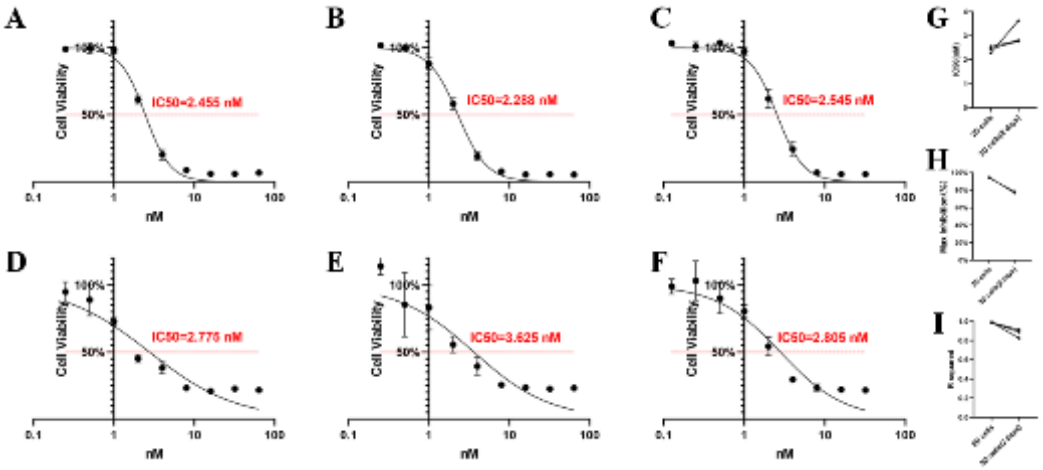

Figure 27. Susceptibility of 2D/3D LNCaP cells exposed to docetaxel treatment.

A-C. Drug testing experiments on 2D cultured LNCaP cells exposed to varying docetaxel concentrations: the IC50 values were 2.455 nM, 2.288 nM, and 2.545 nM. **D-F.** Drug testing experiments of 3D cultured LNCaP cells exposed to varying docetaxel concentrations: the IC50 values were 2.775 nM, 3.625 nM, and 2.805 nM. **G.** Results of the permutation test of IC50. **H.** Maximum inhibition values. **I.** R-squared values.

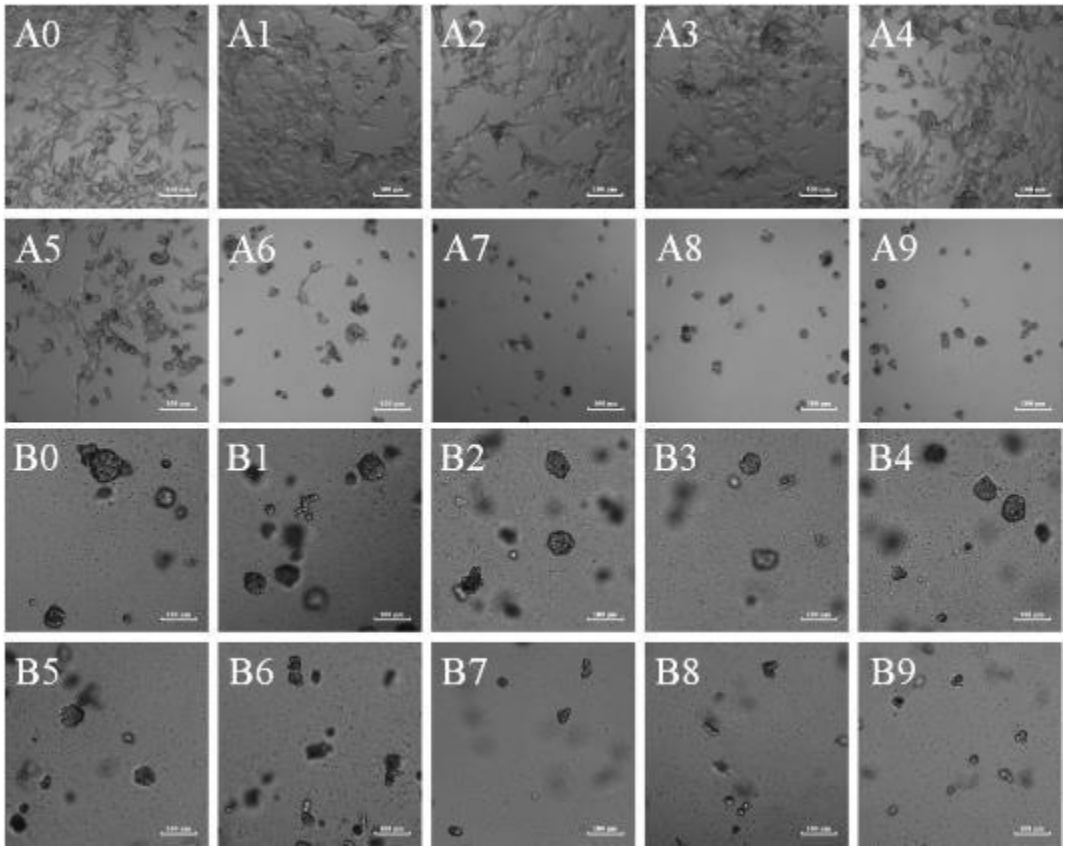

Figure 28. Images of drug testing experiments based on 2D/3D LNCaP cells exposed to docetaxel treatment.

A0-A9. Images of drug testing experiments based on 2D-cultured LNCaP cells exposed to varying docetaxel concentrations. A0: Image of negative control without docetaxel; A1-A9: Images of the LNCaP cells exposed to varying docetaxel concentrations for five days (0.125 nM, 0.25 nM, 0.5 nM, 1 nM, 2 nM, 4 nM, 8 nM, 16 nM, and 32 nM). **B0-B9.** Images of drug testing experiments based on 3D-cultured LNCaP cells exposed to varying docetaxel concentrations. B0: Image of negative control without docetaxel; B1-B9: Images of the LNCaP cells exposed to varying docetaxel concentrations for five days (0.125 nM, 0.25 nM, 0.5 nM, 1 nM, 2 nM, 4 nM, 8 nM, 16 nM, and 32 nM).

3.5.2.2 Susceptibility of 2D/3D LNCaP cells exposed to JQ1 treatment

The protocols of JQ1 drug testing experiments based on 2D- and 3D-cultured LNCaP cells were equal to the protocols described above for docetaxel. The differences in IC50 values between 2D and 3D LNCaP cells were not significant (Figure 29. A-F). The cell images also showed that JQ1 significantly inhibited the proliferation of 2D-cultured cells at high concentrations (Figure 30. A0-A9). In contrast, the inhibition of 3D-cultured cells was reflected in cell numbers and spheroid sizes (Figure 30. B0-B9). We did not describe the maximum inhibitions since the second flatforms of the JQ1 drug testing experiments were not complete with the highest JQ1

concentrations. We also found that the R^2 of 2D drug testing experiments were higher than in corresponding 3D drug testing experiments (Figure 29. H).

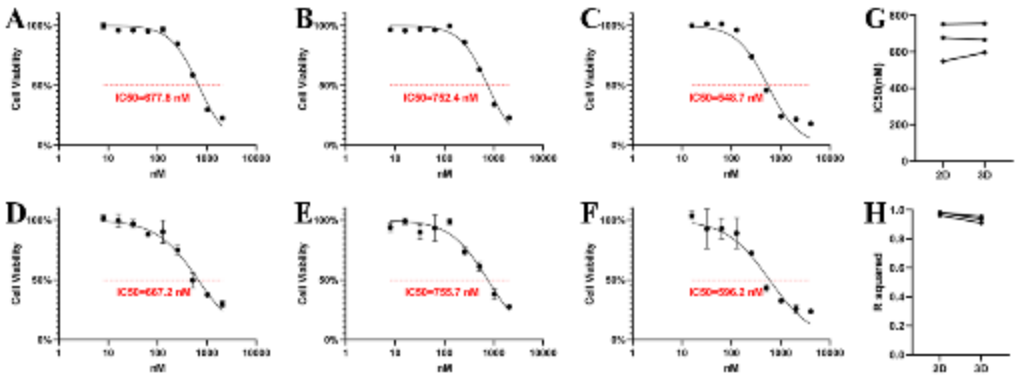

Figure 29. Susceptibility of 2D/3D LNCaP cells exposed to JQ1 treatment.

A-C. Drug testing experiments on 2D-cultured LNCaP cells exposed to varying JQ1 concentrations: the IC50 values were 677.8 nM, 752.4 nM, and 548.7 nM. **D-F.** Drug testing experiments on 3D-cultured LNCaP cells exposed to varying JQ1 concentrations: the IC50 values were 667.2 nM, 755.7 nM and 569.2 nM. **G.** IC50 values. **H.** R-squared values.

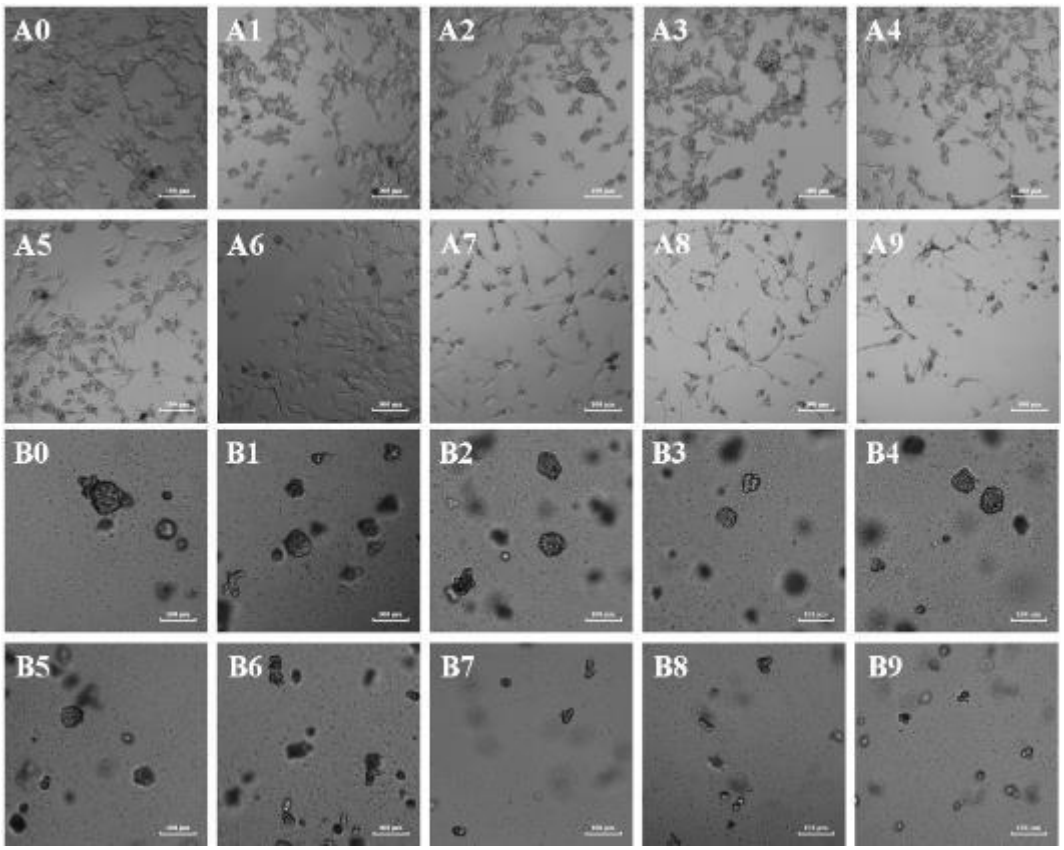

Figure 30. Images of drug testing experiments based on 2D/3D LNCaP cells exposed to JQ1 treatment.

A0-A9. Images of drug testing experiments based on 2D-cultured LNCaP cells exposed to varying JQ1 concentrations: A0. Image of negative control without JQ1; A1-A9: Images of the LNCaP cells exposed to varying JQ1 concentrations for five days (16 nM, 32 nM, 64 nM, 128 nM, 256 nM, 512 nM, 1024 nM, 2048 nM, and 4096 nM). **B0-B9.** Images of drug testing experiments based on 3D-cultured LNCaP cells exposed to varying JQ1 concentrations: B0: Image of negative control without JQ1; B1-B9: Images of the LNCaP cells exposed to varying JQ1 concentrations for five days (16 nM, 32 nM, 64 nM, 128 nM, 256 nM, 512 nM, 1024 nM, 2048 nM, and 4096 nM).

3.5.3 Susceptibility of embedded cultured LNCaP spheroid aliquots exposed to docetaxel treatment

In some previous studies(Devarasetty *et al.*, 2017; Skardal *et al.*, 2015), aliquots of organoids were seeded into the microplates at the beginning of the drug testing experiment to ensure similar cell numbers in each well while plating. We also performed this protocol, based on embedded cultured LNCaP spheroids, which is described in Subheading 2.6.5. We found that the numbers and sizes of LNCaP spheroids were significantly unequal before docetaxel addition (Figure 31. B1-B6), and the cell viability did not fit the IC50 curve (R^2=0.2957). The standard deviation (SD) of this curve was much higher than the SD of the 2D and 3D LNCaP cell drug testing experiments described above and the spheroid drug testing experiments described below (Figure 31. A). The IC50 values were much lower than the other drug testing experiments based on LNCaP spheroids described below. Based on these results, we decided that the protocol based on the aliquots of LNCaP spheroids embedded in Matrigel was not the right choice for LNCaP spheroid drug testing.

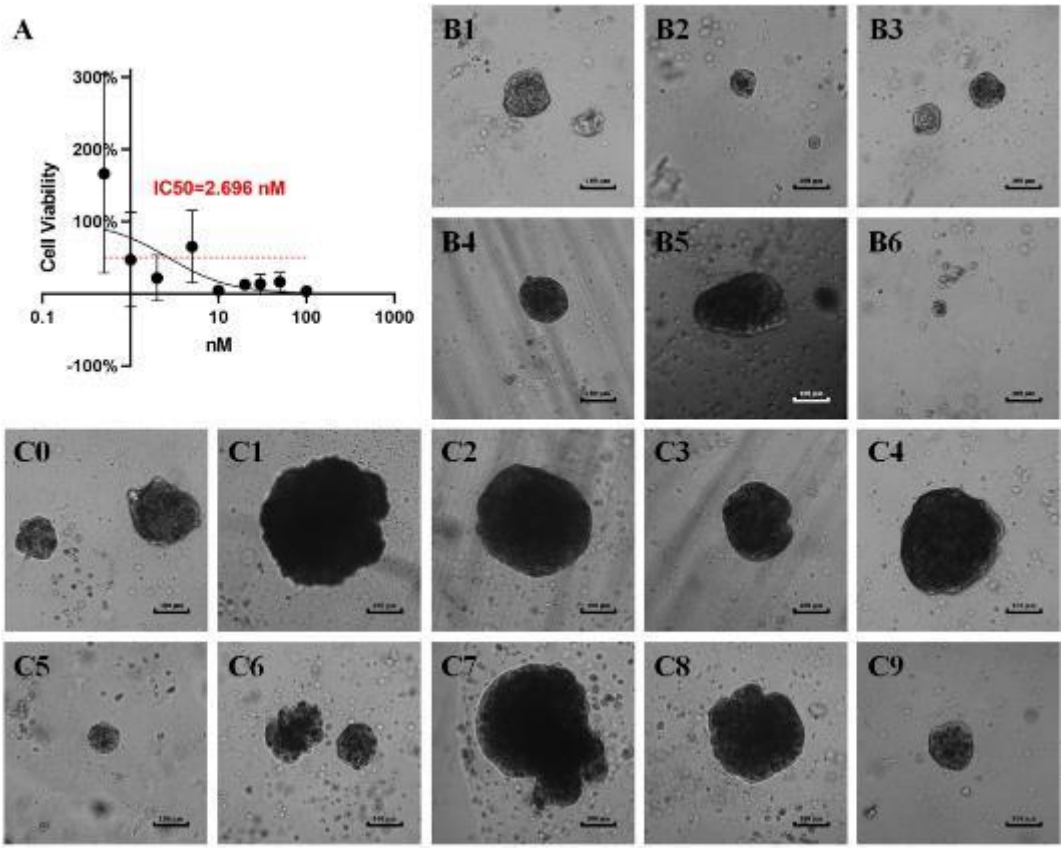

Figure 31. Susceptibility of embedded cultured LNCaP spheroid aliquots exposed to docetaxel treatment.

A. IC50 curve of the embedded cultured LNCaP spheroid aliquots exposed to docetaxel treatment: IC50=2.696 nM, R^2=0.2957. **B1-B6.** Images of the LNCaP spheroid aliquots before docetaxel addition. **C0-C9.** Images of drug testing experiments based on embedded cultured LNCaP spheroid aliquots exposed to varying docetaxel concentrations: C0: Image of negative control well without JQ1; C1-C9: Images of the embedded cultured LNCaP spheroid aliquots exposed to varying docetaxel concentrations for 5 days (0.5 nM, 1 nM, 2 nM, 5 nM, 10 nM, 20 nM, 30 nM, 50 nM, and 100 nM).

3.5.4 Susceptibility of LNCaP floating spheroids exposed to docetaxel treatment

Unlike the embedded cultured LNCaP cells/spheroids in TC-treated 96-well microplates, the different-sized spheroids were harvested quicker from the low attachment U-bottom 96-well spheroid microplates based on different cell numbers while plating. We first evaluated the spheroid formation based on different LNCaP cell plating numbers (Subheading 2.3.2 & 2.6.6.1), and then performed the drug testing experiments according to the protocol described in Subheading 2.6.6.2.

3.5.4.1 Evaluation of floating LNCaP spheroid formation based on different cell numbers while plating in spheroid microplates: The images showed that LNCaP spheroids were formed 24 hours after cell plating, and that they grow over time. Regular spheroids were observed in the wells with 312 - 2500 LNCaP cells/well while plating.

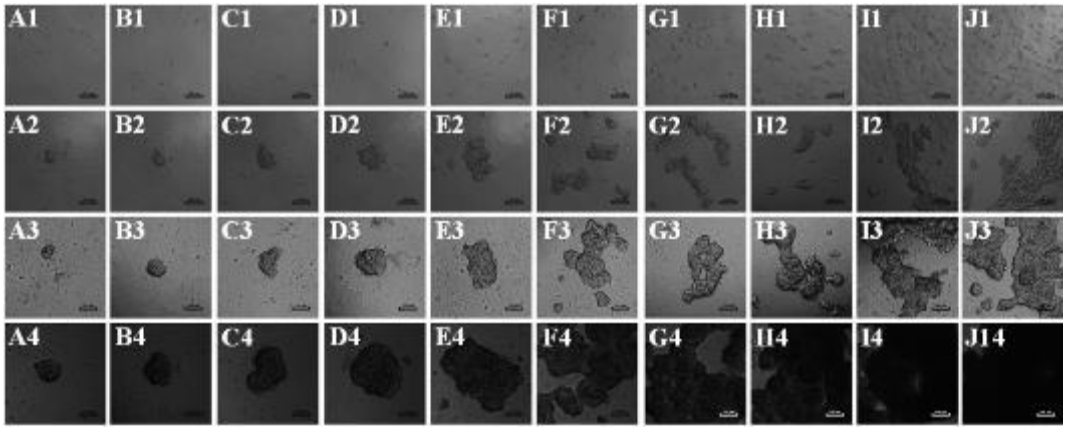

Figure 32. Representative images of LNCaP spheroids in spheroid microplates.

A1-J1. Images of LNCaP cells (cells plating): A1: 312 cells/well, B1: 625 cells/well, C1: 1250 cells/well, D1: 2500 cells/well, F1: 5000 cells/well, G1: 10^4 cells/well, H1: 2×10^4 cells/well, I1: 4×10^4 cells/well, J1: 8×10^4 cells/well, and K1: 16×10^4 cells/well. **A2-J2.** Images of LNCaP spheroids (24 hours after plating): A1: 312 cells/well while plating, B1: 625 cells/well while plating, C1: 1250 cells/well while plating, D1: 2500 cells/well while plating, F1: 5000 cells/well while plating, G1: 10^4 cells/well while plating, H1: 2×10^4 cells/well while plating, I1: 4×10^4 cells/well while plating, J1: 8×10^4 cells/well while plating, and K1: 16×10^4 cells/well while plating. **A3-J3.** Images of LNCaP spheroids (3 days after plating): A1: 312 cells/well while plating, B1: 625 cells/well while plating, C1: 1250 cells/well while plating, D1: 2500 cells/well while plating, F1: 5000 cells/well while plating, G1: 10^4 cells/well while plating, H1: 2×10^4 cells/well while plating, I1: 4×10^4 cells/well while plating, J1: 8×10^4 cells/well while plating, and K1: 16×10^4 cells/well while plating. **A4-J4.** Images of LNCaP spheroids (7 days after plating): A1: 312 cells/well while plating, B1: 625 cells/well while plating, C1: 1250 cells/well while plating, D1: 2500 cells/well while plating, F1: 5000 cells/well while plating, G1: 10^4 cells/well while plating, H1: 2×10^4 cells/well while plating, I1: 4×10^4 cells/well while plating, J1: 8×10^4 cells/well while plating, and K1: 16×10^4 cells/well while plating.

3.5.4.2 Susceptibility of floating LNCaP spheroids of variable size exposed to docetaxel treatment

Two types of LNCaP spheroids were acquired based on 300 and 3000 LNCaP cells in the same spheroid microplates. The experiments were tested in triplicate and showed that the IC50 values

of bigger LNCaP spheroids were higher than those of smaller spheroids. The R^2 values of bigger LNCaP spheroids were 0.9378, 0.6223, and 0.949, and the R^2 values of smaller LNCaP spheroids were 0.7433, 0.9319, and 0.9327. The maximum inhibition of the bigger and smaller LNCaP spheroids in the first and third experiments showed similar results (Figure 33 A vs. D, C vs. F), while the second experiment showed a higher maximum inhibition in the bigger spheroids group (Figure 33 B vs. E). The images showed that the size of the LNCaP spheroids was inhibited by docetaxel treatment, and some LNCaP spheroids exposed to higher docetaxel concentrations (Figure 34) appeared loose and flat, in which case, the size of the spheroids in the images under the microscope were not able to demonstrate the cell viability exactly.

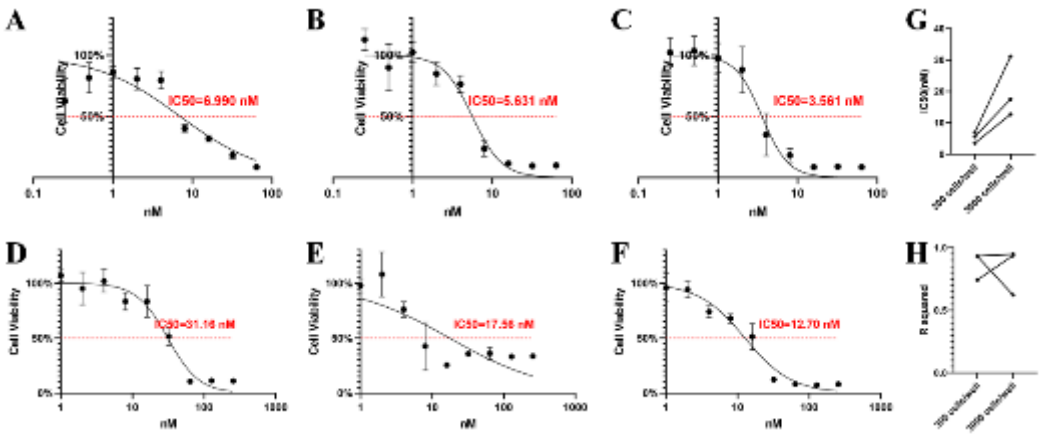

Figure 33. Susceptibility of floating LNCaP spheroids of variable sizes exposed to docetaxel treatment.

A-C. Drug testing experiments on smaller LNCaP spheroids (300 cells/well while plating) exposed to varying docetaxel concentrations: the IC50 values were 6.990 nM, 5.631 nM, and 3.561 nM. **D-F.** Drug testing experiments on bigger LNCaP spheroids (3000 cells/well while plating) exposed to varying docetaxel concentrations: the IC50 values were 31.16 nM, 17.56 nM, and 12.70 nM. **G.** IC50 values. **H.** R-squared values.

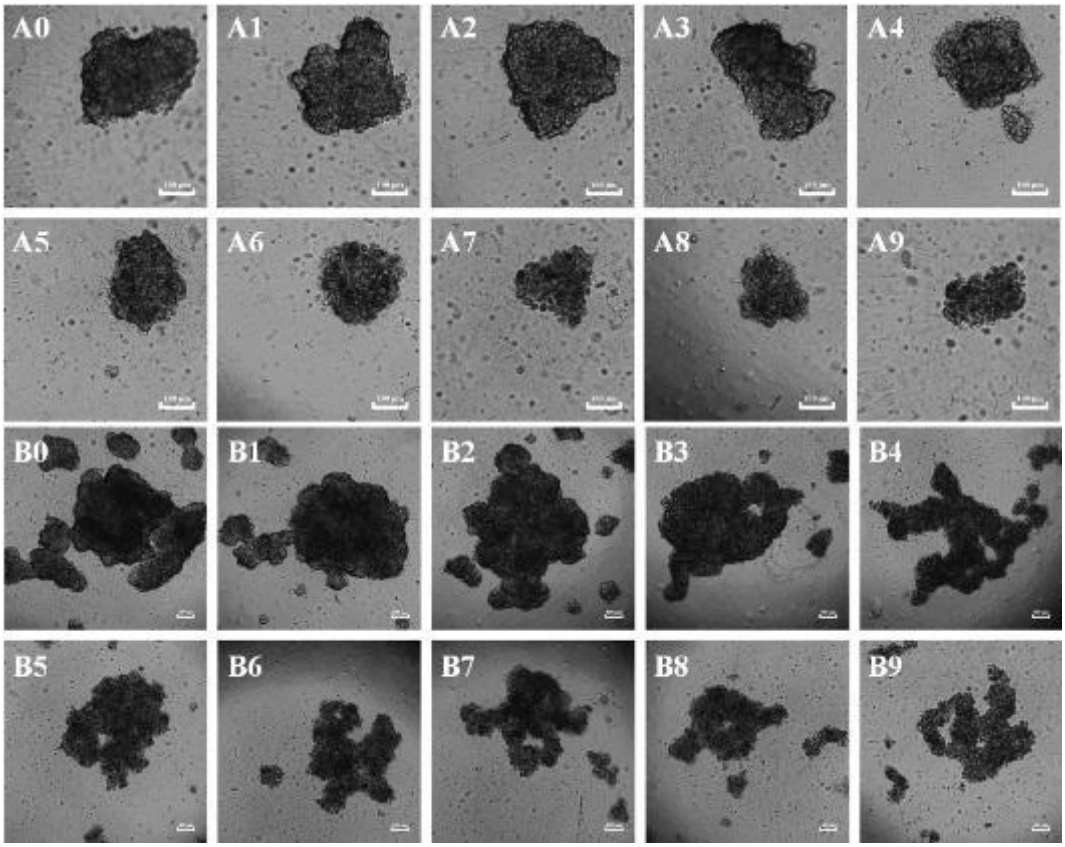

Figure 34. Images of drug testing experiments based on floating LNCaP spheroids of variable sizes exposed to docetaxel treatment.

A0-A9. Images of drug testing experiments based on smaller LNCaP spheroids (300 cells/well while plating) exposed to varying docetaxel concentrations: A0: Image of negative control without docetaxel; A1-A9: Images of the LNCaP cells exposed to varying docetaxel concentrations for five days (0.25 nM, 0.5 nM, 1 nM, 2 nM, 4 nM, 8 nM, 16 nM, 32 nM, and 64 nM). **B0-B9.** Images of drug testing experiments based on bigger LNCaP spheroids (3000 cells/well while plating) exposed to varying docetaxel concentrations: B0: Image of negative control without docetaxel; B1-B9: Images of the LNCaP cells exposed to varying docetaxel concentrations for five days (1 nM, 2 nM, 4 nM, 8 nM, 16 nM, 32 nM, 64 nM, 128 nM, and 256 nM).

3.5.5 Susceptibility of embedded cultured LNCaP cells/spheroids exposed to docetaxel treatment

3.5.5.1 Susceptibility of LNCaP cells cultured in Matrigel for 4 days: Based on our previous results, LNCaP cells remained single cells in Matrigel for 4 days (Subheading 3.3), and we compared the susceptibility of the LNCaP cells cultured in Matrigel for two days with 2D-cultured LNCaP cells, which showed similar IC50 values but different R-squared/maximum

inhibition values (Subheading 3.5.2.1). In this stage, we first cultured the LNCaP cells in the Matrigel for 4 days and then exposed the cells to docetaxel. The IC50 values were 4.140, 5.553, and 3.630 nM (Figure 35. A-C). The images also showed that the LNCaP spheroid formation was inhibited by docetaxel (Figure 35. D0-D9).

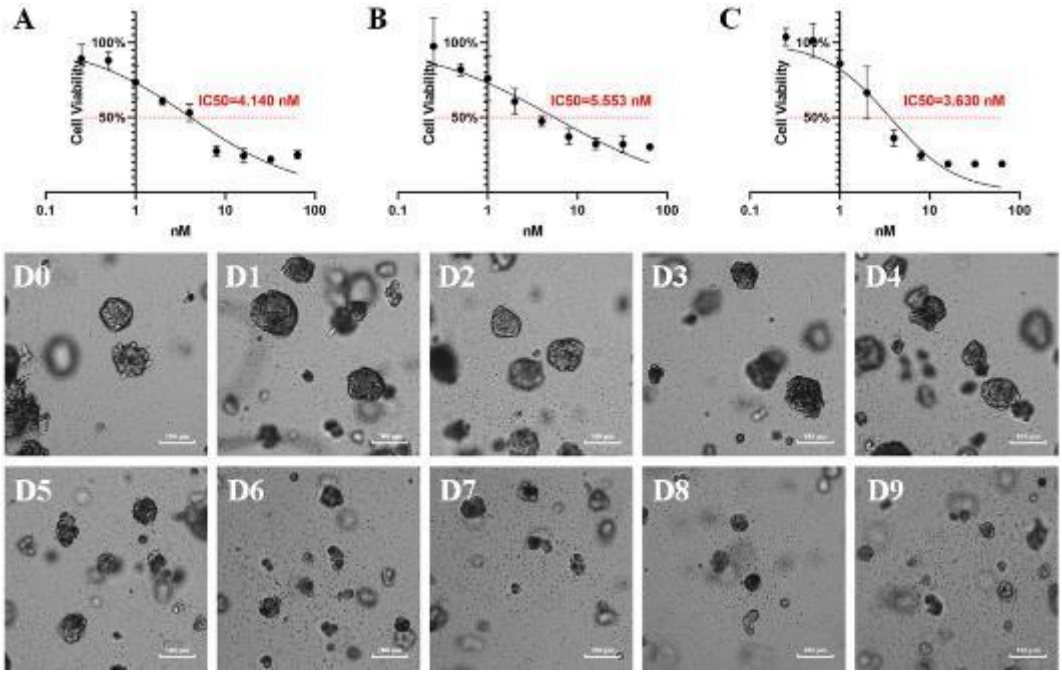

Figure 35. Susceptibility of LNCaP cells cultured for 4 days in Matrigel to docetaxel treatment.

A-C. Drug testing results. **D0-D9.** Images of drug testing experiments of LNCaP cells cultured for four days in Matrigel exposed to varying docetaxel concentrations: D0: Image of negative control without docetaxel; D1-D9: Images of the LNCaP cells exposed to varying docetaxel concentrations for five days (0.25 nM, 0.5 nM, 1 nM, 2 nM, 4 nM, 8 nM, 16 nM, 32 nM, and 64 nM).

3.5.5.2 Susceptibility of LNCaP spheroids cultured in Matrigel for 7 days: Our previous results indicated that small-sized LNCaP spheroids were formed in Matrigel when LNCaP cells were cultured for seven days (Subheading 3.3). The drug testing experiments in this stage were based on these small-sized spheroids instead of single LNCaP cells. The IC50 values in this experiment were 9.903, 16.07, and 15.23 nM (Figure 36. A-C). The images showed that the growth of LNCaP spheroids was inhibited by docetaxel, and some LNCaP spheroids exposed to higher docetaxel concentrations appeared loose and flat (Figure 36. D0-D9).

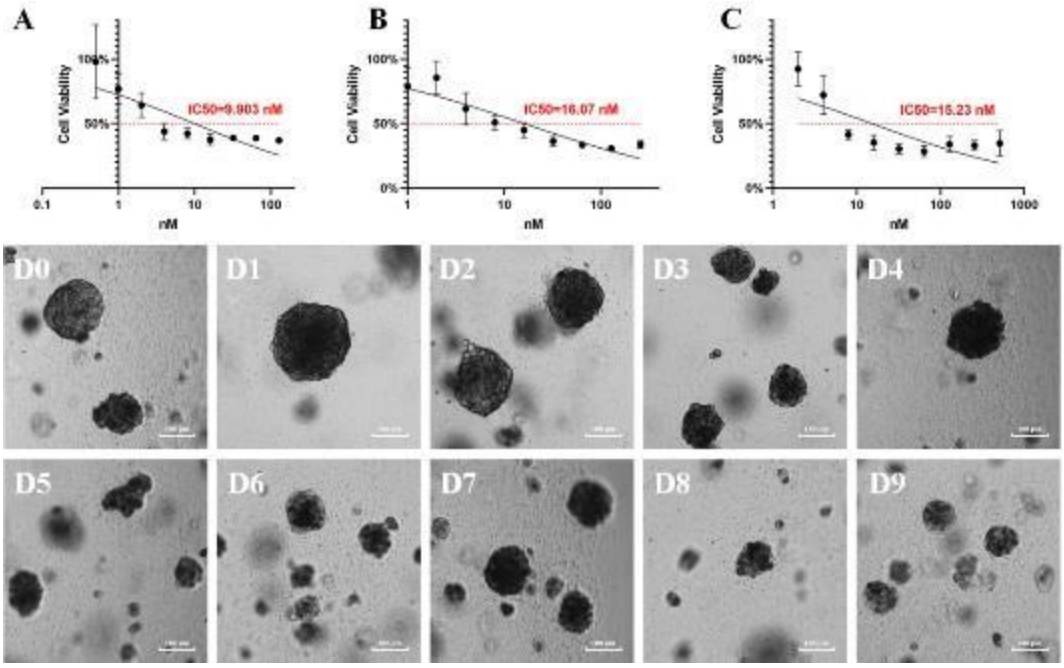

Figure 36. Susceptibility to docetaxel treatment of LNCaP spheroids cultured for 7 days in Matrigel.

A-C. Drug testing results. **D0-D9.** Images of drug testing experiments in LNCaP spheroids cultured for 7 days in Matrigel exposed to varying docetaxel concentrations: D0: Image of negative control without docetaxel; D1-D9: Images of the LNCaP spheroids exposed to varying docetaxel concentrations for 5 days (1 nM, 2 nM, 4 nM, 8 nM, 16 nM, 32 nM, 64 nM, 128 nM, and 256 nM).

3.5.5.3 Susceptibility of LNCaP spheroids cultured in Matrigel for 14 days: Our previous results indicated that LNCaP spheroids were formed in Matrigel when the LNCaP cells were cultured for 14 days (Subheading 3.3). The drug testing experiments in this stage were based on these LNCaP spheroids, and the IC50 values in this experiment were 31.38, 38.35, and 28.13 nM (Figure 37 A-C), much higher than those of 2D cells, 3D cells, and smaller spheroids. No significant differences in the spheroids were observed in the images, while the LNCaP spheroids exposed to higher docetaxel concentrations appeared loose and flat (Figure 37. D0-D9).

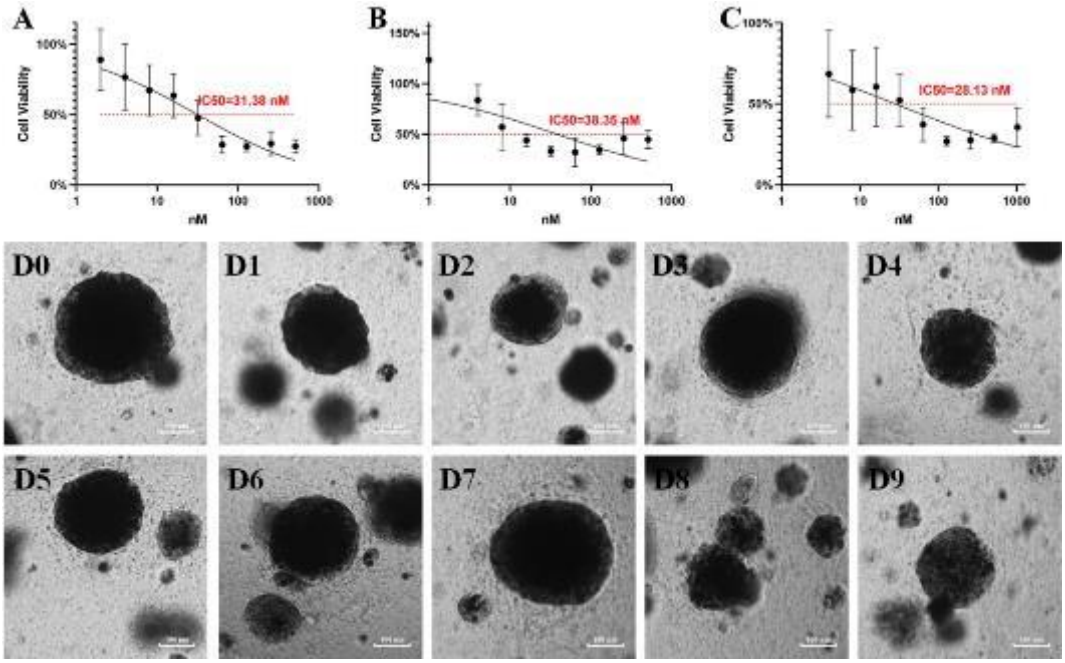

Figure 37. Susceptibility of LNCaP spheroids cultured for 14 days in Matrigel to docetaxel treatment.

A-C. Drug testing results. **D0-D9.** Images of drug testing experiments in LNCaP spheroids cultured for 14 days in Matrigel exposed to varying docetaxel concentrations: D0: Image of negative control without docetaxel; D1-D9: Images of the LNCaP spheroids exposed to varying docetaxel concentrations for 5 days (2 nM, 4 nM, 8 nM, 16 nM, 32 nM, 64 nM, 128 nM, 256 nM, and 512 nM).

3.5.5.4 Susceptibility of LNCaP spheroids cultured in Matrigel for 21 days: The LNCaP spheroids cultured in Matrigel for three weeks were also used to evaluate the susceptibility to docetaxel treatment. The mean values of the cell viability were all higher than 50%. Though we elevated the maximum docetaxel concentration in the drug testing experiments from 256 nM to 2048 nM, the cell viability curves reached the second plateau phase before 50% (Figure 38. A-C). No significant differences in the spheroids' formation were observed in the images, and the LNCaP spheroids exposed to higher docetaxel concentrations did not appear loose and flat in these experiments (Figure 38. D0-D9).

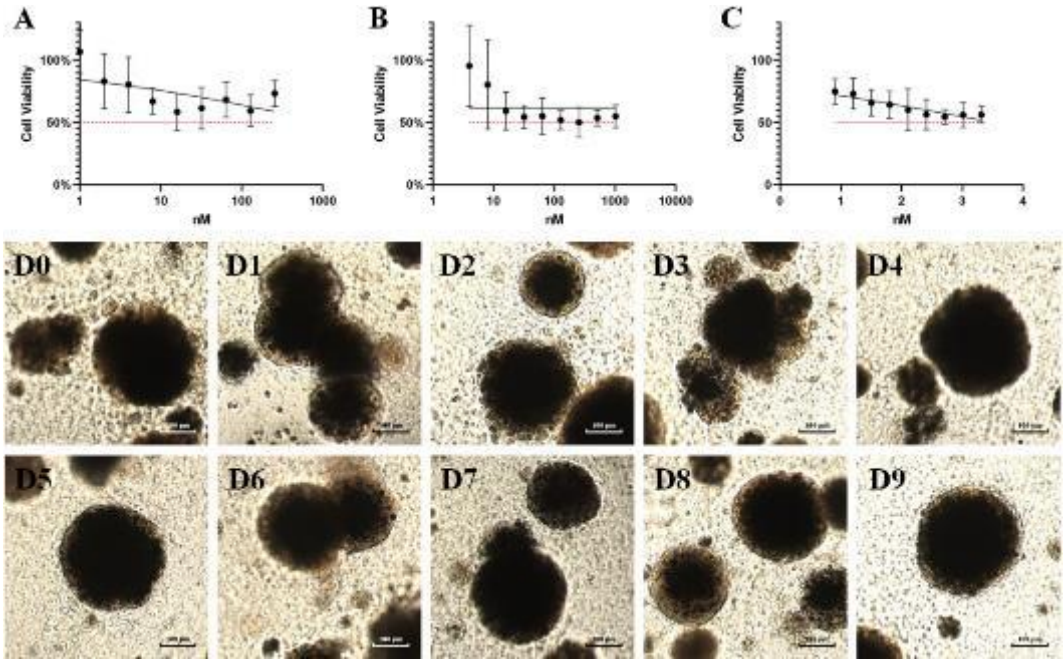

Figure 38. Susceptibility of LNCaP spheroids cultured for 21 days in Matrigel to docetaxel treatment.

A-C. Drug testing results. **D0-D9.** Images of drug testing experiments in LNCaP spheroids cultured for 21 days in Matrigel exposed to varying docetaxel concentrations: D0: Image of negative control without docetaxel; D1-D9: Images of the LNCaP spheroids exposed to varying docetaxel concentrations for 5 days (4 nM, 8 nM, 16 nM, 32 nM, 64 nM, 128 nM, 256 nM, 512 nM, and 1024 nM).

3.5.5.5 Parameters of 2D and 3D drug testing experiments

The IC50 values and R-squared values of the drug testing experiments based on 2D LNCaP cells and 3D-embedded cultured LNCaP cells were roughly the same (Subheading 3.5.2.1 and 3.5.2.2). However, the 3D-embedded cultured LNCaP cells' maximum inhibition values were much lower than that of 2D LNCaP cells. Additionally, we found that the IC50 values and SD values became higher according to the cell/spheroid size (Figure 39. A, D), while the R-squared values and maximum inhibition become lower (Figure 39. B, C). Lower SD values were found after the IC50 was reached in the IC50 curves than those of before it was reached (Figure 39. D). Combined with the drug testing images, we concluded that this was because most of the small-sized LNCaP spheroids died, resulting in the reduction of data volatility in different wells. The IC50 curves also became flatter according to the cell/spheroid size (Figure 39. E-J), and the lower R-squared values of the larger-sized spheroids also indicated poor goodness of fit.

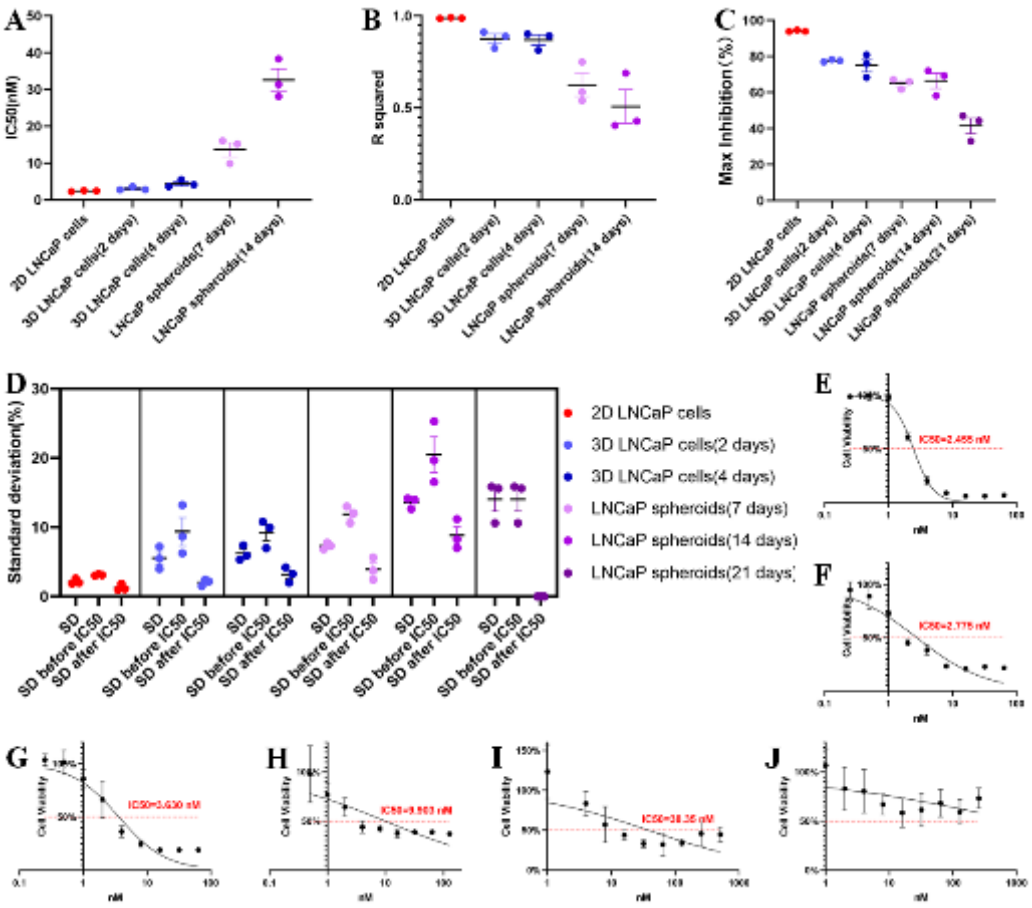

Figure 39. Parameters of the drug testing experiments based on 2D LNCaP cells and 3D embedded cultured LNCaP cells/spheroids exposed to docetaxel and the IC50 curves with the median R-squared values.

A. IC50 values of 2D LNCaP cells and 3D-embedded cultured LNCaP cells/spheroids exposed to docetaxel. **B.** R-squared values of 2D LNCaP cells and 3D-embedded cultured LNCaP cells/spheroids exposed to docetaxel. **C.** The maximum inhibition of 2D LNCaP cells and 3D-embedded cultured LNCaP cells/spheroids exposed to docetaxel. **D.** SD values of 2D LNCaP cells and 3D-embedded cultured LNCaP cells/spheroids exposed to docetaxel. **E-J.** IC50 curves with the median R-squared values**:** E: IC50 curve of 2D LNCaP cells exposed to docetaxel; F: IC50 curve of 3D-embedded cultured LNCaP cells (cultured for 2 days before plating); G: IC50 curve of 3D-embedded cultured LNCaP cells (cultured for 4 days before plating); H: IC50 curve of 3D-embedded cultured LNCaP spheroids (cultured for 7 days before plating); I: IC50 curve of 3D-embedded cultured LNCaP spheroids (cultured for 14 days before plating); J: IC50 curve of 3D-embedded cultured LNCaP spheroids (cultured for 21 days before plating).

Two kinds of LNCaP spheroids were used in the above drug testing experiments: embedded cultured LNCaP spheroids and floating spheroids. We also compared the images of embedded

cultured spheroids and the floating spheroids exposed to 64 nM docetaxel. The floating spheroids became loose and flat when exposed to 64 nM docetaxel for five days (Figure 40. F2). However, the embedded LNCaP spheroids of a similar size exposed to 64 nM docetaxel (Figure 40. E2) seemed roughly the same as the spheroids in negative control wells (Figure 40. E1). These loose and flat spheroids were also observed with the small-sized spheroids (Figure 40. B2, C2), which were more drug-sensitive than large-sized spheroids in the drug testing results.

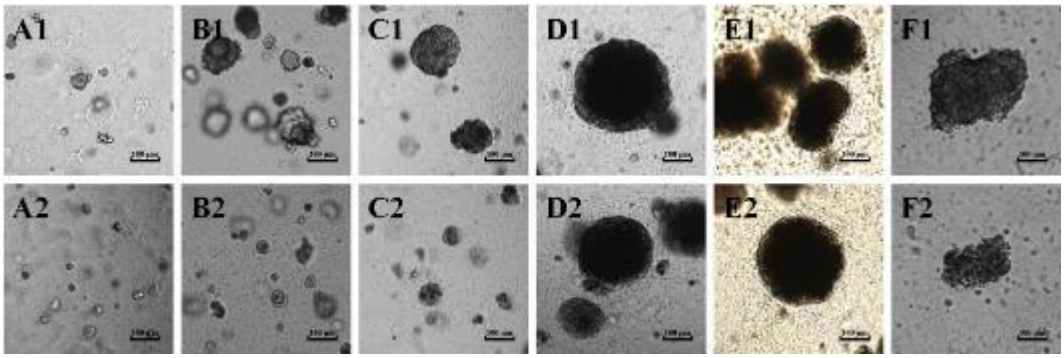

Figure 40. Images of LNCaP cells and spheroids exposed to 64nM docetaxel treatment. **A1.** Image of 3D-embedded cultured LNCaP cells (cultured for 2 days before docetaxel addition) in negative control wells; **A2.** Image of 3D-embedded cultured LNCaP cells (cultured for 2 days before docetaxel addition) exposed to 64 nM docetaxel for five days. **B1.** Image of 3D-embedded cultured LNCaP cells (cultured for 4 days before docetaxel addition) in negative control wells; **B2.** Image of 3D-embedded cultured LNCaP cells (cultured for 4 days before docetaxel addition) exposed to 64 nM docetaxel for five days. **C1.** Image of 3D-embedded cultured LNCaP spheroids (cultured for 7 days before docetaxel addition) in negative control wells; **C2.** Image of 3D embedded cultured LNCaP spheroids (cultured for 7 days before docetaxel addition) exposed to 64 nM docetaxel for five days. **D1.** Image of 3D embedded cultured LNCaP spheroids (cultured for 14 days before docetaxel addition) in negative control wells; **D2.** Image of 3D embedded cultured LNCaP spheroids (cultured for 14 days before docetaxel addition) exposed to 64 nM docetaxel for five days. **E1.** Image of 3D embedded cultured LNCaP spheroids (cultured for 21 days before docetaxel addition) in negative control wells; **E2.** Image of 3D embedded cultured LNCaP spheroids (cultured for 21 days before docetaxel addition) exposed to 64 nM docetaxel for five days. **F1.** Image of floating LNCaP spheroids in negative control wells; **C2.** Image of floating LNCaP spheroids exposed to 64 nM docetaxel for five days.

3.6 Susceptibility of 2D/3D LNCaP cells exposed to docetaxel/JQ1 combination treatment

3.6.1 Susceptibility of 2D LNCaP cells exposed to docetaxel and JQ1 combination treatment by the diagonal method: The diagonal method was performed to evaluate whether different concentrations of JQ1 could amplify the docetaxel-induced cell inhibition. We found that 128 nM and 256 nM significantly amplified cell inhibition in comparison to docetaxel alone (Figure 41. E, F).

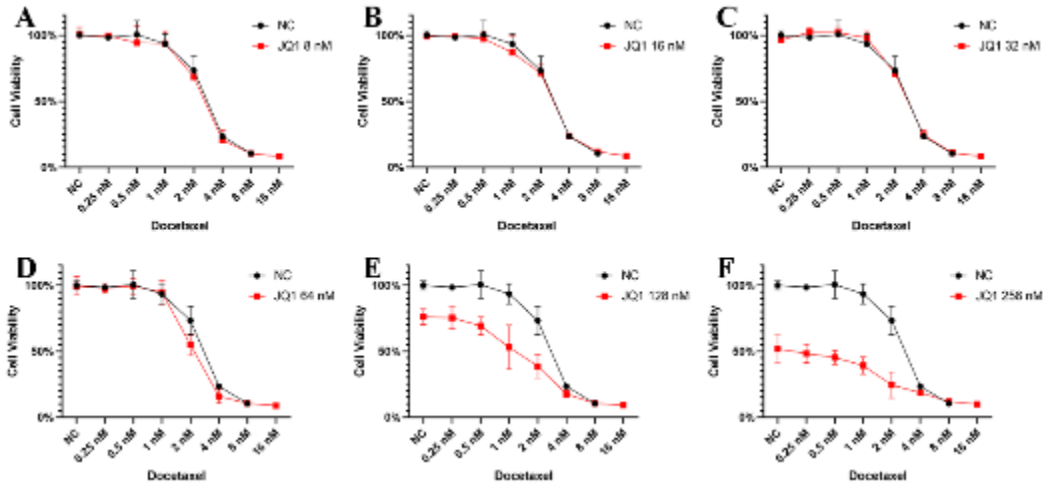

Figure 41. Diagonal method to evaluate whether variable concentrations of JQ1 could amplify the cell inhibition caused by docetaxel.

A. Cell viability of 2D-cultured LNCaP cells exposed to varying docetaxel concentrations and a fixed concentration of JQ1 (8 nM); **B.** Cell viability of 2D-cultured LNCaP cells exposed to varying docetaxel concentrations and a fixed concentration of JQ1 (16 nM); **C.** Cell viabilities of 2D cultured LNCaP exposed to varying docetaxel concentrations and a fixed concentration of JQ1 (32 nM); **D.** Cell viabilities of 2D cultured LNCaP cells exposed to varying docetaxel concentrations and a fixed concentration of JQ1 (64 nM); **E.** Cell viabilities of 2D cultured LNCaP cells exposed to varying docetaxel concentrations and a fixed concentration of JQ1 (128 nM); **F.** Cell viabilities of 2D cultured LNCaP cells exposed to varying docetaxel concentrations and a fixed concentration of JQ1 (256 nM).

3.6.2 Susceptibility of 2D and 3D LNCaP cells exposed to docetaxel and JQ1 combination treatment: Based on the results described above, we performed a combination treatment to evaluate the susceptibility of 2D and 3D LNCaP cells exposed to the docetaxel and JQ1 combination treatment. We found that JQ1 at 128 nM amplified the cell inhibition of docetaxel single treatment in both the 2D-cultured LNCaP cells and the 3D-embedded cultured LNCaP cells (Figure 42).

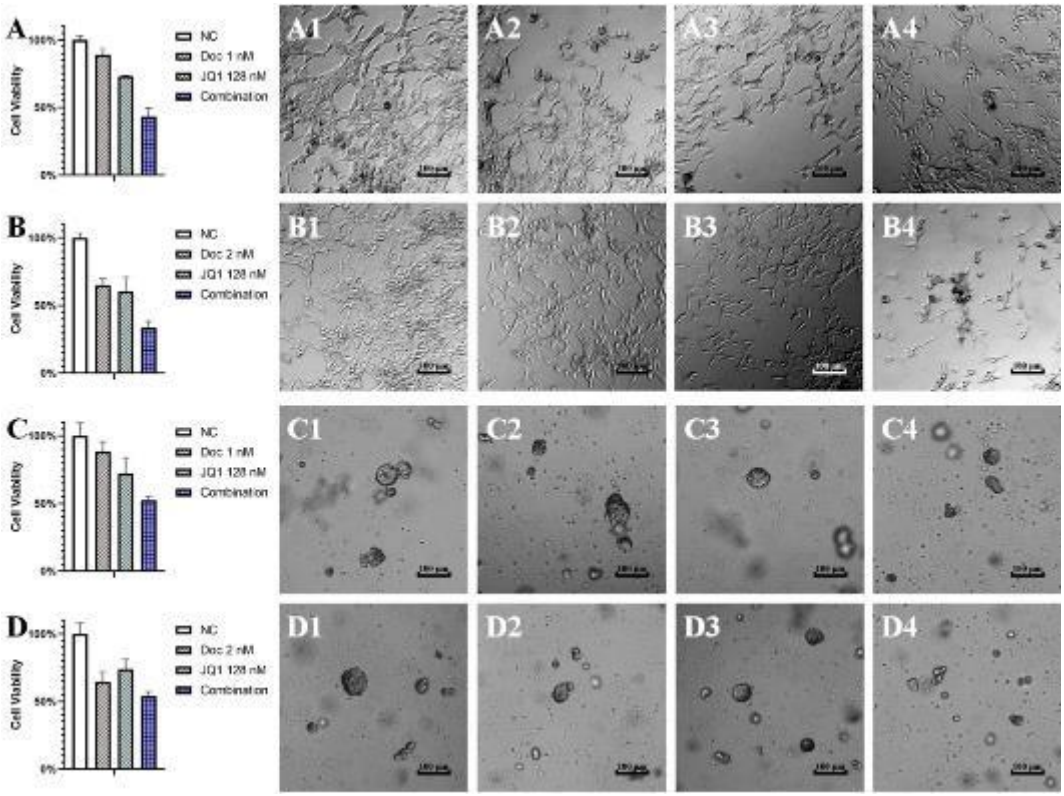

Figure 42. Susceptibility of 2D and 3D LNCaP cells exposed to the docetaxel and JQ1 combination treatment.

A. Cell viability of 2D LNCaP cells exposed to 1 nM docetaxel and 128 nM JQ1 alone or in combination. **A1:** Image of negative control without docetaxel and JQ1; **A2:** Image of 2D LNCaP cells exposed to 1 nM docetaxel; **A3:** Image of 2D LNCaP cells exposed to 128 nM JQ1; **A4:** Image of 2D LNCaP cells exposed to 1 nM docetaxel and 128 nM JQ1. **B.** Cell viability of 2D LNCaP cells exposed to 2 nM docetaxel and 128 nM JQ1 alone or in combination. **B1:** Image of negative control without docetaxel and JQ1; **B2:** Image of 2D LNCaP cells exposed to 2 nM docetaxel; **B3:** Image of 2D LNCaP cells exposed to 128 nM JQ1; **B4:** Image of 2D LNCaP cells exposed to 2 nM docetaxel and 128 nM JQ1. **C.** Cell viability of 3D-embedded cultured LNCaP cells exposed to 1 nM docetaxel and 128 nM JQ1 alone or in combination. **C1:** Image of negative control without docetaxel and JQ1; **C2:** Image of 3D-embedded cultured LNCaP cells exposed to 1 nM docetaxel; **C3:** Image of 3D-embedded cultured LNCaP cells exposed to 128 nM JQ1; **C4:** Image of 3D-embedded cultured LNCaP cells exposed to 1 nM docetaxel and 128 nM JQ1. **D.** Cell viability of 3D-embedded cultured LNCaP cells exposed to 2 nM docetaxel and 128 nM JQ1 alone or in combination. **D1:** Image of negative control without docetaxel and JQ1; **D2:** Image of 3D-embedded cultured LNCaP cells exposed to 2 nM docetaxel; **D3:** Image of 3D embedded cultured LNCaP cells exposed to 128 nM JQ1; **D4:** Image of 3D embedded cultured LNCaP cells exposed to 2 nM docetaxel and 128 nM JQ1.

3.6.3 LNCaP spheroid formation when exposed to docetaxel and JQ1 combination treatment

3.6.3.1 Spheroid formation when exposed to docetaxel or JQ1 treatment alone

Our previous drug testing results based on 3D-cultured LNCaP cells suggested that the spheroid formation could be inhibited by docetaxel and JQ1 treatment. To determine whether there are any synergistic effects of docetaxel and JQ1, we first performed experiments in 24-well plates to explore a suitable drug concentration for docetaxel and JQ1. We found that LNCaP spheroid formation was significantly inhibited when exposing it to docetaxel concentrations higher than 0.5 nM or JQ1 concentration higher than 128 nM (Figure 43).

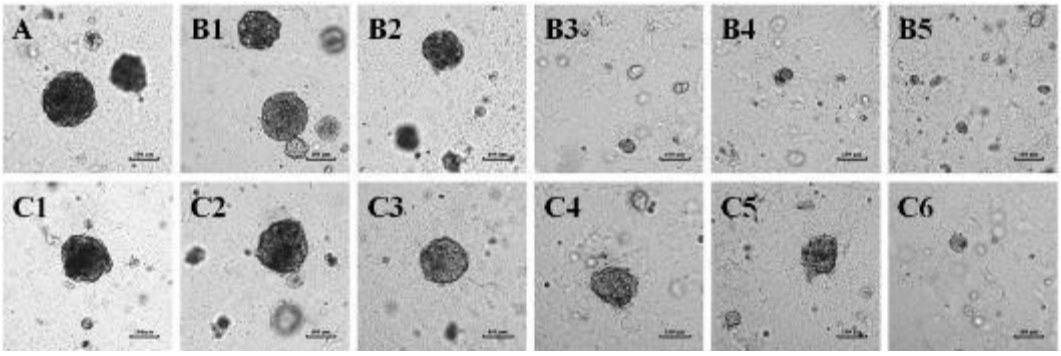

Figure 43. LNCaP spheroid formation when exposed to docetaxel or JQ1 treatment alone. **A.** LNCaP spheroid formation in complete growth medium without docetaxel or JQ1 for 14 days. **B1-B5.** LNCaP spheroid formation when exposed to varying docetaxel concentrations (0.25 nM, 0.5 nM, 1 nM, 2 nM, and 4 nM) for 14 days. **C1-C6.** LNCaP spheroid formation when exposed to varying JQ1 concentrations (8 nM, 16 nM, 32 nM, 64 nM, 128 nM, and 256 nM) for 14 days.

3.6.3.2 Spheroid formation when exposed to docetaxel and JQ1 combination treatment:

Based on the results above, we performed spheroid formation experiments by exposing the spheroids to 0.5 nM docetaxel and 128 nM JQ1 alone or in combination treatment. We found that the combination treatment significantly inhibited the LNCaP spheroid formations compared with docetaxel or JQ1 alone (Figure 44).

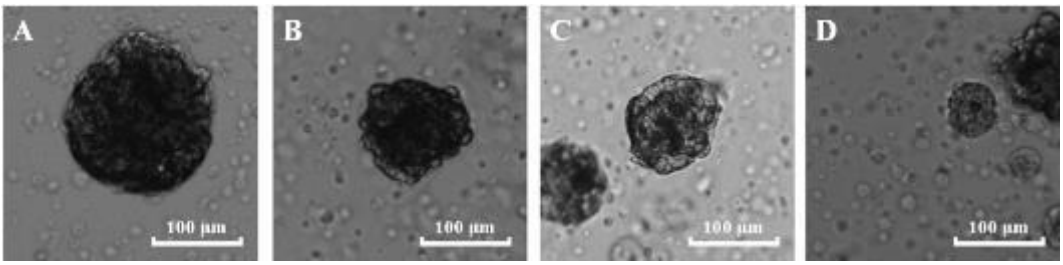

Figure 44. Images of the median LNCaP spheroids exposed to docetaxel and JQ1 combination treatment.

A. Image of the median LNCaP spheroids cultured in complete growth medium without docetaxel or JQ1 for 14 days. **B.** Image of the median LNCaP spheroids exposed to 0.5 nM of docetaxel for 14 days. **C.** Image of the median LNCaP spheroids exposed to 128 nM of JQ1 for 14 days. **D.** Image of the median LNCaP spheroids exposed to docetaxel (0.5 nM) and JQ1 (128 nM) treatment for 14 days.

According to the previous results, d_{max} and lg volume were good parameters for LNCaP cell/spheroid size displaying and the evaluation of growth kinetics (Subheading 3.3). We additionally collected the d_{max} and lg volume data of 100 embedded cultured LNCaP spheroids in each group (NC, treatment of 0.5 nM docetaxel, treatment of 128 nM JQ1, and the combination treatment). GraphPad Prism 8 was used for the normality tests, unpaired t-test, histograms, and violin plots.

3.6.3.2.1 d_{max} of LNCaP spheroids exposed to docetaxel and JQ1 for 14 days

The d_{max} distributions of the LNCaP spheroids for each group are shown in Figure 42 A-D. The frequency distributions and D'Agostino-Pearson omnibus normality tests showed that all the d_{max} data were normaly distributed ($P > 0.05$). Therefore, we used mean values of d_{max} to describe the size of the spheroids (Figure 45. F). The unpaired tests showed that the d_{max} of LNCaP spheroids exposed to the combination treatment was significantly smaller than the d_{max} in the docetaxel, JQ1, and NC groups ($P < 0.0001$, Figure 45. F). The same trends were also observed in the violin plot of d_{max} (Figure 45. E) and the LNCaP spheroid numbers bigger than the median spheroids in the NC group (Figure 45. G).

Group	NC	Docetaxel	JQ1	Combination
D'Agostino-Pearson omnibus (K2)	1.761	5.019	1.46	0.2779
p-value	0.4145	0.0813	0.4819	0.8703
Passed normality test (alpha=0.05)?	Yes	Yes	Yes	Yes

Table 7. Results of the normality tests for LNCaP spheroids exposed to docetaxel/JQ1 for 14 days (d_{max}).

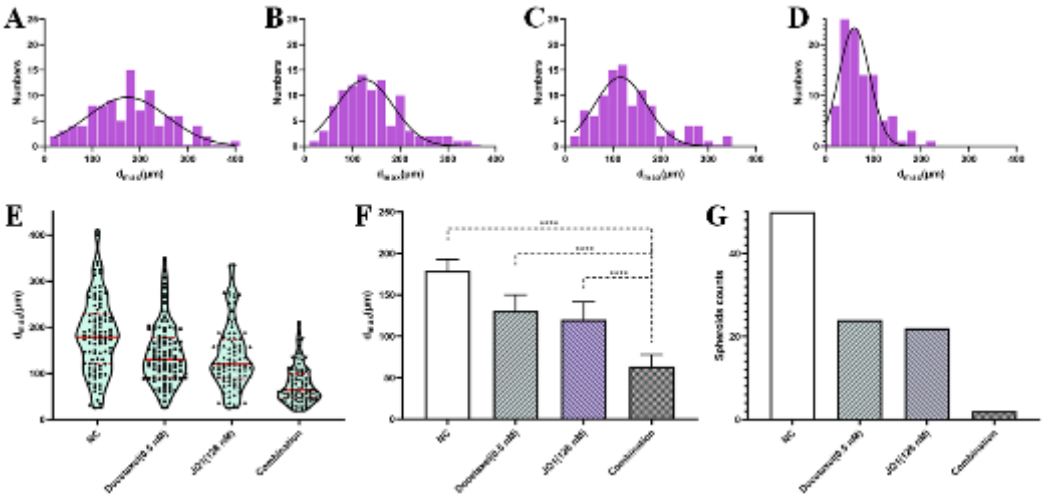

Figure 45. Analyses of spheroid distribution and spheroid size exposed to docetaxel or JQ1 alone or the combination treatment (according to d_{max}).

A. Histogram of d_{max} of LNCaP spheroids cultured in complete growth medium without docetaxel or JQ1 for 14 days (NC group) (P=0.4145). **B.** Histogram of the d_{max} of LNCaP spheroids exposed to 0.5 nM docetaxel (P=0.0813). **C.** Histogram of the d_{max} of LNCaP spheroids exposed to 128 nM JQ1(P=0.4819). **D.** Histogram of the d_{max} of LNCaP spheroids exposed to the combination treatment (0.5 nM docetaxel and 128 nM JQ1) (P=0.8703). **E.** Violin plot of the LNCaP spheroids distribution. **F.** Mean values of the d_{max} of LNCaP spheroids for each group (Mean with SEM) (****: P < 0.0001). **G.** Numbers of LNCaP spheroids bigger than the median spheroids in NC group (according to d_{max}).

3.6.3.2.2 lg volume of LNCaP spheroids exposed to docetaxel and JQ1 for 14 days

The lg volume distributions of the LNCaP spheroids for each group are shown in Figure 46 A-D. The frequency distributions and D'Agostino-Pearson omnibus normality tests showed that all the lg volume data were normally distributed (P > 0.05). The unpaired tests showed that the lg volume of LNCaP spheroids exposed to the combination treatment was significantly smaller than the lg volume in the docetaxel, JQ1, and NC groups (P < 0.0001, Figure 46. F). The same trends were also observed in the violin plot of lg volume comparison (Figure 46. E) and the LNCaP spheroid numbers bigger than the median spheroids in NC group (Figure 46. G).

Group	NC	Docetaxel	JQ1	Combination
D'Agostino-Pearson omnibus (K2)	2.836	2.13	0.1604	0.8124
p-value	0.2422	0.3447	0.9229	0.6662
Passed normality test (alpha=0.05)?	Yes	Yes	Yes	Yes

Table 8. Results of the normality tests for LNCaP spheroids exposed to docetaxel/JQ1 for 14 days (lg volume).

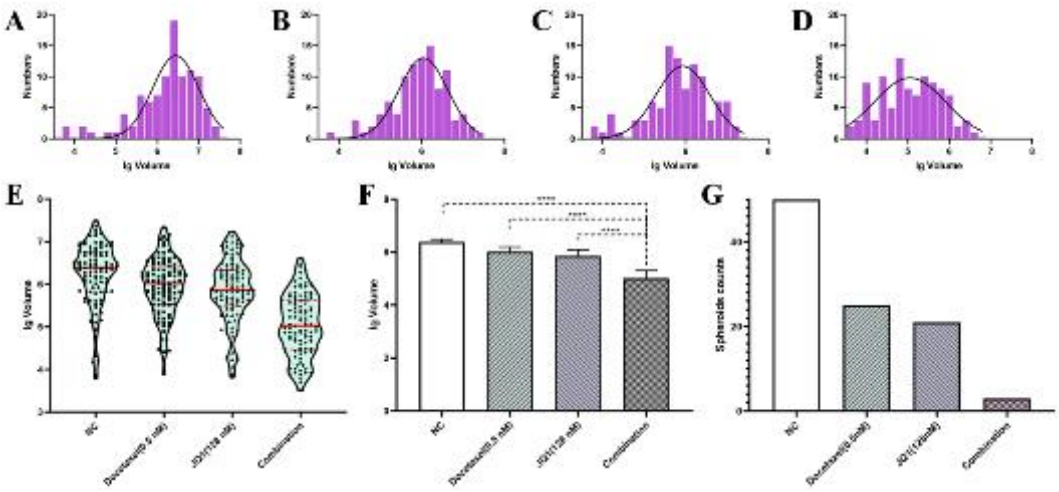

Figure 46. Analyses of spheroid distribution and spheroid size exposed to docetaxel or JQ1 alone or the combination treatment (according to lg volume).

A. Histogram of the lg volume of LNCaP spheroids culturing in complete growth medium without docetaxel or JQ1 for 14 days (NC group) (P=0.2422). **B.** Histogram of the lg volume of LNCaP spheroids exposed to 0.5 nM docetaxel (P=0.3447). **C.** Histogram of the lg volume of LNCaP spheroids exposed to 128 nM JQ1 (P=0.9229). **D.** Histogram of the lg volume of LNCaP spheroids exposed to the combination treatment (0.5 nM docetaxel and 128 nM JQ1) (P=0.6662). **E.** Violin plot of the LNCaP spheroids distribution. **F.** Mean values of lg volume of LNCaP spheroids for each group (Mean with SEM) (****: $P < 0.0001$). **G.** Numbers of LNCaP spheroids bigger than the median spheroids in NC group (according to lg volume).

4 Discussion

Establishing preclinical cancer models which could precisely mimic *in vivo* cancer is critical to novel anti-cancer drug research and development(Elbadawy et al., 2020). 3D organoid/spheroid culture systems and PDX models more appropriately reflect cellular heterogeneity, cell-cell interactions, and molecular divergence than 2D-cultured cell lines. However, the efficiency of PCa organoid and PDX establishment is relatively low(Lin et al., 2014; Gao et al., 2014). PCa spheroids based on suitable cell lines are also good choices in drug screening. Almost all of the evaluation indices of drug screening have been based on 2D-cultured cells, which have shown limitations in 3D drug testing experiments. In this study, we first evaluated the susceptibilities of LNCaP cells and spheroids exposed to the same anti-cancer drug. We then performed suitable protocols for the combination treatment of docetaxel and JQ1.

4.1 Formation inconsistency of embedded cultured LNCaP spheroids and suitable parameters to describe the size of the LNCaP spheroids

One of the challenges of spheroid drug testing experiments is to conveniently mass produce uniformly sized spheroids since the susceptibility for similar-sized spheroids shows convergence(Shahi Thakuri et al., 2016). Therefore, we first explored the suitable culture condition for LNCaP spheroids, and we then evaluated if the formation of embedded cultured LNCaP spheroids were consistent. In contrast to some published literature(Härmä et al., 2015; Ziaee and Chung, 2014; Song et al., 2003), our results indicate that 3D-embedded cultured LNCaP cells cannot survive in medium with an FBS concentration lower than 7.5%. The cause of this could be that the LNCaP cells were embedded cultured in Matrigel, which might serve as a barrier between the cells and the complete growth medium. The embedded cultured LNCaP spheroids started to form between the fourth to seventh day and grew over time. Unlike the spheroid formation consistency in round-bottom microplates(Shahi Thakuri et al., 2016), we found that the embedded cultured LNCaP spheroids in flat-bottom plates had a significant formation inconsistency, since the differences in the size of the LNCaP spheroids gradually widened over time. These results indicate that the capability of spheroid formation based on single LNCaP cells was significantly different even though the cells were from the same cell line with the same background genotype. Compared with d_{max} and lg volume, the spheroid volume seemed an unsuitable parameter to describe LNCaP cell/spheroid size. This is because the large-sized spheroids were not normally distributed, and the small-sized cells/spheroids could not be displayed significantly in the spheroid growth curves.

4.2 Pros and cons of the drug testing protocols based on embedded culture LNCaP spheroids, spheroid aliquots and floating spheroids

Two kinds of 96-well microplates (TC-treated microplates and U-bottom spheroid microplates) are usually used in 3D drug testing experiments, which provide the embedded cultured spheroids and floating spheroids with different drug diffusivity, frequency of cell proliferation, and tightness of the packed cells. In this study, three drug testing protocols were evaluated for the susceptibility of the 3D-cultured LNCaP cells and spheroids. The first protocol was based on the embedded cultured single LNCaP cells with the same initial plating numbers. According to the spheroid images and distribution results described above, the size of the LNCaP spheroids was not consistent. The spheroid size was also restricted by the longest culturing time in Matrigel, since the Matrigel became unstable after a long culturing time (Subheading 3.4). The second protocol based on spheroid aliquots overcame the spheroid size limitation restrictions due to the culturing time, while the spheroid sizes and numbers before drug addition varied much more than those obtained with the first protocol. The SD values in the spheroid aliquot experiments were much larger than those in the other protocols, showing that the different wells' cell viabilities differed significantly. These factors could have resulted in inaccurate IC50 values. The third protocol for drug testing was based on the floating spheroids from U-bottom spheroid microplates, in which we were able to quickly harvest consistent LNCaP spheroids(Shahi Thakuri et al., 2016). However, only one floating spheroid could be harvested from each well, and the progress of spheroid formation based on single cells could not be easily observed in this type of microplate. According to the images of the spheroids exposed to 64 nM docetaxel (Subheading 3.5.5.5, Figure 40), the floating spheroids were more sensitive to docetaxel than similar-sized embedded cultured LNCaP spheroids. The LNCaP spheroid formation in the spheroid microplates was based on cell fusion within a shorter time frame, the dynamic cell-cell and cell-matrix interaction of which should still be evaluated in future experiments. There are some limitations to this part of the study. Firstly, we could not fully distinguish whether the differences found originated from the Matrigel or variations in cell-cell and cell-matrix interactions, since the floating spheroids were not embedded in Matrigel. Secondly, the drug diffusivity, frequency of cell proliferation, and cell maturation ages of different kinds of spheroids were not detected in this study, which should be assessed further in future projects. Another limitation is that the maximum inhibition of the floating spheroids was significantly different in same-sized spheroids (Subheading 3.5.4.2). More experiments should be performed in spheroid microplates to confirm our results.

4.3 Relationship between docetaxel susceptibility and the size of LNCaP cells and spheroids

In this study, we described the IC50 curves of differently sized LNCaP cells/spheroids exposed to docetaxel. The same cell line's susceptibility exposed to docetaxel should be similar, but we found that the IC50 values and the other parameters differ significantly in differently sized LNCaP cells/spheroids. Several studies(Gao *et al.*, 2015; Atefi *et al.*, 2014; Godugu *et al.*, 2013) showed that 3D-cultured skin cancer cells generally showed greater resistance to many types of cytotoxic drugs than 2D-cultured cells. Some 3D-cultured breast cancer cells display complete resistance to paclitaxel, while producing a dose-dependent response in 2D-cultured cells(Lemmo *et al.*, 2014). More interestingly, another study(IMAMURA *et al.*, 2015) in breast cancer showed that spheroids based on BT-549, Bt-474, and T-47D cell lines were more resistant to paclitaxel and doxorubicin than 2D-cultured cells, while the spheroids based on MCF-7, HCC-1954, and MDA-MB-231 cell lines showed similar drug sensitivities in the corresponding 2D-culture cells. One unpublished study(Berrouet *et al.*, 2020) revealed that the IC50 curves for both 2D and 3D cultures of fast proliferating cells mostly overlap. However, for slowly proliferating cells, the IC50 curves for the 3D cultures attain higher half-inhibitory values. The LNCaP cell line is one kind of slower proliferating cell line. Further studies should also be performed to clarify if those differences in susceptibility can also be detected in fast proliferating PCa cells. Another limitation of those experiments is that the differences in the susceptibilities of the differently sized spheroids were evaluated based on inconsistently sized spheroids instead of similar-sized spheroids, the latter of which should be further explored in the future.

4.4 How should the susceptibility of 3D-cultured LNCaP cells/spheroids be evaluated?

As we described above, the same cell line's susceptibility to the same anti-cancer drug should be similar, but we might get different results from differently sized LNCaP cells/spheroids. So how should we evaluate the susceptibility of 3D cultured LNCaP cells/spheroids?

2D cell culture was introduced as a tool for anti-cancer drug screening in the 1950s(EAGLE and FOLEY, 1958) and has since become an essential part of preclinical drug discovery. 2D-cultured cells are grown as a monolayer in plates and flasks, which provides a flat "full-on-display" structure, different from cells *in vivo*. The drug testing experiments based on these flat cells showed more sensitivity than 3D-cultured cells and PDX models. This is one reason why the success rate of novel anti-cancer drugs selected by preclinical models is so low in clinical

trials(Stock et al., 2016; Hay *et al.*, 2014). 3D-cultured cells and PDX models provide more *in vivo*-like preclinical models that better mirror *in vivo* responses(Duval *et al.*, 2017), but the efficiency of PCa organoid/PDX establishment has been relatively low(Gao et al., 2014; Shi *et al.*, 2019). Spheroids established from PCa cell lines with the same gene characteristics as PCa tissues are another effective preclinical model in anti-cancer drug screening, but the suitable experimental procedures and evaluation indexes are still in development.

Drug-dose-response curves are widely used to measure anti-cancer drug sensitivities(Berrouet et al., 2020) and are developed based on drug testing work in 2D monolayer cultured cells. Similar-sized cancer cells were covered with medium containing uniform drug concentrations and cultured for a timeframe long enough for the cancer cells to passage 1-2 times, usually resulting in plunges (around IC50 values) in the curves(Turner and Charlton, 2005; Hafner *et al.*, 2016). IC50 values were shown to be an imperfect evaluation index in 3D drug testing experiments, which means that a multiparametric evaluation system should be established for spheroids and organoids. Since there were no standard experimental protocols for assessing spheroids' susceptibility when exposed to anti-cancer drugs, we performed different experiments based on embedded spheroids and floating spheroids. We found that the IC50 values of the larger-sized LNCaP spheroids were much higher than those of 2D LNCaP cells, 3D-embedded cultured LNCaP cells, and small-sized spheroids. The maximum inhibition of the spheroids increased with the size of the spheroids, and the cell viability did not decrease below 50% when the size of the spheroids had become large enough. The R-squared values of the larger-sized spheroids did not fit the IC50 curves. Nonuniformity of the size of spheroids can result in different biological activities, so recently, great efforts have been made to produce consistently sized spheroids/organoids in standard labware(Shahi Thakuri et al., 2016). However, it is essential to note that, even if we could produce similarly sized spheroids, the susceptibility to anti-cancer drug sensitivity would not be able to be evaluated by unfit curves. The maximum inhibition and area under the dose-response curve have been shown to be efficacy parameters to assess the susceptibility to drug testing in spheroids(Shahi Thakuri et al., 2016). According to our results, the IC50 curves of 3D-embedded cultured LNCaP single cells fit IC50 curves, but for the large-sized LNCaP spheroids with a low maximum inhibition and a low R-squared value, the IC50 curves were not suitable for evaluating the susceptibility to the drug. At the level of experimental operation, similar numbers of LNCaP cells could easily be plated into each well when cell plating, though this is challenging to achieve in the protocol based on spheroid aliquots. A limitation of the protocol based on 3D-embedded cultured LNCaP cells is that it only allows evaluation of single LNCaP cells' susceptibility, instead of LNCaP

spheroids. In this study, we chose drug testing experiments based on 2D and 3D-embedded LNCaP cells to evaluate the susceptibility to the docetaxel/JQ1 combination treatment. To assess the susceptibility of LNCaP spheroids, we additionally performed LNCaP spheroid formation experiments when exposed to docetaxel/JQ1 treatment to evaluate the inhibition of spheroid formation.

4.5 JQ1 and docetaxel: a potential combination therapy for PCa

Since Prof. Huggins and Hodges first discovered the hormonal dependence of PCa in 1941(Huggins and Hodges, 1941), hormonal therapy has become the backbone of mPCa treatments. A variety of strategies focusing on blocking androgen-AR signaling are available to treat PCa, and most have been shown to induce significant tumor regressions and normalize serum PSA levels(Lochrin *et al.*, 2014). However, almost all patients with mPCa become resistant to hormonal therapy and succumb to mCRPC. Deregulated androgen-AR signaling, such as AR amplification, mutation, and alternative splicing, can drive CRPC progression(Holzbeierlein *et al.*, 2004), and at least one of these aberrations can be detected in more than 50% of patients with CRPC(Asangani et al., 2014). Since resistance can be conferred to PCa cells after various hormonal treatments, novel non-AR dependent therapeutic strategies should be explored in the future.

JQ1 is a potent small-molecule inhibitor of BRD4, which has been shown to reduce the transcription of AR target genes(Seton-Rogers, 2014). It can also reduce the proliferation of PCa cells and organoids with known AR mutations, AR amplification, and AR-V7 expression(Welti *et al.*, 2018). JQ1 is thought to be a potential novel PCa therapy to overcome AR aberrant signaling, improving the outcome of patients beyond current PCa treatments(Welti et al., 2018). However, new literature has shown that JQ1 can promote PCa invasion and metastasis in a BET protein-independent manner when the PCa cell growth was inhibited(Leiming Wang, 2020). Docetaxel is an effective anti-cancer drug for patients with mPCa, and the effects of JQ1 can be synergistically amplified by docetaxel addition both *in vitro* and *in vivo* in esophageal adenocarcinoma(Song et al., 2020). However, that synergistic amplification was not observed when docetaxel was combined with a BRD4-proteolysis targeting chimeric in breast cancer(Noblejas-López et al., 2019). In this study, we performed drug testing experiments based on 2D and 3D preclinical models, which showed that JQ1 can amplify the cell inhibition of the single docetaxel treatment. The same tendency was observed in LNCaP spheroid formation. So, for the first time, we showed that JQ1 and docetaxel are a potential combination therapy for patients with PCa. The limitation of these studies was that

we only discovered a potential combination treatment for prostate cancer. Further projects should systematically explore if the drug pair of JQ1 and docetaxel is synergistic (such as miniaturized checkerboard assays), and its mechanism should also be explored in the future.

4.6 Conclusions

Our results identified the different fitness of IC50 curves for 2D and 3D preclinical models, and indicated a potential combination treatment (docetaxel and JQ1) for PCa patients. Specifically, IC50 curves appear to be suitable for evaluating the susceptibility of 3D single LNCaP cells exposed to docetaxel. However, for large-sized LNCaP spheroids, IC50 curves may not be suitable for assessing drug testing results' susceptibility. More evaluation indices (such as maximum inhibition) and experiments (such as spheroid formation) should be explored and performed to evaluate the susceptibility systematically. Our results also indicated that JQ1 and docetaxel might be a potentially successful combination treatment for patients with PCa.

4.7 Outlook

There has been a rapid development of BRD-inhibitors in recent years, and some have already entered clinical trials(Alqahtani *et al.*, 2019). BET-inhibitors induce cytostatic, instead of cytotoxic effects, which indicates that their combination with other drugs might be a better strategy in cancer treatment(Pervaiz *et al.*, 2018). JQ1, the ground-breaking BET-inhibitor drug, is a new and effective treatment strategy for patients with mPCa. However, a recent study showed that JQ1 promoted PCa invasion and metastasis in a BET protein-independent manner when the PCa cell growth was inhibited(Leiming Wang, 2020), indicating that combining other treatments with JQ1 might be more promising than JQ1 alone. Docetaxel could be one such choice for a combination strategy, since it is an irreplaceable first-line systemic chemotherapy drug for patients with mPCa. Our results suggest that JQ1 and docetaxel are a potentially successful combination therapy for PCa. More experiments are needed to explore if these drugs indeed act synergistically. The mechanism of action also should be explored, as better understandings could lead to more rationally designed combinations of treatments. Other combination strategies of future interest for JQ1 include hormonal therapies and PARP inhibitors (such as olaparib).

References:

Alghamdi, S., Khan, I., Beeravolu, N., McKee, C., Thibodeau, B., Wilson, G. & Chaudhry, G. R. (2016), "BET protein inhibitor JQ1 inhibits growth and modulates WNT signaling in mesenchymal stem cells", *Stem Cell Research & Therapy,* Vol. 7 No. 1, pp.

Alqahtani, A., Choucair, K., Ashraf, M., Hammouda, D. M., Alloghbi, A., Khan, T., Senzer, N. & Nemunaitis, J. (2019), "Bromodomain and extra-terminal motif inhibitors: a review of preclinical and clinical advances in cancer therapy", *Future Science OA,* Vol. 5 No. 3, pp. FSO372.

Archie Bleyer, F. S. R. B. (2020), "Prostate cancer in young men: An emerging young adult and older adolescent challenge", *Cancer,* Vol. 126 No. 1, pp. 46-57.

Arrowsmith, J. (2011), "Phase III and submission failures: 2007–2010", *Nature Reviews Drug Discovery,* Vol. 10 No. 2, pp. 87-87.

Asangani, I. A., Dommeti, V. L., Wang, X., Malik, R., Cieslik, M., Yang, R., Escara-Wilke, J., Wilder-Romans, K., Dhanireddy, S., Engelke, C., Iyer, M. K., Jing, X., Wu, Y., Cao, X., Qin, Z. S., Wang, S., Feng, F. Y. & Chinnaiyan, A. M. (2014), "Therapeutic targeting of BET bromodomain proteins in castration-resistant prostate cancer", *Nature,* Vol. 510 No. 7504, pp. 278-282.

Atefi, E., Lemmo, S., Fyffe, D., Luker, G. D. & Tavana, H. (2014), "High Throughput, Polymeric Aqueous Two-Phase Printing of Tumor Spheroids", *Advanced Functional Materials,* Vol. 24 No. 41, pp. 6509-6515.

Ballangrud, A. M., Yang, W. H., Charlton, D. E., McDevitt, M. R., Hamacher, K. A., Panageas, K. S., Ma, D., Bander, N. H., Scheinberg, D. A. & Sgouros, G. (2001), "Response of LNCaP spheroids after treatment with an alpha-particle emitter (213Bi)-labeled anti-prostate-specific membrane antigen antibody (J591)", *Cancer Res,* Vol. 61 No. 5, pp. 2008-2014.

Ballangrud, A. M., Yang, W. H., Dnistrian, A., Lampen, N. M. & Sgouros, G. (1999), "Growth and characterization of LNCaP prostate cancer cell spheroids", *Clin Cancer Res,* Vol. 5 No. 10 Suppl, pp. 3171s-3176s.

Barsouk, A., Padala, S. A., Vakiti, A., Mohammed, A., Saginala, K., Thandra, K. C., Rawla, P. & Barsouk, A. (2020), "Epidemiology, Staging and Management of Prostate Cancer", *Medical Sciences,* Vol. 8 No. 3, pp. 28.

Berrouet, C., Dorilas, N., Rejniak, K. A. & Tuncer, N. (2020), "Comparison of drug inhibitory effects (IC50) in monolayer and spheroid cultures", *bioRxiv,*.

Chen, R. C., Rumble, R. B., Loblaw, D. A., Finelli, A., Ehdaie, B., Cooperberg, M. R., Morgan, S. C., Tyldesley, S., Haluschak, J. J., Tan, W., Justman, S. & Jain, S. (2016), "Active Surveillance for the Management of Localized Prostate Cancer (Cancer Care Ontario Guideline): American Society of Clinical Oncology Clinical Practice Guideline Endorsement", *Journal of clinical oncology,* Vol. 34 No. 18, pp. 2182-2190.

Cheng, H. H., Gulati, R., Azad, A., Nadal, R., Twardowski, P., Vaishampayan, U. N., Agarwal, N., Heath, E. I., Pal, S. K., Rehman, H., Leiter, A., Batten, J. A., Montgomery, R. B., Galsky, M. D., Antonarakis, E. S., Chi, K. N. & Yu, E. Y. (2015), "Activity of enzalutamide in men with metastatic castration-resistant prostate cancer is affected by prior treatment with abiraterone and/or docetaxel", *Prostate Cancer and Prostatic Diseases,* Vol. 18 No. 2, pp. 122-127.

Cho, S. (2020), "Patient-derived xenografts as compatible models for precision oncology", *Laboratory Animal Research,* Vol. 36 No. 1, pp.

Claire H Pernar, E. M. E. K. (2018), "The Epidemiology of Prostate Cancer", *Cold Spring Harb Perspect Med,* Vol. 8 No. 12, pp. a030361.

Colella, G., Fazioli, F., Gallo, M., De Chiara, A., Apice, G., Ruosi, C., Cimmino, A. & de Nigris, F. (2018), "Sarcoma Spheroids and Organoids—Promising Tools in the Era of Personalized Medicine", *International Journal of Molecular Sciences,* Vol. 19 No. 2, pp. 615.

Cornford, P., Bellmunt, J., Bolla, M., Briers, E., De Santis, M., Gross, T., Henry, A. M., Joniau, S., Lam, T. B., Mason, M. D., van der Poel, H. G., van der Kwast, T. H., Rouvière, O., Wiegel, T. & Mottet, N. (2017), "EAU-ESTRO-SIOG Guidelines on Prostate Cancer. Part II: Treatment of Relapsing, Metastatic, and Castration-Resistant Prostate Cancer", *European Urology,* Vol. 71 No. 4, pp. 630-642.

Crawford, E. D., Heidenreich, A., Lawrentschuk, N., Tombal, B., Pompeo, A. C. L., Mendoza-Valdes, A., Miller, K., Debruyne, F. M. J. & Klotz, L. (2019), "Androgen-targeted therapy in men with prostate cancer: evolving practice and future considerations", *Prostate Cancer and Prostatic Diseases,* Vol. 22 No. 1, pp. 24-38.

de Bono, J. S., Oudard, S., Ozguroglu, M., Hansen, S., Machiels, J., Kocak, I., Gravis, G., Bodrogi, I., Mackenzie, M. J., Shen, L., Roessner, M., Gupta, S. & Sartor, A. O. (2010), "Prednisone plus cabazitaxel or mitoxantrone for metastatic castration-resistant prostate cancer progressing after docetaxel treatment: a randomised open-label trial", *The Lancet,* Vol. 376 No. 9747, pp. 1147-1154.

Devarasetty, M., Wang, E., Soker, S. & Skardal, A. (2017), "Mesenchymal stem cells support growth and organization of host-liver colorectal-tumor organoids and possibly resistance to chemotherapy", *Biofabrication,* Vol. 9 No. 2, pp. 021002.

Duval, K., Grover, H., Han, L., Mou, Y., Pegoraro, A. F., Fredberg, J. & Chen, Z. (2017), "Modeling Physiological Events in 2D vs. 3D Cell Culture", *Physiology*, Vol. 32 No. 4, pp. 266-277.

EAGLE, H. & FOLEY, G. E. (1958), "Cytotoxicity in Human Cell Cultures as a Primary Screen for the Detection of Anti-Tumor Agents", *Cancer Res*, Vol. 18 No. 9, pp. 1017-1025.

Elbadawy, M., Abugomaa, A., Yamawaki, H., Usui, T. & Sasaki, K. (2020), "Development of Prostate Cancer Organoid Culture Models in Basic Medicine and Translational Research", *Cancers*, Vol. 12 No. 4, pp. 777.

Evans, A. J. (2018), "Treatment effects in prostate cancer", *Mod Pathol*, Vol. 31 No. S1, pp. S110-121.

Gao, D., Vela, I., Sboner, A., Iaquinta, P. J., Karthaus, W. R., Gopalan, A., Dowling, C., Wanjala, J. N., Undvall, E. A., Arora, V. K., Wongvipat, J., Kossai, M., Ramazanoglu, S., Barboza, L. P., Di, W., Cao, Z., Zhang, Q. F., Sirota, I., Ran, L., MacDonald, T. Y., Beltran, H., Mosquera, J., Touijer, K. A., Scardino, P. T., Laudone, V. P., Curtis, K. R., Rathkopf, D. E., Morris, M. J., Danila, D. C., Slovin, S. F., Solomon, S. B., Eastham, J. A., Chi, P., Carver, B., Rubin, M. A., Scher, H. I., Clevers, H., Sawyers, C. L. & Chen, Y. (2014), "Organoid Cultures Derived from Patients with Advanced Prostate Cancer", *Cell*, Vol. 159 No. 1, pp. 176-187.

Gao, Y., Foster, R., Yang, X., Feng, Y., Shen, J. K., Mankin, H. J., Hornicek, F. J., Amiji, M. M. & Duan, Z. (2015), "Up-regulation of CD44 in the development of metastasis, recurrence and drug resistance of ovarian cancer", *Oncotarget*, Vol. 6 No. 11, pp. 9313-9326.

Godugu, C., Patel, A. R., Desai, U., Andey, T., Sams, A. & Singh, M. (2013), "AlgiMatrix™ Based 3D Cell Culture System as an In-Vitro Tumor Model for Anticancer Studies", *PLoS ONE*, Vol. 8 No. 1, pp. e53708.

Gravis, G., Fizazi, K., Joly, F., Oudard, S., Priou, F., Esterni, B., Latorzeff, I., Delva, R., Krakowski, I., Laguerre, B., Rolland, F., Théodore, C., Deplanque, G., Ferrero, J. M., Pouessel, D., Mourey, L., Beuzeboc, P., Zanetta, S., Habibian, M., Berdah, J. F., Dauba, J., Baciuchka, M., Platini, C., Linassier, C., Labourey, J. L., Machiels, J. P., El Kouri, C., Ravaud, A., Suc, E., Eymard, J. C., Hasbini, A., Bousquet, G. & Soulie, M. (2013), "Androgen-deprivation therapy alone or with docetaxel in non-castrate metastatic prostate cancer (GETUG-AFU 15): a randomised, open-label, phase 3 trial", *The Lancet Oncology*, Vol. 14 No. 2, pp. 149-158.

Hafner, M., Niepel, M., Chung, M. & Sorger, P. K. (2016), "Growth rate inhibition metrics correct for confounders in measuring sensitivity to cancer drugs", *Nature Methods*, Vol. 13 No. 6, pp. 521-527.

Ham, S. L., Joshi, R., Thakuri, P. S. & Tavana, H. (2016), "Liquid-based three-dimensional tumor models for cancer research and drug discovery", *Experimental biology and medicine (Maywood, N.J.)*, Vol. 241 No. 9, pp. 939-954.

Härmä, V., Haavikko, R., Virtanen, J., Ahonen, I., Schukov, H., Alakurtti, S., Purev, E., Rischer, H., Yli-Kauhaluoma, J., Moreira, V. M., Nees, M. & Oksman-Caldentey, K. (2015), "Optimization of Invasion-Specific Effects of Betulin Derivatives on Prostate Cancer Cells through Lead Development", *PLOS ONE*, Vol. 10 No. 5, pp. e0126111.

Hay, M., Thomas, D. W., Craighead, J. L., Economides, C. & Rosenthal, J. (2014), "Clinical development success rates for investigational drugs", *Nature Biotechnology*, Vol. 32 No. 1, pp. 40-51.

Hepburn, A. C., Sims, C. H. C., Buskin, A. & Heer, R. (2020), "Engineering Prostate Cancer from Induced Pluripotent Stem Cells—New Opportunities to Develop Preclinical Tools in Prostate and Prostate Cancer Studies", *International Journal of Molecular Sciences*, Vol. 21 No. 3, pp. 905.

Holzbeierlein, J., Lal, P., LaTulippe, E., Smith, A., Satagopan, J., Zhang, L., Ryan, C., Smith, S., Scher, H., Scardino, P., Reuter, V. & Gerald, W. L. (2004), "Gene Expression Analysis of Human Prostate Carcinoma during Hormonal Therapy Identifies Androgen-Responsive Genes and Mechanisms of Therapy Resistance", *The American Journal of Pathology*, Vol. 164 No. 1, pp. 217-227.

IMAMURA, Y., MUKOHARA, T., SHIMONO, Y., FUNAKOSHI, Y., CHAYAHARA, N., TOYODA, M., KIYOTA, N., TAKAO, S., KONO, S., NAKATSURA, T. & MINAMI, H. (2015), "Comparison of 2D- and 3D-culture models as drug-testing platforms in breast cancer", *Oncology Reports*, Vol. 33 No. 4, pp. 1837-1843.

James, N. D., Sydes, M. R., Clarke, N. W., Mason, M. D., Dearnaley, D. P., Spears, M. R., Ritchie, A. W. S., Parker, C. C., Russell, J. M., Attard, G., de Bono, J., Cross, W., Jones, R. J., Thalmann, G., Amos, C., Matheson, D., Millman, R., Alzouebi, M., Beesley, S., Birtle, A. J., Brock, S., Cathomas, R., Chakraborti, P., Chowdhury, S., Cook, A., Elliott, T., Gale, J., Gibbs, S., Graham, J. D., Hetherington, J., Hughes, R., Laing, R., McKinna, F., McLaren, D. B., O'Sullivan, J. M., Parikh, O., Peedell, C., Protheroe, A., Robinson, A. J., Srihari, N., Srinivasan, R., Staffurth, J., Sundar, S., Tolan, S., Tsang, D., Wagstaff, J., Parmar, M. K. B. & Investigators, S. (2016), "Addition of docetaxel, zoledronic acid, or both to first-line long-term hormone therapy in prostate cancer (STAMPEDE): survival results from an adaptive, multiarm, multistage, platform randomised controlled trial", *Lancet*, Vol. 387 No. 10024, pp. 1163-1177.

Kimura, T. & Egawa, S. (2018), "Epidemiology of prostate cancer in Asian countries", *International Journal of Urology*, Vol. 25 No. 6, pp. 524-531.

Kopetz, S., Lemos, R. & Powis, G. (2012), "The Promise of Patient-Derived Xenografts: The Best Laid Plans of Mice and Men", *Clinical Cancer Research*, Vol. 18 No. 19, pp. 5160-5162.

Leiming Wang, M. X. C. K. (2020), "Small molecule JQ1 promotes prostate cancer invasion via BET-independent inactivation of FOXA1", *J Clin Invest*, Vol. 130 No. 4, pp. 1782-1792.

Lemmo, S., Atefi, E., Luker, G. D. & Tavana, H. (2014), "Optimization of Aqueous Biphasic Tumor Spheroid Microtechnology for Anti-cancer Drug Testing in 3D Culture", *Cellular and Molecular Bioengineering,* Vol. 7 No. 3, pp. 344-354.

Lin, D., Wyatt, A. W., Xue, H., Wang, Y., Dong, X., Haegert, A., Wu, R., Brahmbhatt, S., Mo, F., Jong, L., Bell, R. H., Anderson, S., Hurtado-Coll, A., Fazli, L., Sharma, M., Beltran, H., Rubin, M., Cox, M., Gout, P. W., Morris, J., Goldenberg, L., Volik, S. V., Gleave, M. E., Collins, C. C. & Wang, Y. (2014), "High Fidelity Patient-Derived Xenografts for Accelerating Prostate Cancer Discovery and Drug Development", *Cancer Research,* Vol. 74 No. 4, pp. 1272-1283.

Lochrin, S. E., Price, D. K. & Figg, W. D. (2014), "BET bromodomain inhibitors—A novel epigenetic approach in castration-resistant prostate cancer", *Cancer Biology & Therapy,* Vol. 15 No. 12, pp. 1583-1585.

Ma, L., Li, J., Nie, Q., Zhang, Q., Liu, S., Ge, D. & You, Z. (2017), "Organoid culture of human prostate cancer cell lines LNCaP and C4-2B", *American journal of clinical and experimental urology,* Vol. 5 No. 3, pp. 25-33.

Mezynski, J., Pezaro, C., Bianchini, D., Zivi, A., Sandhu, S., Thompson, E., Hunt, J., Sheridan, E., Baikady, B., Sarvadikar, A., Maier, G., Reid, A. H. M., Mulick Cassidy, A., Olmos, D., Attard, G. & de Bono, J. (2012), "Antitumour activity of docetaxel following treatment with the CYP17A1 inhibitor abiraterone: clinical evidence for cross-resistance?", *Annals of Oncology,* Vol. 23 No. 11, pp. 2943-2947.

Min Yuen Teo, D. E. R. P. (2019), "Treatment of Advanced Prostate Cancer", *Annu Rev Med,* Vol. 70479-499.

Mottet, N., Bellmunt, J., Bolla, M., Briers, E., Cumberbatch, M. G., De Santis, M., Fossati, N., Gross, T., Henry, A. M., Joniau, S., Lam, T. B., Mason, M. D., Matveev, V. B., Moldovan, P. C., van den Bergh, R. C. N., Van den Broeck, T., van der Poel, H. G., van der Kwast, T. H., Rouvière, O., Schoots, I. G., Wiegel, T. & Cornford, P. (2017), "EAU-ESTRO-SIOG Guidelines on Prostate Cancer. Part 1: Screening, Diagnosis, and Local Treatment with Curative Intent", *Eur Urol,* Vol. 71 No. 4, pp. 618-629.

Mulholland, T., McAllister, M., Patek, S., Flint, D., Underwood, M., Sim, A., Edwards, J. & Zagnoni, M. (2018), "Drug screening of biopsy-derived spheroids using a self-generated microfluidic concentration gradient", *Scientific Reports,* Vol. 8 No. 1, pp.

Nadal, R., Zhang, Z., Rahman, H., Schweizer, M. T., Denmeade, S. R., Paller, C. J., Carducci, M. A., Eisenberger, M. A. & Antonarakis, E. S. (2014), "Clinical activity of enzalutamide in Docetaxel-naïve and Docetaxel-pretreated patients with metastatic castration-resistant prostate cancer", *The Prostate,* Vol. 74 No. 15, pp. 1560-1568.

Nader, R., Amm, J. E. & Aragon-Ching, J. B. (2018), "Role of chemotherapy in prostate cancer", *Asian J Androl,* Vol. 20 No. 3, pp. 221-229.

Nguyen, H. M., Vessella, R. L., Morrissey, C., Brown, L. G., Coleman, I. M., Higano, C. S., Mostaghel, E. A., Zhang, X., True, L. D., Lam, H., Roudier, M., Lange, P. H., Nelson, P. S. & Corey, E. (2017), "LuCaP Prostate Cancer Patient-Derived Xenografts Reflect the Molecular Heterogeneity of Advanced Disease an--d Serve as Models for Evaluating Cancer Therapeutics", *The Prostate,* Vol. 77 No. 6, pp. 654-671.

Noblejas-López, M. D. M., Nieto-Jimenez, C., Burgos, M., Gómez-Juárez, M., Montero, J. C., Esparís-Ogando, A., Pandiella, A., Galán-Moya, E. M. & Ocaña, A. (2019), "Activity of BET-proteolysis targeting chimeric (PROTAC) compounds in triple negative breast cancer", *Journal of Experimental & Clinical Cancer Research,* Vol. 38 No. 1, pp.

Oudard, S., Fizazi, K., Sengeløv, L., Daugaard, G., Saad, F., Hansen, S., Hjälm-Eriksson, M., Jassem, J., Thiery-Vuillemin, A., Caffo, O., Castellano, D., Mainwaring, P. N., Bernard, J., Shen, L., Chadjaa, M. & Sartor, O. (2017), "Cabazitaxel Versus Docetaxel As First-Line Therapy for Patients With Metastatic Castration-Resistant Prostate Cancer: A Randomized Phase III Trial — FIRSTANA", *J Clin Oncol,* Vol. 35 No. 28, pp. 3189-3197.

Pervaiz, M., Mishra, P. & Günther, S. (2018), "Bromodomain Drug Discovery – the Past, the Present, and the Future", *The Chemical Record,* Vol. 18 No. 12, pp. 1808-1817.

Petrylak, D. P., Tangen, C. M., Hussain, M. H. A., Lara, P. N., Jones, J. A., Taplin, M. E., Burch, P. A., Berry, D., Moinpour, C., Kohli, M., Benson, M. C., Small, E. J., Raghavan, D. & Crawford, E. D. (2004), "Docetaxel and Estramustine Compared with Mitoxantrone and Prednisone for Advanced Refractory Prostate Cancer", *The New England journal of medicine,* Vol. 351 No. 15, pp. 1513-1520.

Pienta, K. J. (2001), "Preclinical mechanisms of action of docetaxel and docetaxel combinations in prostate cancer", *Semin Oncol,* Vol. 28 No. 4 Suppl 15, pp. 3-7.

Rebecca L Siegel, K. D. M. A. (2020), "Cancer statistics, 2020", *CA Cancer J Clin,* Vol. 70 No. 1, pp. 7-30.

Scannell, J. W., Blanckley, A., Boldon, H. & Warrington, B. (2012), "Diagnosing the decline in pharmaceutical R&D efficiency", *Nature Reviews Drug Discovery,* Vol. 11 No. 3, pp. 191-200.

Scher, H. I., Fizazi, K., Saad, F., Taplin, M., Sternberg, C. N., Miller, K., de Wit, R., Mulders, P., Chi, K. N., Shore, N. D., Armstrong, A. J., Flaig, T. W., Fléchon, A., Mainwaring, P., Fleming, M., Hainsworth, J. D., Hirmand, M., Selby, B., Seely, L. & de Bono, J. S. (2012), "Increased Survival with Enzalutamide in Prostate Cancer after Chemotherapy", *New England Journal of Medicine,* Vol. 367 No. 13, pp. 1187-1197.

Schweizer, M. T., Zhou, X. C., Wang, H., Bassi, S., Carducci, M. A., Eisenberger, M. A. & Antonarakis, E. S.

(2014), "The Influence of Prior Abiraterone Treatment on the Clinical Activity of Docetaxel in Men with Metastatic Castration-resistant Prostate Cancer", *European Urology*, Vol. 66 No. 4, pp. 646-652.
Seton-Rogers, S. (2014), "BETting on epigenetic therapy", *Nature Reviews Cancer*, Vol. 14 No. 6, pp. 385-385.
Shahi Thakuri, P., Ham, S. L., Luker, G. D. & Tavana, H. (2016), "Multiparametric Analysis of Oncology Drug Screening with Aqueous Two-Phase Tumor Spheroids", *Molecular Pharmaceutics*, Vol. 13 No. 11, pp. 3724-3735.
Shahi Thakuri, P., Luker, G. D. & Tavana, H. (2019), "Cyclical Treatment of Colorectal Tumor Spheroids Induces Resistance to MEK Inhibitors", *Translational Oncology*, Vol. 12 No. 3, pp. 404-416.
Shen, M. M. & Abate-Shen, C. (2010), "Molecular genetics of prostate cancer: new prospects for old challenges", *Genes & Development*, Vol. 24 No. 18, pp. 1967-2000.
Shi, C., Chen, X. & Tan, D. (2019), "Development of patient-derived xenograft models of prostate cancer for maintaining tumor heterogeneity", *Translational Andrology and Urology*, Vol. 8 No. 5, pp. 519-528.
Shi, X., Liu, C., Liu, B., Chen, J., Wu, X. & Gong, W. (2018), "JQ1: a novel potential therapeutic target", *Pharmazie*, Vol. 73 No. 9, pp. 491-493.
Skardal, A., Devarasetty, M., Rodman, C., Atala, A. & Soker, S. (2015), "Liver-Tumor Hybrid Organoids for Modeling Tumor Growth and Drug Response In Vitro", *Annals of Biomedical Engineering*, Vol. 43 No. 10, pp. 2361-2373.
Smith-Palmer, J., Takizawa, C. & Valentine, W. (2019), "Literature review of the burden of prostate cancer in Germany, France, the United Kingdom and Canada", *BMC Urology*, Vol. 19 No. 1, pp.
Song, H., O'Connor, K. C., David, O., Giordano, C. L., Pappas-LeBeau, H. & Clejan, S. (2003), "Immunohistochemical analysis of differentiation in static and mixed prostate cancer spheroids", *Journal of Cellular and Molecular Medicine*, Vol. 7 No. 2, pp. 180-186.
Song, S., Li, Y., Xu, Y., Ma, L., Pool Pizzi, M., Jin, J., Scott, A. W., Huo, L., Wang, Y., Lee, J. H., Bhutani, M. S., Weston, B., Shanbhag, N. D., Johnson, R. L. & Ajani, J. A. (2020), "Targeting Hippo coactivator YAP1 through BET bromodomain inhibition in esophageal adenocarcinoma", *Molecular oncology*, Vol. 14 No. 6, pp. 1410-1426.
Stein, M. N., Goodin, S. & DiPaola, R. S. (2012), "Abiraterone in Prostate Cancer: A New Angle to an Old Problem", *Clinical Cancer Research*, Vol. 18 No. 7, pp. 1848-1854.
Stock, K., Estrada, M. F., Vidic, S., Gjerde, K., Rudisch, A., Santo, V. E., Barbier, M., Blom, S., Arundkar, S. C., Selvam, I., Osswald, A., Stein, Y., Gruenewald, S., Brito, C., van Weerden, W., Rotter, V., Boghaert, E., Oren, M., Sommergruber, W., Chong, Y., de Hoogt, R. & Graeser, R. (2016), "Capturing tumor complexity in vitro: Comparative analysis of 2D and 3D tumor models for drug discovery", *Scientific Reports*, Vol. 6 No. 1, pp.
Sweeney, C. J., Chen, Y., Carducci, M., Liu, G., Jarrard, D. F., Eisenberger, M., Wong, Y., Hahn, N., Kohli, M., Cooney, M. M., Dreicer, R., Vogelzang, N. J., Picus, J., Shevrin, D., Hussain, M., Garcia, J. A. & DiPaola, R. S. (2015), "Chemohormonal Therapy in Metastatic Hormone-Sensitive Prostate Cancer", *New England Journal of Medicine*, Vol. 373 No. 8, pp. 737-746.
Takebe, T., Imai, R. & Ono, S. (2018), "The Current Status of Drug Discovery and Development as Originated in United States Academia: The Influence of Industrial and Academic Collaboration on Drug Discovery and Development", *Clinical and Translational Science*, Vol. 11 No. 6, pp. 597-606.
Tannock, I. F., de Wit, R., Berry, W. R., Horti, J., Pluzanska, A., Chi, K. N., Oudard, S., Théodore, C., James, N. D., Turesson, I., Rosenthal, M. A., Eisenberger, M. A. & TAX, I. (2004), "Docetaxel plus Prednisone or Mitoxantrone plus Prednisone for Advanced Prostate Cancer", *The New England journal of medicine*, Vol. 351 No. 15, pp. 1502-1512.
Thakuri, P. S., Gupta, M., Plaster, M. & Tavana, H. (2019), "Quantitative Size-Based Analysis of Tumor Spheroids and Responses to Therapeutics", *ASSAY and Drug Development Technologies*, Vol. 17 No. 3, pp. 140-149.
Turner, R. J. & Charlton, S. J. (2005), "Assessing the Minimum Number of Data Points Required for Accurate IC50 Determination", *ASSAY and Drug Development Technologies*, Vol. 3 No. 5, pp. 525-531.
Vale, C. L., Burdett, S., Rydzewska, L. H. M., Albiges, L., Clarke, N. W., Fisher, D., Fizazi, K., Gravis, G., James, N. D., Mason, M. D., Parmar, M. K. B., Sweeney, C. J., Sydes, M. R., Tombal, B., Tierney, J. F. & STOpCaP, S. G. (2016), "Addition of docetaxel or bisphosphonates to standard of care in men with localised or metastatic, hormone-sensitive prostate cancer: a systematic review and meta-analyses of aggregate data", *The lancet oncology*, Vol. 17 No. 2, pp. 243-256.
van Soest, R. J., van Royen, M. E., de Morrée, E. S., Moll, J. M., Teubel, W., Wiemer, E. A. C., Mathijssen, R. H. J., de Wit, R. & van Weerden, W. M. (2013), "Cross-resistance between taxanes and new hormonal agents abiraterone and enzalutamide may affect drug sequence choices in metastatic castration-resistant prostate cancer", *European Journal of Cancer*, Vol. 49 No. 18, pp. 3821-3830.
Welti, J., Sharp, A., Yuan, W., Dolling, D., Nava Rodrigues, D., Figueiredo, I., Gil, V., Neeb, A., Clarke, M., Seed, G., Crespo, M., Sumanasuriya, S., Ning, J., Knight, E., Francis, J. C., Hughes, A., Halsey, W. S., Paschalis, A., Mani, R. S., Raj, G. V., Plymate, S. R., Carreira, S., Boysen, G., Chinnaiyan, A. M., Swain, A. & de Bono, J. S. (2018), "Targeting Bromodomain and Extra-Terminal (BET) Family Proteins in Castration-Resistant Prostate Cancer (CRPC)", *Clinical Cancer Research*, Vol. 24 No. 13, pp. 3149-3162.

Ziaee, S. & Chung, L. W. (2014), "Induction of integrin α 2 in a highly bone metastatic human prostate cancer cell line: roles of RANKL and AR under three-dimensional suspension culture", *Molecular Cancer*, Vol. 13 No. 1, pp. 208.

Statutory Declaration

“I, Yipeng Xu, by personally signing this document in lieu of an oath, hereby affirm that I prepared the submitted dissertation on the topic [Evaluation of the combination treatment docetaxel and JQ1 in 2D and 3D preclinical models of prostate cancer / Bewertung der Kombinationsbehandlung Docetaxel und JQ1 in präklinischen 2D- und 3D-Modellen von Prostatakrebs], independently and without the support of third parties, and that I used no other sources and aids than those stated.
All parts which are based on the publications or presentations of other authors, either in letter or in spirit, are specified as such in accordance with the citing guidelines. The sections on methodology (in particular regarding practical work, laboratory regulations, statistical processing) and results (in particular regarding figures, charts and tables) are exclusively my responsibility.

[In the case of having conducted your doctoral research project completely or in part within a working group:] Furthermore, I declare that I have correctly marked all of the data, the analyses, and the conclusions generated from data obtained in collaboration with other persons, and that I have correctly marked my own contribution and the contributions of other persons (cf. declaration of contribution). I have correctly marked all texts or parts of texts that were generated in collaboration with other persons.

My contributions to any publications to this dissertation correspond to those stated in the below joint declaration made together with the supervisor. All publications created within the scope of the dissertation comply with the guidelines of the ICMJE (International Committee of Medical Journal Editors; www.icmje.org) on authorship. In addition, I declare that I shall comply with the regulations of Charité – Universitätsmedizin Berlin on ensuring good scientific practice.

I declare that I have not yet submitted this dissertation in identical or similar form to another Faculty.

The significance of this statutory declaration and the consequences of a false statutory declaration under criminal law (Sections 156, 161 of the German Criminal Code) are known to me.”

Date Signature

Curriculum Vitae

My curriculum vitae does not appear in the electronic version of my paper for reasons of data protection

Acknowledgments

First and foremost, I would like to extend my heartfelt gratitude to Professor Ulrich Keilholz for his constant encouragement and guidance. He not only provided me with such an excellent opportunity to work in his lab, but also taught me a lot of knowledge in cancer research. Without his consistent and illuminating instruction, this thesis could not reach its present form.

I am also deeply indebted to Prof. Reinhold Schäfer, my second supervisor. He had given me so many good suggestions and help in my researches. And high tribute shall be paid to Przybilla Dorothea, Loredana Vecchione, Anna Kotarac, Anastasia Dielmann, Christoph Hapke, Sandra Liebs, Anika Nonnenmacher, Gabriela Pachnikova, Soo Ann Yap. They helped me a lot in the lab. I gratefully acknowledge the help of all the researchers in the Urology lab and Urology department of Charité Campus Mitte. They provided me with the LNCaP cell line and told me their useful experiences in 3D cell culture.

I also owe a special debt of gratitude to Zhonghua Helmke, Yanyan Xu, Pamela Glowacki and all the people in Charité International Cooperations (ChIC) and Charité Welcome Center. They have helped me to resolve a lot of life problems and public affairs.

Special thanks should go to Prof. Shaoxing Zhu, Matron Yibo Cai and all my other colleagues in China. All the people in our department were so busy, and they have taken on much more work when I work in Germany. I also want to express my gratitude to all the people in Zhejiang Cancer Hospital and Zhejiang Association for Science and Technology. They provided me with the financial support and valuable chance to study and research in Charité.

Finally, I am indebted to my parents, my wife, my lovely daughter and son. They have expressed their longing to me many times, and I could accept all their unconditional love even they are thousands of miles away. I will give them more loves when I come back to China.

I love all of you.

Thank you so much!

Certification by the statistician

CHARITÉ

CharitéCentrum für Human- und Gesundheitswissenschaften

Charité | Campus Charité Mitte | 10117 Berlin

Institut für Biometrie und klinische Epidemiologie (iBikE)

Direktor: Prof. Dr. Geraldine Rauch

Postantschrift:
Charitéplatz 1 | 10117 Berlin
Besucheranschrift:
Reinhardtstr. 58 | 10117 Berlin

Tel. +49 (0)30 450 562171
geraldine.rauch@charite.de
https://biometrie.charite.de/

Name, Vorname: Xu, Yipeng

Emailadresse: yipeng.xu@charite.de

Matrikelnummer: 226446

PromotionsbetreuerIn: Prof. Dr. Ulrich Keilholz

Promotionsinstitution / Klinik: Charité Comprehensive Cancer Center

Bescheinigung

Hiermit bescheinige ich, dass Herr Yipeng Xu innerhalb der Service Unit Biometrie des Instituts für Biometrie und klinische Epidemiologie (iBikE) bei mir eine statistische Beratung zu einem Promotionsvorhaben wahrgenommen hat. Folgende Beratungstermine wurden wahrgenommen:

- Termin 1: 23.11.2020

Folgende wesentliche Ratschläge hinsichtlich einer sinnvollen Auswertung und Interpretation der Daten wurden während der Beratung erteilt:

- Descriptive analysis of the data using tables and figures
- Tests of univariate normality
- Fitting a dose-response curve to find the absolute IC50
- Coefficient of determination (R^2 value)
- Two-sample *t*-test

Diese Bescheinigung garantiert nicht die richtige Umsetzung der in der Beratung gemachten Vorschläge, die korrekte Durchführung der empfohlenen statistischen Verfahren und die richtige Darstellung und Interpretation der Ergebnisse. Die Verantwortung hierfür obliegt allein dem Promovierenden. Das Institut für Biometrie und klinische Epidemiologie übernimmt hierfür keine Haftung.

Datum: 23.11.2020 Name des Beraters/der Beraterin: Dr. Asanka Gunawardana

CHARITÉ
UNIVERSITÄTSMEDIZIN BERLIN
Institut für Biometrie und
Klinische Epidemiologie
Campus Charité Mitte
Charitéplatz 1 | D-10117 Berlin
Sitz: Reinhardtstr. 58

Unterschrift BeraterIn, Institutsstempel